Dmit

X-581-73-369
PREPRINT

NASA TM X- 70535

AE-C ATTITUDE DETERMINATION AND CONTROL PRELAUNCH ANALYSIS AND OPERATIONS PLAN

R. D. WERKING
R. D. HEADRICK
C. F. MANDERS
R. D. WOOLLEY

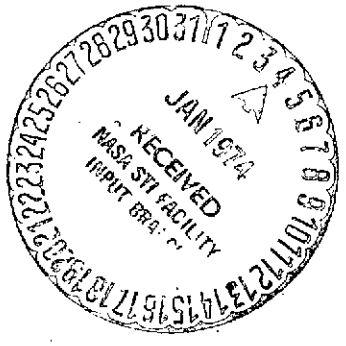

DECEMBER 1973

GODDARD SPACE FLIGHT CENTER
GREENBELT, MARYLAND

FOREWORD

This document has been prepared by the Attitude Determination and Control Section and Computer Sciences Corporation to provide a description of attitude control support being supplied by the Mission and Data Operations Directorate. Included are descriptions of the computer programs being used to support the missions for attitude determination, prediction, and control. In addition, descriptions of the operating procedures which will be used to accomplish mission objectives are provided.

TABLE OF CONTENTS

TABLE OF CONTENTS (Cont'd)

LIST OF ILLUSTRATIONS

Figure

LIST OF TABLES

Table

SECTION 1 - INTRODUCTION

1.1 MISSION PLAN

The objective of Atmosphere Explorer-C (AE-C) is to continue investigation of the upper atmosphere begun by AE-1 and AE-2, earlier spacecraft. It is designed to determine energy input at lower altitudes (120 to 300 kilometers) by measuring structural parameters (neutral and charged particle composition, density, and temperature), solar ultraviolet input, and airglow line intensities.

The AE-C orbit has an initial perigee of 157 kilometers, an apogee of 4300 kilometers, and an inclination of 68.1 degrees, chosen to give a slow rotation (-0.61 degree per day) of the argument of perigee. The latest available launch elements are listed in Appendix A. Perigee will be lowered periodically to altitudes as low as 120 kilometers for 1-day periods. These low-altitude operations are possible because of the onboard Orbit Adjust Propulsion System (OAPS) and the additional stability provided by the momentum wheel. To assure performance of the mission, the spacecraft attitude must be maintained within the following constraints:

- The spin-axis attitude is to be maintained within 2 degrees (arc) of the orbit normal (either positive or negative to maintain the Z-axis Sun angle less than or equal to 90 degrees).
- The total angular momentum must be maintained within 10 percent of the nominal value of 1200 in.-lb-sec.
- These attitude constraints will be met by operation of MSAD/AE for attitude determination, primarily on near real-time (apogee) passes and by Multi-Satellite Attitude Prediction/Atmosphere Explorer (MSAP/AE) for attitude control command generations.

1.2 ATTITUDE SENSORS AND CONTROL SYSTEMS

Attitude sensing is provided by wheel horizon scanners (WHSs); a body horizon scanner (BHS), as shown in Figure 1-1; a fan-shaped digital solar aspect sensor; a magnetometer triad; and an elevation gimbal. Data from the Miniature Electrostatic Accelerometer (MESA) will be provided to the Orbit Determination group during OAPS firings.

The horizon sensors respond to infrared radiation in the 14- to-16-micron CO_2 band, chosen to minimize cloud noise. The WHS detectors receive radiation which is reflected off mirrors rotating on the momentum wheel at effective polar mounting angles of 104 and 118 degrees with respect to the spin (Z) axis. The WHS telemetry consists of Earth widths (elapsed time) for both sensors, split-to-index time (equivalent to a rotational angle), and wheel spin period. The BHS sensor has a similar detector mounted at a 110-degree polar angle to the Z-axis. A second BHS sensor is mounted at the same angle for redundancy, but data from only one of them is telemetered down in the form of Earth width and spin period.

The Digital Solar Aspect Indicator (DSAI) has a fan-shaped field of view (FOV) which covers Sun angles, β , with 1-degree resolution from 0 to 180 degrees from the spin axis. The solar gate sensor enables the DSAI when the Sun is within 0.75 degree arc of the DSAI Y-Z plane.

A set of biaxial gimbals will be provided to aim a solar experiment to the center of the Sun with an accuracy of 1 minute of arc. The elevation gimbal angle with respect to the spacecraft will be determined with an accuracy of ± 0.5 degree.

An orthogonal triad of magnetometers is planned for the AE-C mission: one will be mounted parallel to the +Z-axis and the others will lie in the X-Y plane, 90 degrees out of phase. Each component will be sampled in telemetry at the main frame rate. No specification is made against magnetic materials, and spacecraft magnetic fields may be substantial.

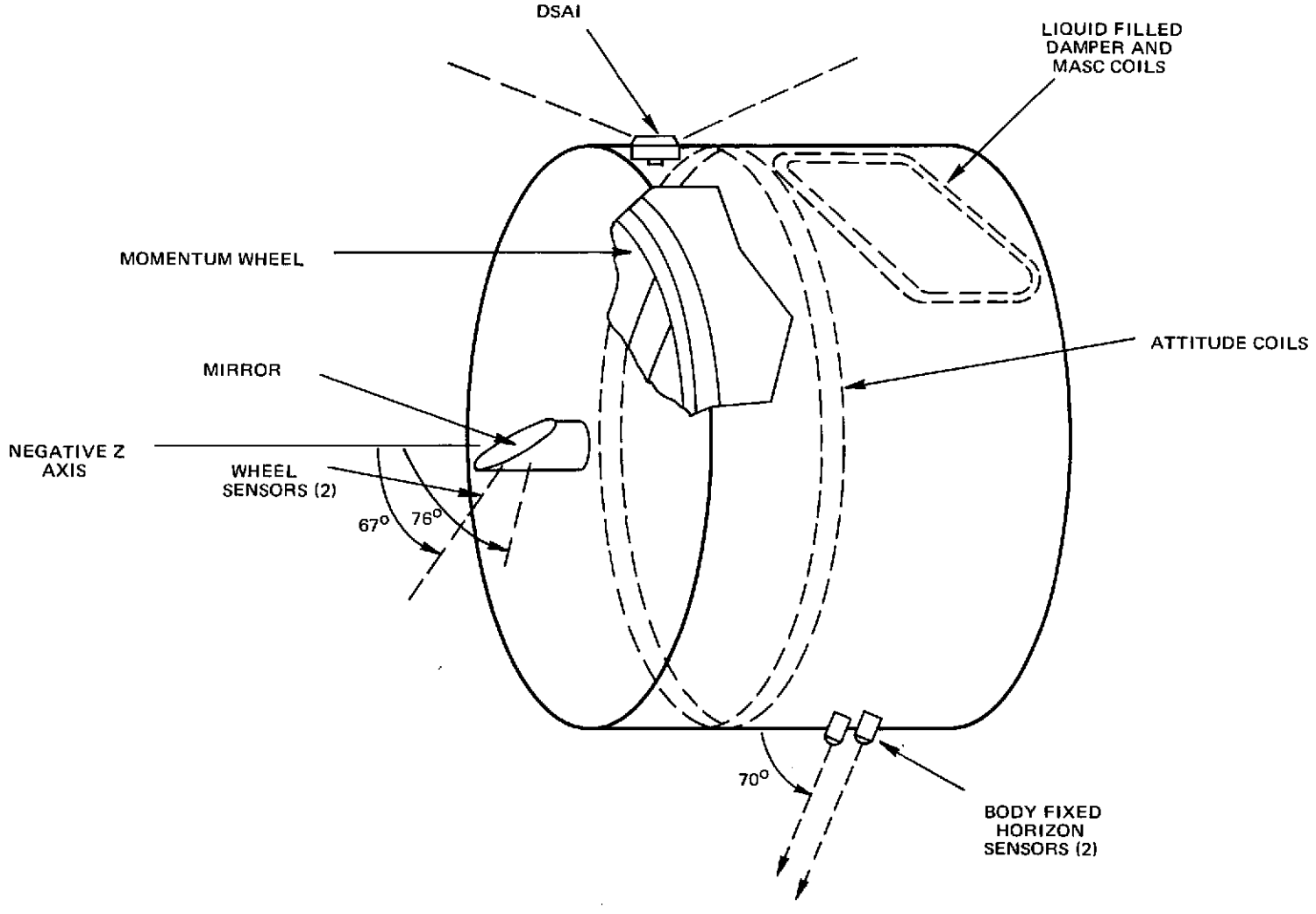

Figure 1-1. Location of Components of the Attitude Control System

An orthogonal triad of MESAs will be available to measure acceleration due to thrusting and atmospheric drag. One will be mounted along the Z-axis and the other two will have their sensitive axes at ±45 degrees to the X-axis. There will be three constraintment ranges (A, B, and C), the most sensitive of which (C) permits measurements from 2×10^{-5} g (full scale) to 4×10^{-8} g. Constraintment range A permits measurement from 8×10^{-3} g (full scale) to 1.6×10^{-5} g. This range will normally be used during spacecraft thruster firing.

The AE spacecraft has two modes of operation: the pitch loop control mode and a freewheeling, or tachometer, loop mode. In the pitch loop mode, the spacecraft rotates about the spin axis (Z), at either a 4-revolution-per-minute or despun (Earth-pointing) mode of 1 revolution per orbit. In the tachometer mode, the spin rate can be selected by ground command from 1 rpm to approximately 8 rpm. In the despun mode, the spin axis is normal to the orbital plane and the spacecraft Y-axis can be aligned with the local vertical or at any commanded pitch angle from this position.

The attitude control system consists of a momentum wheel assembly, magnetic torquers, nutation dampers, automatic roll control, pitch control, and yaw thruster.

Figure 1-1 shows the location of the attitude control system components.

Momentum consists of the sum of the body and the wheel inertia-velocity products. The simplest and most accurate (±0.1 percent) determination of total momentum can be made from the telemetered wheel period when despun. During contact passes while spinning, both wheel and body rate data are also available from the horizon and Sun sensors. Thus, a running record of body inertia can be kept, so that subsequent momentum determination during the spin mode is possible.

The momentum wheel provides a momentum reference for stabilizing the spacecraft and a reaction torque for controlling the spin rate and despun attitude. The initial angular momentum will be attained by spinning the spacecraft, using the delta vehicle. Momentum will be maintained by appropriate transfers between the spacecraft and the wheel. (In the despun mode, essentially all the momentum will be transferred to the wheel, but in the spin mode, it will be distributed between the wheel and the spacecraft.) The spin rate will be set to the rate commanded from the ground by sensing the rotation rate with respect to the local vertical and controlling wheel speed appropriately.

The magnetic torquers control spacecraft orientation and momentum magnitude. After horizon sensors have determined the orientation, a magnetic precession torque, generated by a Z-axis coil either automatically or by ground command, is applied to the spin axis to align the axis normal to the orbit plane. Momentum magnitude control will be accomplished via a magnetic torque applied about the spin axis. Appropriate switching of the magnetic field of a spin coil in the spacecraft X-Y plane provides an interaction with the Earth's magnetic field to effect the desired momentum magnitude change.

Passive nutation dampers on the despun portion of the spacecraft will be used to damp spacecraft oscillations induced by aerodynamic drag, thruster firing, and other disturbing forces.

During low-perigee passes and apogee restoration maneuvers, the primary attitude disturbance results in roll deviations in the vicinity of perigee. Automatic roll control is provided for backup in case of missed station contacts to reduce this attitude error by automatic sensing and magnetic torquing. Because roll deviations occurring at perigee appear as roll deviations at the subsequent apogee, closed-loop (i.e., automatic) roll sensing will take place at apogee.

Spin or pitch angle control is provided in either a closed-loop mode or in an open-loop (or tachometer) mode. In the closed-loop mode, control is achieved

by momentum transfer between the flywheel and the main body by means of a direct current torque motor. In the open-loop mode, the desired value of the wheel speed can be set by ground command at any of 32 values from 10 to 41 radians per second, to allow control of the body spin rate in the range of 1 to 8 rpm. The closed-loop mode is employed either during the despun mode (one revolution per orbit) and at a spin rate of 4 rpm.

Pitch error is measured by one of the two wheel horizon sensors. The sky-Earth and Earth-sky transitions are used to generate a pulse that bisects the two horizon pulses. This pulse represents a local vertical reference that can then be compared with the encoder-generated index pulse to obtain the pitch error.

The necessary horizon splitting is accomplished by gating a clock to a counter for sensor Earth-time duration and, beginning with the next sky-Earth transition, counting down at twice the frequency. This process produces a time-bisecting pulse during the next wheel spin.

Two redundant pitch axis control loops will be available. Either of the torque motors with its corresponding electronic loop can be selected by ground command and either horizon sensor can be used with the selected loop.

The pitch electromechanical assembly for pitch control consists of an outer fixed housing that interfaces with the spacecraft and of an inner rotating turntable. Mounted onto these two items are an encoder with redundant coils, labyrinth seals, redundant brushless torque motors; an oil reservoir; the flywheel; a mirror assembly; and bolometers and associated electronics. The turntable assembly is supported by the external housing through a single bearing.

1.3 GROUND DATA FLOW

The ground data flow is shown in Figure 1-2.

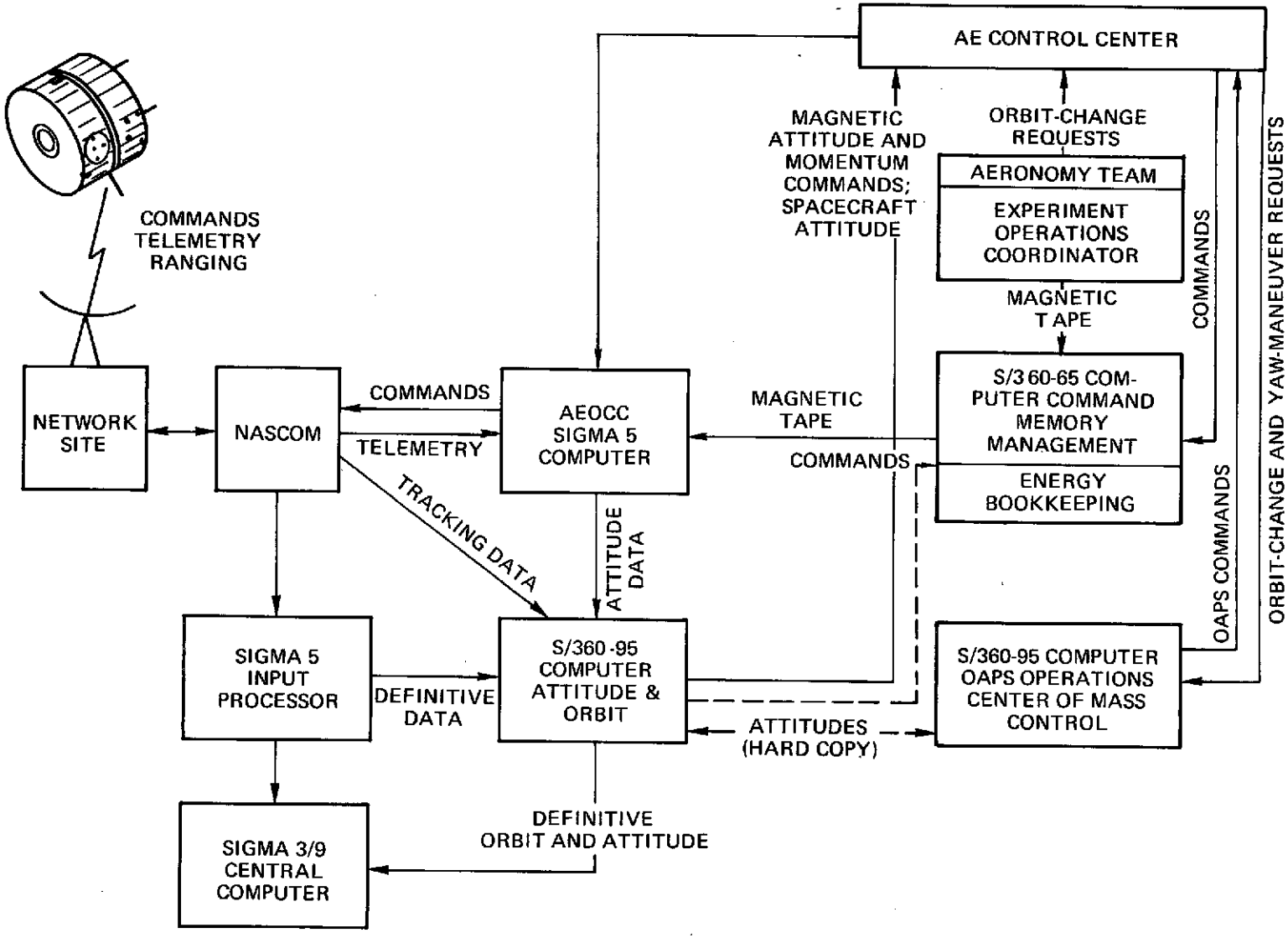

Figure 1-2. Ground Data Flow

To maintain the attitude and momentum within mission constraints, the established procedure is followed: attitude determination, prediction, and control. Because of the relatively strong torques and tight constraints, special care must be taken in attitude accuracy, bias determination, and estimation of spacecraft parameters.

2.1 ATTITUDE DETERMINATION

The basic method used for real-time spin-axis attitude determination is the conic intersection technique for both deterministic and least-squares processing. Sensor data from WHS, Sun sensors, and magnetometers are converted into cone angles about the reference vectors. Special filtering methods are used to average the cone angles to reduce the sensitivity to body dynamics. In terms of vectors on a unit sphere, the equations can be written as:

$$\begin{aligned} \hat{Z} \cdot \hat{E} &= \cos \mathbf{n} \\ \hat{Z} \cdot \hat{S} &= \cos \beta \\ \hat{Z} \cdot \hat{B} &= \cos \chi \end{aligned} \tag{2-1}$$

where $\hat{Z}$ = spacecraft spin-axis unit vector

$\hat{E}$ = satellite-Earth unit vector

$\hat{S}$ = satellite-Sun unit vector

$\hat{B}$ = Earth's B-field unit vector

$\mathbf{n}$ = nadir cone angle between $\hat{Z}$ and $\hat{E}$

β = Sun angle between $\hat{Z}$ and $\hat{S}$

χ = magnetometer cone angle between $\hat{Z}$ and $\hat{B}$

The horizon scanners, which operate in the 14-to-16-micron band, respond to radiation from the CO_2 molecules in the upper atmosphere, and thus are not

subject to terminator problems that are common to optical sensors. They are sensitive, however, to other error sources, such as threshold drift, radiance variations, orbit error, and Earth oblateness. The Earth widths from the WHS telemetry are converted to nadir angles from the spherical triangle relationship:

$$\cos \rho = \cos \gamma_2 \cos n + \sin \gamma_2 \sin n \cos f_2 \qquad (2\text{-}2)$$

where γ_2 = sensor mounting (cant) angle, 118 degrees

f_2 = half width of the Earth from $f_2 = \pi$ EW2/SP

EW2 = measured Earth width from WHS2

SP = selected spin period

ρ = angular radius of the Earth, calculated from the following:

$$\sin \rho = \frac{R_E + HT_{CO_2}}{r}$$

where r = distance from the center of the Earth to the satellite

HT_{CO_2} = height of the CO_2 effective horizon

R_E = radius of the Earth at the averaged horizon-crossing points

The correction has been made for oblateness using a two-parameter model:

$$R_E = R_{EQ}\left(1 - \epsilon_1 \sin^2 \phi_{LAT} + \epsilon_2 \sin \phi_{LAT}\right)$$

where R_{EQ} = equatorial radius

ϵ_1 = flattening coefficient

ϕ_{LAT} = horizon-crossing latitude

ϵ_2 = empirical coefficient for seasonal effects

Although Equation (2-2) yields ambiguous values for n, the two solutions are easily resolved when the attitude is near the orbit normal. With both WHS sensors operational, the term $\cos \rho$ can be eliminated, removing the dependence on orbit ephemeris. The resulting dual-scanner equation is

$$\tan n = \frac{\cos \gamma_2 - \cos \gamma_1}{\sin \gamma_1 \cos f_1 - \sin \gamma_2 \cos f_2}$$

without ambiguity. At apogee, the orbit and oblateness errors are small and the WHS2 single-scanner solution is more accurate ($\sigma_n = 0.3$ degree) because of fewer sensor-electronic errors. At apogee, the WHS2 sensor can tolerate roll angles of -9 degrees ($n = 81$ degrees) before missing the Earth.

Sun angles are read directly from the DSAI Gray-coded telemetry with 1-degree resolution or an accuracy of $\sigma_\beta = 0.5$ degree. The DSAI range is from 0 to 180 degrees, and thus will provide data as long as the spacecraft is in sunlight and in the spinning mode. When the SPS is tracking the Sun, the elevation gimbal gives a separate Sun-angle measurement to about the same accuracy, but one which is more subject to performance errors. The gimbal range is 0 to 90 degrees and can provide data also when the body is despun.

The magnetometer cone angle, χ, is obtained from

$$\cos \chi = \frac{H_z}{\sqrt{H_x^2 + H_y^2 + H_z^2}}$$

These magnetometers are subject to rather large errors due to quantization alone ($\sigma_\chi = 1.25$ degrees), and spacecraft magnetic fields are expected to be large and variable due to coils, transmitters, tape recorders, experiments, and the iron momentum wheel. Constant biases can be resolved and removed

by routines in the telemetry processor (BAMN and RESIDU). The magnetometers will be used as backup data for another reference vector for conic intersection when the spacecraft is in shadow. Although the magnetometer data is available at the main-frame rate (16 per second), it will ordinarily be sifted down to about 1 per second to reduce the data volume.

2.2 DISTURBANCE TORQUES

A nominal launch will place the spin axis at negative orbit normal, and to satisfy mission requirements, the spin axis must track the orbit normal to within 2 degrees. The orbit normal describes a cone in inertial space, with the right ascension decreasing about 1.5 degrees per day because of the Earth's oblateness.

In addition to the tracking error caused by attitude sensing and control limitations, there are several external torques which precess the spin axis away from its proper orientation.

The torques considered include aerodynamic, magnetic, solar pressure, gravity gradient, and the delta-V thruster. The effects of these disturbance torques are assessed by use of MSAP/AE simulation runs.

The simulations were made with an orbit generator using the following preliminary orbit elements:

Epoch	December 7, 1973
Epoch time	5.53 hours U.T.
Semimajor axis	8625.1195 kilometers
Eccentricity	0.2421825
Inclination	68.1104
Mean anomaly	359.4129 degrees
Argument of perigee	165.7542 degrees
Right ascension of ascending node	236.8955

and the initial attitude at negative orbit normal.

One-day simulation runs were made 3 days after launch date by turning on various torque-calculation indicators in the MSAP satellite-dependent input. The effect of the varying perigee height was studied by changing the semimajor axis and the eccentricity to achieve the desired perigee altitude. The results are presented by MSAP/AE-C attitude summary and various MSAP plots. The summary of the attitude drift rate due to these torques is given in Table 2-1. An example of a typical run (120 kilometers, aerodynamic torque) is given in Appendix B. The increase in momentum in this run was caused by having the integration stepsize a multiple of the spin period.

Because of the low perigee altitude, aerodynamic torque will be the primary cause of attitude disturbance for the AE-C mission.

The aerodynamic torque is modeled by the following equation, using the simple drag-force model:

$$\vec{T}_{aero} = \vec{r} \times \vec{F}$$

and

$$\vec{F} = C_D \left(\rho \frac{V^2}{2} \right) A_p \, (-\hat{V})$$

where C_D = drag coefficient $\cong 2.0$

ρ = atmospheric density

V = magnitude of the satellite velocity

A_p = surface area of the satellite projected on the plane perpendicular to $\hat{V}$

$\hat{V}$ = unit vector in the direction of satellite velocity

$\vec{r}$ = the vector displacement of the satellite center of pressure from the center of mass

Table 2-1. Attitude Drift Rate Summary

PERIGEE HEIGHT (KM)	TYPE OF TORQUE	SPIN RATE (RPM)	CONDITIONS	$\Delta\alpha$ (DEG)	$\Delta\delta$ (DEG)	ΔL (IN.-LB -SEC)
120	AERODYNAMIC	4	$C_D = 2.$ YCMOFF = 0.1"	4.9	1.4	57.7
		0	ZCMOFF = 0.1"	5.0	1.4	98.9
161	AERODYNAMIC	4	$C_D = 2.$ YCMOFF = 0.1"	0.4	0.1	1.7
		0	ZCMOFF = 0.1"	0.4	0.1	8.6
161	MAGNETIC	4	ZBIAS = 500 POLE-CM	0.1	0.0	0
		4	ZBIAS = 1000 POLE-CM	0.2	0.0	0
161	MAGNETIC	0	XBIAS = 50 POLE-CM	0.0	0.0	0
161	GRAVITY	4	NEGATIVE ORBIT NORMAL	0.0	0.0	0
			2-DEGREE CONING	0.0	0.0	0.1
161	SOLAR	4	ZCMOFF = 0.1"	0.0	0.0	0
161	NONE	4		0.0	0.0	0

It is assumed here that shadowing effects which might be caused by solar pointing subsystem are negligible. The projected area of the AE-C satellite surface is given by

$$A_p = \left| hD \sin \theta_i \right| + \frac{\pi D^2}{4} \cos \theta_i$$

where D = diameter of cylinder

h = length of cylinder

θ_i = angle between $\hat{V}$ and cylinder axis

The aerodynamic force is proportional to the atmospheric density at perigee. The drift rate is proportional to the force and the offset of the centroid from the center of mass.

The other disturbance torque which is observable from the drift rates is the magnetic torque, given by

$$\vec{T}_{mag} = \vec{M} \times \vec{B}$$

where $\vec{M}$ = magnetic dipole moment

$\vec{B}$ = Earth's magnetic field

Cases were simulated for residual dipole moments of 500 and 1000 pole-cm along the Z-axis, with results as shown in Table 2-1. In the despun mode, a dipole moment of 50 pole-cm along the X-axis produced no effect.

When the delta-V thruster is fired it will produce a disturbance torque

$$\vec{T} = \vec{r} \times \vec{F}$$

where $\vec{F}$ = force vector along the thrust axis

$\vec{r}$ = thrust offset vector from the center of mass of the spacecraft

Because $\vec{F}$ is nearly along the X-axis, the center of mass offset along $\hat{x}$ will not produce any torque. The torque from the y and z components can be evaluated separately for roll and spin-rate changes.

Using the impulse approximation,

$$\Delta H_y = \Delta z \cdot F_x \Delta t$$

When the firing occurs along or against the velocity vector of

$$\Delta\varphi_r = \pm \frac{\Delta H_y}{H_{TOTAL}}$$

at perigee or apogee, this results in a change in roll angle, φ_r.

For typical values ($\Delta z = 0.1$ inch, $F_x = 4.0$ pounds, $\Delta t = 260$ seconds, and $H_{TOTAL} = 1200$ in.-lb-sec), we have $\Delta\varphi_r \cong 5.0$ degrees. For perigee-lowering maneuvers, it will be necessary to preroll the spacecraft to avoid entering the atmosphere with the attitude far from the orbit normal.

The Δy offset gives a spin rate change

$$\Delta H_z = - \Delta y \, F \, \Delta t$$

of -104.0 in.-lb-sec for $\Delta y = 0.1$ inch.

2.3 CONTROL TORQUES

An optimal magnetic attitude control method has been developed for AE-C to maintain the spin-axis direction within 2 degrees of orbit normal. The control law has been shown to be optimal in the sense of minimum time, minimum

energy, and minimum attitude deviation. The deviation and some comparitive results is presented in the paper included as Appendix C.

The yaw thruster is provided for emergency maneuvers, and produces a torque

$$\vec{T} = \vec{r} \times \vec{F}$$

where $\vec{F}$ = force vector along the thrust axis

$\vec{r}$ = thrust offset vector from the center of mass of the spacecraft

The thruster is located on the spacecraft to produce a strong torque along the Y-axis that can be used to perform a 180-degree yaw maneuver and can also be used for rapid correction of the spin-axis orientation.

The Magnetic Attitude Spin Coil (MASC) is commutated to produce a torque along the Z-axis to adjust the total angular momentum of the system. It is anticipated that the action of the nutation damper and momentum wheel under external torques will increase the total momentum of the system and necessitate periodic "dumping" by the MASC.

The partitioning of the total momentum between wheel and body is achieved through the action of the pitch control electronics (PCE) in either a closed-loop mode (despun or 4 rpm) or open-loop mode (1 to 8 rpm). Details of command generation are given in another document.[1]

2.4 CONTINGENCIES

Two contingencies have been analyzed extensively:

- Recovery from zero angular momentum failure.
- Torquing to check out the Extreme Solar Ultraviolet Measurement (ESUM) field of view.

---

[1] Computer Sciences Corporation Memorandum, Pitch Control Electronics Commands, R.D. Woolley, September 21, 1973.

2.4.1 Recovery From Zero Angular Momentum Failure Mode

Prior to separation, the Delta launch vehicle is scheduled to spin up the AE spacecraft to about 10 rpm to impart the required angular momentum to stabilize the system. Failure to spinup (the zero angular momentum failure mode) results in serious consequences which endanger the mission.

- With the spacecraft tumbling, the experiments cannot function
- Attitude data is severely impaired
- No orbit adjustment maneuvers can be performed

It should be noted that the actual angular momentum will never be exactly zero, but will always have some finite value.

The following procedure will be used to determine the angular momentum (magnitude and direction) if this failure to spinup occurs.

- Spinup wheel to 10 radians per second
- Determine H_3 from commanded wheel and measured body rates from Sun times and magnetometers
- Determine nutation angle, θ, from Sun angles and magnetometers
- Determine total angular momentum from $H_T = H_3/\cos\theta$.
- Determine angular momentum direction with Sun and magnetometer data.

Three recovery methods are possible:

- Off-loading one tank with a delta-V thruster
- Yaw thruster firing into a flat spin with passive nutation decay, using the momentum wheel to ensure positive spin

- Yaw thruster firing into a flat spin with active ground-controlled real-time nutation damping using the momentum wheel and magnetic coil

These methods are described in the following subsections.

2.4.1.1 Off-Loading One Tank With the Delta-V Thruster

If fuel is drawn continuously from the number 4 tank (along the -y-axis), the center of mass shift gives a moment arm along -y , providing a torque along the z-axis (Figure 2-1).

$$T_Z = -\Delta y \times F_X$$

Because the center of mass shift is linear in time, the angular momentum increases quadratically. Table 2-2 shows the values at 100-second intervals, where the impulsive approximation has been used for ΔH :

$$\Delta H = -\overline{\Delta y}\ \overline{F}\ \Delta t$$

An additional source of angular momentum accrues from the momentum carried off by the fuel. Because the body can be made to spin in reverse by commanding the tachometer loop on, subtracting off negative angular momentum will increase the total momentum of the system.

$$\Delta H = -mr^2\ \omega_z$$

The values were calculated at the maximum tachometer rate of 41 radians per second.

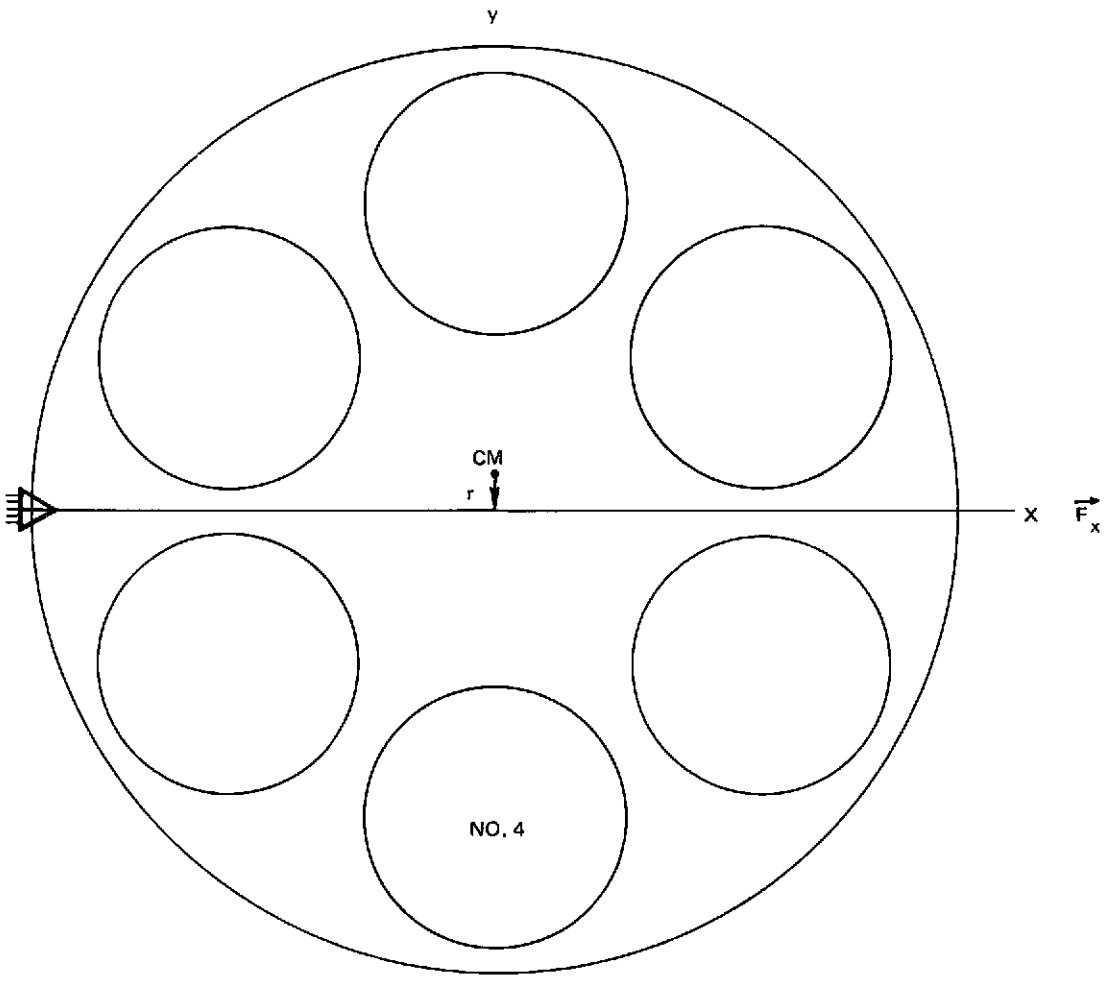

Figure 2-1. Center of Mass Shift From Off-Loading the Number 4 Tank

It is estimated that approximately 1034 seconds of fuel usage (15.7 pounds of fuel) is required to add 318 in.-lb-sec of angular momentum, which will allow the spacecraft to be despun at the lowest tachometer rate of 10 radians per second.

If time is critical, the burn should be performed as quickly as possible. If time is not critical, the burn can be split into three firings, and the following operational procedure is suggested:

Determine tumble contingency from magnetometers and DSAI
Command tachometer loop at 41 radians per second
Load and fire 345-second continuous delta-V burn
Determine attitude from magnetometers and DSAI
Run MSAP for coil commands
Load and execute coil commands to negative orbit normal

[WHS and BHS will acquire the Earth. The nadir programmer will work at a negative spin rate.]

Load and fire second 345-second delta-V burn
Confirm attitude from WHS-Sun data

[OAPS becomes operational (pulsed mode) after nutation has decayed to less than 5 degrees to avoid the risk of the BHS missing the Earth and confusing the nadir programmer.]

Load and fire third 345-second delta-V burn
Confirm attitude and rates

[OAPS becomes operational in despun mode. If necessary, the orbit can be corrected using the opposite tank, and the angular momentum will increase further.]

Run MSAP for spin coil commands

Table 2-2. Angular Momentum From Off-Loading One Tank With Delta-V Thruster

t	F (POUND)	$\bar{F}$ (POUND)	Δy (INCH)	$\Delta\bar{y}$ (INCH)	ΔH_{rxF} (IN.-LB-SEC)	ω_z (RAD/SEC)	$\Delta H_{mr^2\omega_z}$ (IN.-LB-SEC)	H_{TOTAL} (IN.-LB-SEC)
0	3.983		10^{-14}					
100	3.916	3.950	−0.0156	−0.0078	3.081	−1.3469	4.774	7.855
200	3.842	3.879	−0.0311	−0.0234	9.058	−1.3388	4.665	21.578
300	3.750	3.796	−0.0463	−0.0387	14.690	−1.3246	4.529	40.797
400	3.650	3.700	−0.0615	−0.0539	19.943	−1.3048	4.354	65.094
500	3.551	3.600	−0.0765	−0.0690	24.843	−1.2796	4.156	94.094
600	3.459	3.505	−0.0913	−0.0839	29.407	−1.2497	3.949	127.450
700	3.376	3.418	−0.1061	−0.0982	33.730	−1.2152	3.741	164.921
800	3.303	3.340	−0.1207	−0.1134	37.870	−1.1765	3.535	206.295
900	3.238	3.270	−0.1352	−0.1280	41.846	−1.1338	3.333	251.474
1000	3.181	3.210	−0.1496	−0.1424	45.703	−1.0871	3.132	300.309
1034	3.165	3.173	−0.1544	−0.1520	16.657	−1.0166	0.976	317.942

[Leave attitude at a negative rate; run the spin coil to decrease this rate.]

Command tachometer loop at 10 radians per second

Spinup to 1080 in.-lb-sec

[Will require about 3 days at 24 in.-lb-sec per orbit.]

The three firings can be accomplished at successive perigees to minimize the risk of changing the orbit.

2.4.1.2 Yaw Thruster--Passive Damping

This technique uses very little fuel (less than 0.5 pound) because of the 15-inch moment arm of the yaw thruster. The yaw thruster is fired for about 18 seconds to achieve slightly less than the nominally required angular momentum of 1200 in.-lb-sec. Then the spacecraft is placed in 10 radians per second tachometer mode to maximize the rate of nutation damping toward the positive Z-axis. After the nutation half cone angle has decreased to less than 5 degrees (from the initial value of 90 degrees) and after the angular momentum vector has been maneuvered to the negative orbit normal using magnetics, orbit adjust maneuvers can be performed in either a spinning or a despun mode.

If the perigee altitude is high enough so that aerodynamic pumping of nutation is small, the technique results in an operational spacecraft capable of orbit adjustment maneuvers within 2 to 3 days. If the perigee altitude is below 150 kilometers, then aerodynamic nutation pumping might significantly increase the time required for this technique, or perhaps even prevent the eventual success of this technique. The following procedure is required to implement this method:

[Pitch control electronics is off, so the wheel is not spinning significantly relative to the body.]

Determine tumble contingency from MAGS and DSAI

[Verify that perigee is above 150 kilometers.]

Fire yaw thruster for 18 seconds to achieve approximately 1100 in.-lb-sec angular momentum

Command spacecraft into tachometer loop at 10 radians per second

Wait (1/2 to 1 day) for nutation to decay to about a 30-degree half cone angle
[Determine attitude while waiting.]

Load and execute coil commands maneuvering to the negative orbit normal

Wait for nutation to decay below a 5-degree half cone angle.

Load and execute MASC commands to trim the angular momentum to 1200 in.-lb-sec.

2.4.1.3 Yaw Thruster--Active Damping

This method could result in an operational spacecraft within 1 to 2 days, and uses less than 0.5 pound of fuel. However, it requires the development of nutation damping computer programs to operate in the Atmosphere Explorer Operations Control Center (AEOCC), phasing real-time commands about every 5 seconds with quantities calculated from real-time telemetry. The efficiency of this technique in speeding up nutation damping over the passive damping case depends on the command timing accuracy (fractions of a second) achieved by that presently undeveloped software.

After the nutation half cone angle has decreased to less than 5 degrees and after the angular momentum vector has been maneuvered to the negative orbit normal using magnetics, orbit adjust maneuvers can be performed in either a spinning or a despun mode. The time required before this operational capability is

possible is 1 to 2 days. The following procedure is required to implement this method:

[Pitch control electronics is off, so the wheel is not spinning significantly relative to the body.]

Determine tumble contingency from magnetometers and DSAI

Fire yaw thruster for 18 seconds to achieve 1100 in.-lb-sec angular momentum

Command spacecraft into tachometer loop at 10 radians per second

Initiate active nutation damping maneuvers throughout every real-time station contact until the half cone angle is below 5 degrees

As soon as the half nutation cone angle is below 30 degrees, load and execute (between station contacts) coil commands maneuvering to the negative orbit normal

As soon as the half nutation cone angle is below 5 degrees, load and execute MASC commands to trim the angular momentum to 1200 in.-lb-sec

2.4.2 Torquing to Check Out the ESUM Field of View

The ESUM experimenter has requested that the spin axis be torqued through Sun angles of 35 to 90 degrees to check out the instrument's field of view. The maneuver is requested within 6 weeks of launch to be performed in about 5-degree Sun-angle increments with the attitude determined and experimental data taken at each step. An analysis was made of magnetic maneuvers at two possible times:

- first inversion from negative to positive orbit normal
- six weeks from launch on an uncorrected orbit

2.4.2.1 Inversion Time

Although the time of first inversion on the current mission plan will occur 8 or 9 weeks after launch, these plans may be revised or the experimenter's time requirement may be relaxed. Because a magnetic inversion maneuver is already required at this time, torquing toward the Sun would not impose any additional operations nor any additional time outside mission constraints.

Preliminary analysis established that maneuvers at declinations south of the Sun provided more WHS data than those north of the Sun. When torquing was forbidden for 20 minutes on either side of perigee, the maneuver required 4 days, which seemed too long to have the spacecraft outside mission constraints. Therefore, continuous torquing was used to speed up the maneuver.

To get a somewhat realistic orbit, elements were taken from an EPHEM tape for December 28, 1973 (from a November 1, 1973 launch) corrected for the difference in the node for the current December 7, 1973 launch date, giving an effective epoch at February 2, 1974. These elements were propagated by analytic routines (BRRS or FASTOG) to the maneuver time about February 13, 1974. The perigee altitude is about 145 kilometers.

For MSAP, nominal values were used for:

- drag coefficient, $C_D = 2.0$
- angular momentum - 1200 in.-lb-sec
- CP-CM offset = 0.1 inch along Z-axis
- two coils, 98,000 pole-cm each
- night coil reduction = 5 percent
- initial attitude near the negative orbit normal

Selected points (ϕ_{max} = 130 degrees, 90 degrees, 50 degrees) were input to ODAP to check data availability and shadow times, which are shown on Figure 2-2. With the torquers on continuously, the Z magnetometer will be saturated, and it will be especially important to have the spacecraft in sunlight

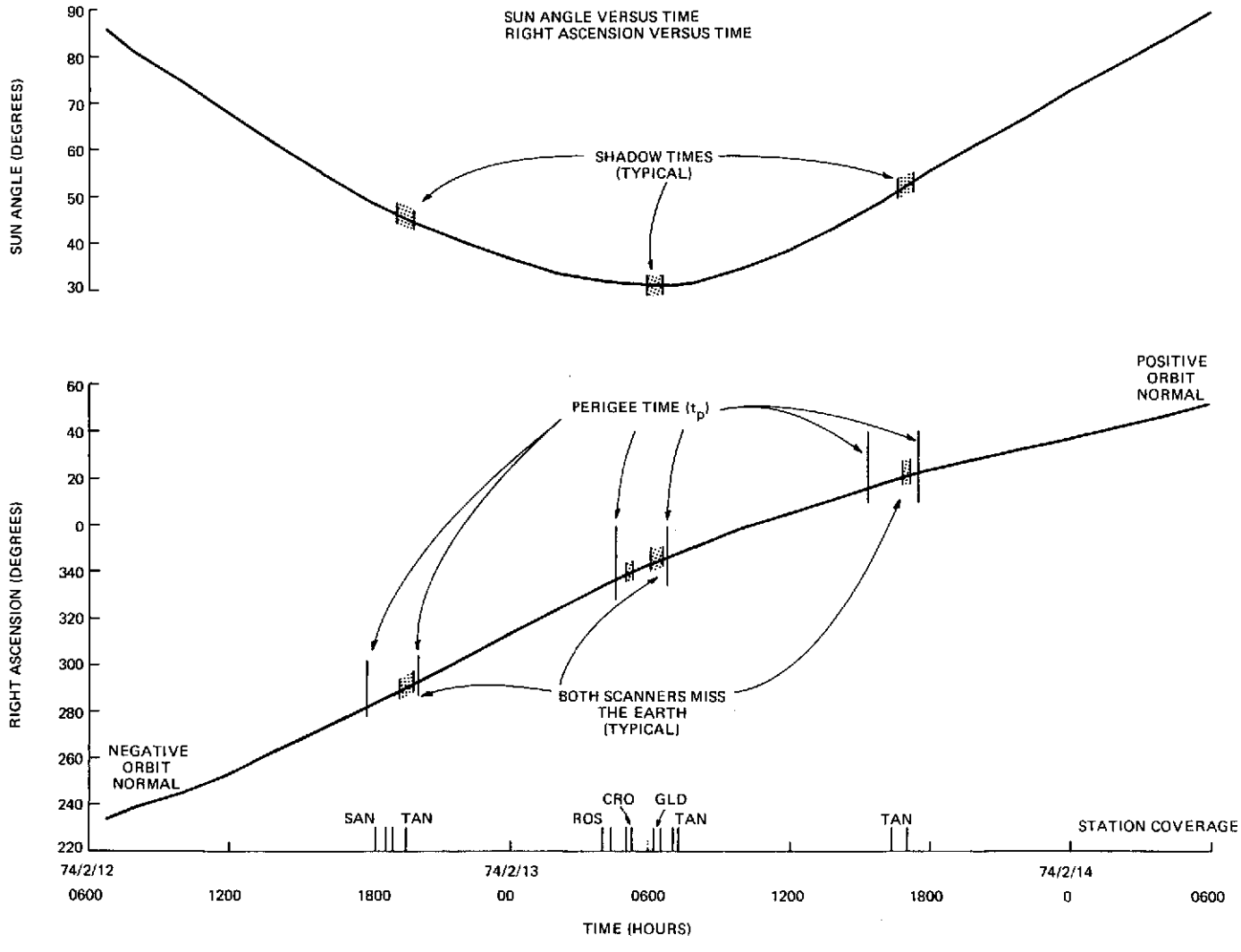

Figure 2-2. Torquing at Inversion

to get a second reference vector for accurate attitudes. The station coverage around the middle orbit (February 13, 1974 0437-0646) illustrates a potential problem in that the station coverage coincides with the times of missed data. Because attitude data might be severely degraded by blind orbits, it would be necessary to either turn on the tape recorders near apogee or to alter the attitude trajectory or maneuver times.

2.4.2.2 Six Weeks After Launch

Approximately 6 weeks after launch on an uncorrected orbit, the Sun angle will be at 35 degrees in a favorable geometry. A magnetic maneuver can be made away from the Sun to 90 degrees and back in about 36 hours. Figure 2-3 illustrates the variation of Sun angle and right ascension with time. At this particular geometry there is no shadow and no time when both WHS sensors miss the Earth (though WHS1 will miss at apogee and WHS2 will miss at perigee at the Sun angle of 90 degrees). The Sun angle is changing at about 7 degrees per orbit, but the torques can be arranged to have a different set of Sun angles at perigee on the two legs of the maneuver.

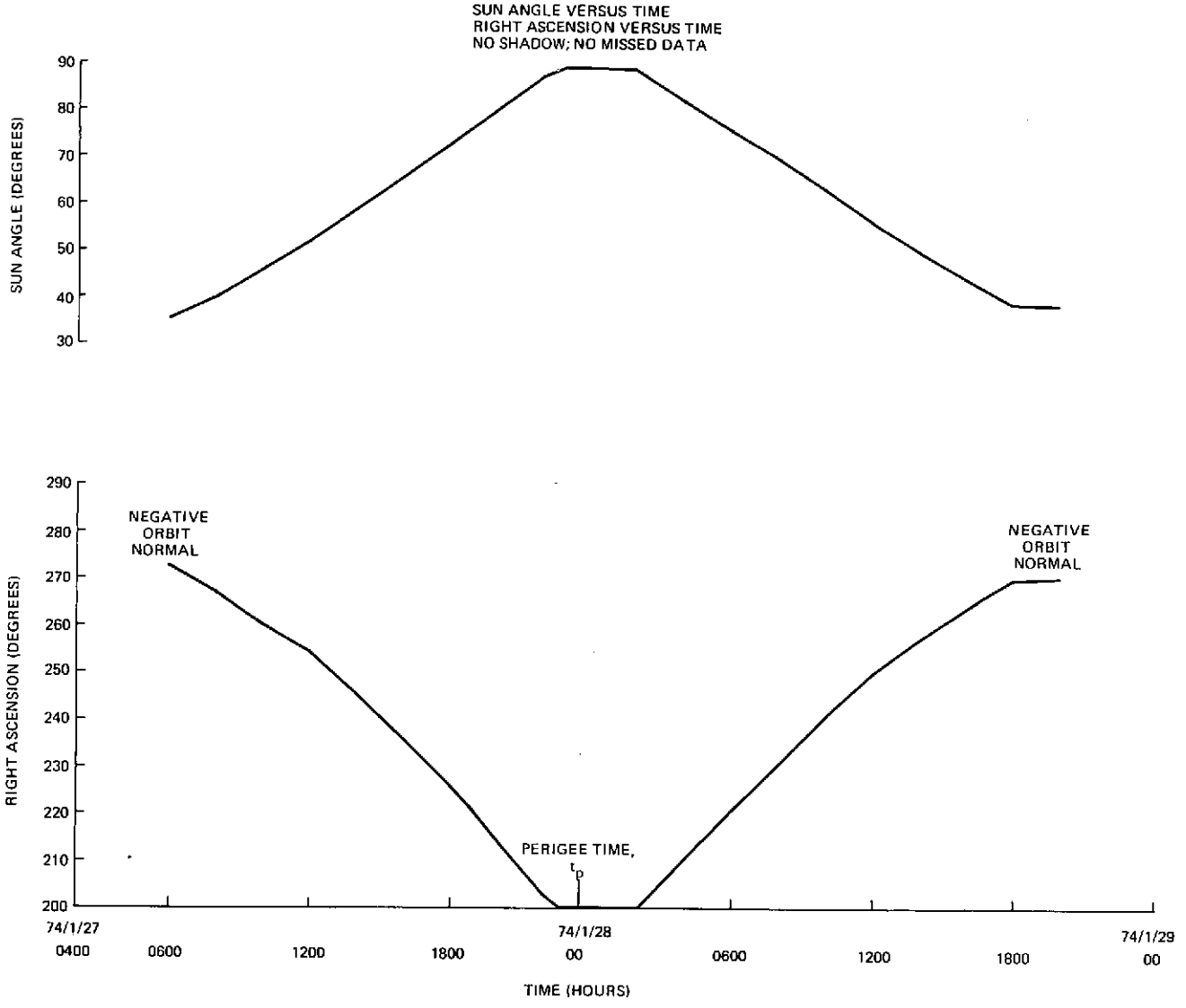

Figure 2-3 ESUM Torquing 6 Weeks After Launch

SECTION 3 - ATTITUDE SUPPORT SYSTEM OVERVIEW

3.1 MSAD EXECUTIVE AND GRAPHICS

The Multi-Satellite Attitude Determination (MSAD) System has been developed for general attitude determination. This executive system employs an interactive control structure to serve as the operational environment or base on which the AE-dependent attitude determination system was built. It is composed of a set of drivers and utility routines to control the sequence of application subsystems, graphic displays, core storage allocation, selection of routines, and error-handling capabilities. MSAD is used in conjunction with the MSAP System for complete attitude support. The total system is referred to as the Multi-Satellite Attitude Program System (MAPS). The MSAD/AE System is composed of a Simulator Subsystem, a Telemetry Processor Subsystem, and an Attitude Determination Subsystem.

3.1.1 Simulator Subsystem Overview

The Atmosphere Explorer Simulator Subsystem (AESIM) is designed to simulate the telemetry data required for attitude determination. During the prelaunch period, the primary function of AESIM will be to test the Telemetry Processor and the Attitude Determination Subsystems; during the postlaunch period, AESIM will be used as an analytical tool in the study of attitude dynamics. In addition, AESIM will create on demand a disk file of simulated data to be used in the prelaunch testing of the Operations Control Center (OCC) and the input processor (IP) data links.

AESIM consists of two separate attitude simulators, TELSIM and ADSIM, each one tailored specifically for one of the functions mentioned above. TELSIM is more suitable in testing the telemetry processor and data links. It makes use of a simplified, non-nutating spacecraft model with either a constant attitude or a time varying attitude read from an MSAP tape. In addition, small-range

attitude maneuvers can easily be simulated with TELSIM by specifying the initial and final attitudes and the time span of the maneuvers.

The Attitude Dynamics Simulator (ADSIM), on the other hand, simulates attitude data from a nutating satellite by numerical integration of Euler's equations. Its inputs are the moments of inertia along the principal axes, the angular momentum vector, the body axes relative to the angular momentum vector, spacecraft position, and relevant data describing the spacecraft's sensor complement. ADSIM is also able to simulate coning, which is caused by an offset between the geometrical and principal axes of the spacecraft.

3.1.2 Telemetry Processor Subsystem Overview

The basic function of the telemetry processor is to convert raw data in telemetry counts from the AE-C spacecraft to geometric entities used in attitude determination. During the conversion process, telemetry data resides in the telemetry processor in three forms: working arrays containing raw data in telemetry counts; intermediate arrays of sensor readings in engineering units; and output arrays of cone angles, dihedral angles, and azimuth determination information.

The telemetry processor is called by TPDRIV, a driver built into the MSAD executive system. Input to the telemetry processor consists of either real or simulated telemetry data contained on disk files. Additional input may include NAMELISTS, sensor data sets consisting of previously processed data in engineering units, and ephemeris information. Output consists of cone angles, dihedral angles, and azimuth determination information. Additional output optionally includes a data set containing accelerometer and OAPS data and a data set containing sensor information in engineering units.

The telemetry processor processes data in both the real-time and definitive modes. The principal difference between the two types of processing is in the handling of output arrays. In the real-time mode, output arrays are passed to the Attitude Determination Subsystem when they are full. In the definitive mode,

full output arrays are written on a data set. Thus, in the real-time mode, several calls to the telemetry processor may be required to process a complete pass of data, whereas in the definitive mode only one call is required.

The basic flow through the telemetry processor is to read a user-specified number of raw data records into a working array, unpack the data from the working arrays and store it in arrays of sensor readings in engineering units, then convert the data in the sensor arrays to cone angles and store these in output arrays. This cycle continues until an output array is filled; processing then proceeds as explained above, depending on whether the system data is in the real-time or the definitive mode.

The telemetry processor subsystem is controlled by an executive which calls individual modules to perform specific functions. The executive also controls looping within the processor. Backward moves to the telemetry processor for reprocessing, either from another subsystem or from within the telemetry processor, always return to the executive. Therefore, reprocessing starts at the beginning of an interval rather than in the middle of a partially processed interval. Reprocessing may start with raw telemetry or with sensor data in engineering units if a sensor data set has been written.

Optional processing available in the telemetry processor includes quality byte checking, time checking, range checking, magnetometer bias determination, addition of constant biases to sensor readings, sifting of high-volume data, and display of data at various steps in the processing.

The telemetry processor can run in either the interactive or the noninteractive mode (MSAD directory array mode). In the interactive mode, operator intervention is required only at the initial control parameter display to minimize attention handling in real-time processing. However, numerous optional displays are available for analysis. These include plots and tables of all intermediate sensor arrays and all output arrays. The intermediate sensor array

displays include displays of all data points for a short period of time or selected data points for a longer period of time. There are also additional control parameter displays which allow operator control over the optional processing features.

In summary, the telemetry processor performs the required functions of reading raw telemetry, converting telemetry counts to engineering units, and converting these readings to cone and dihedral angles. Optionally, it performs various quality checks, displays data, and allows data to be changed or reprocessed.

3.1.3 Attitude Determination Subsystem

The Attitude Determination Subsystem (ADS) has two major functions. In the real-time operational mode, it computes the attitude of the spacecraft's angular momentum vector and writes this information into the active file together with the averaged spin rates of the wheel and the body. This data set is used for control purposes.

In the definitive mode, it computes certain attitude parameters on a uniform time-step basis and writes these parameters in a file for the experimenters. Using the data in this file, a three-axis attitude can be computed for any time T during the time span of the solution.

The two operational modes are interchangeable on the same batch of data, giving either type of output. The mode cannot be changed, however, once the operation has started.

The ADS consists of three modules: the filtering module (FILTER), the angular momentum module (ANGMOM), and the azimuth module (AZIM).

3.1.3.1 Filter Module

The main functions of the filtering module are to reduce data volume, smooth data to remove random noise, and determine and remove the effects of certain types of dynamic motion from the data (precession, coning).

The filtering module processes the cone angle arrays passed from the telemetry processor. There are three types of these cone angle arrays: wheel horizon scanner arrays, Sun sensor arrays, and magnetometer arrays.

In attitude computation, any combination of these sensor data can be used, and any data type can be skipped or downweighted at the user's option. Another option is the sampling time interval for the filter output.

These data arrays are processed by a recursive least-squares filter, which passes the parameters on to the next modules at equal time intervals. The processing of the data takes place point by point. The filter has a fading memory, allowing any slow changes in the attitude parameters to be followed. The model function to describe the sensor cone angles has three parts: one term to describe the cone angle between the angular momentum of the spacecraft and the reference vector, a sinusoidal term to describe the motion of the Z-axis around the angular momentum vector (precession), and a second sinusoidal term for motions that show a periodic feature around the Z-axis with the body period (coning). This model function has seven parameters to fit the data. The initialization of the filter is done by an application of the Fast Fourier Transform.

The filter module also has simpler operational modes. It can be used for N point data averaging (running average mode) or data sifting if required. The recursive filtering mode is used mainly for precession determination in the definitive mode.

The filter module also computes a dihedral angle array at the sampling times to permit resolution of attitude ambiguities in the angular momentum module. For each type of cone angle array there is a corresponding dihedral angle array. These angles are computed with respect to a fixed axis on the body so that the dihedral angle between two sensor events will be simply the difference of these dihedral angles. There is no adjustment for precession on these angles because the only purpose is to resolve ambiguity. The smoothed cone angle arrays and the raw dihedral angles are the data base of the angular momentum module.

3.1.3.2 Angular Momentum Determination Module

The capabilities of the angular momentum module are to determine the attitude of the angular momentum vector of the spacecraft; give one-point attitude in the real-time mode, which represents an average attitude for the pass or the up-to-date attitude after a perigee pass; provide an attitude history for the whole pass in the definitive mode; compute an initial attitude value--based on cone and dihedral angles--to initialize the least-squares scheme (quick-look mode); batch or recursively process sensor data; and to compute third-axis attitude in the definitive mode.

In the definitive mode, the preprocessed (filtered) data is written out in an auxiliary file if current definitive ephemeris data is not available. In the real-time mode, the filtered data array is processed immediately using the most recent ephemeris data. In the first step, the cone and dihedral angle data are used for an initial attitude determination; this is called the quick-look attitude determination mode. This can be done point by point or in batch mode. The output attitude is used to initialize either a batch (DCCONS) or recursive (GRECRS) least-squares differential correction subroutine to compute a refined attitude based entirely on the cone angle data. After the one-point attitude has been determined and written in the archive file together with average wheel and body rates, the operation of the real-time mode ends.

In the definitive mode, as soon as ephemeris information is available, the filtered cone angle data goes through the angular momentum module to obtain angular momentum history. This procedure is identical with the one used in the real-time mode except that the attitude is computed at equal time steps and stored for further processing.

The next step is the determination of the spacecraft Z-axis. The computation is based on the wheel horizon sensor data, with the Sun sensor data as an alternative. The subsystem is flexible enough, however, to use any available data type for Z-axis computation.

Even if both the coning and the precession components are present and separated from the data in the filter module, only the one having the larger contributing bias is considered for Z-axis computation. The Z-axis information is computed at equal time intervals, with about one point each body spin period.

3.1.3.3 Body X-Axis Determination Module

In the definitive mode for three-axis attitude determination, the azimuth angle is also needed. This computation takes place in the azimuth module. The module's capabilities are to compute azimuth angles and rates at equal time intervals, and provide attitude parameters for experimenters, with up to quadratic interpolation terms.

The primary source of data is the body horizon sensor readings in the spinning mode and the split-to-index pulses in the despun mode. In the despun mode, the pulses are converted directly to phase angles in the telemetry processor, and these angles are smoothed in the filter module.

The Sun event times are used for calibration and the magnetometer data for backup. The attitude parameters are written out at equal time intervals, and a quadratic interpolation can be applied to compute three-axis attitude on a continuous basis.

3.2 MSAP SYSTEM OVERVIEW

The AE version of MSAP is designed to generate the attitude control commands necessary to maintain spacecraft attitude within specified constraints. It is executed in the interactive graphics mode, with program flow under optional operator control. Computed spacecraft commands are both printed and written on a nonvolatile disk-file archive dedicated to AE for ease in subsequent handling.

The MSAP/AE system has been designed to provide a flexible attitude prediction and optimal control system that may be expanded to support additional satellites. The system's essential features are described in the following subsections.

There are two archives used by MSAP/AE: Command History and Attitude History.

The determined attitudes (along with appropriate times) are in the Attitude History archive and are entered by the Attitude Determination Subsystem, providing the link between the attitude determination and control functions.

The Command History archive contains sequential entries of two types:

1. spacecraft commands affecting attitude control
2. determined values of changing parameters (x, y, z CP-CM offsets) essential to computing required commands

These two archives are read by setting two FORTRAN NAMELIST parameters enabling the operator to streamline initialization for parameter estimation.

Spacecraft attitude control commands (and their times) are determined by MSAP/AE and written into the archive for use in command displays and in subsequent simulations with overlapping time periods. Canceled commands are not deleted from the archive; their canceled status is indicated by entry of a flag which allows reinitialization of their initial types and times for control center use.

Estimated values of the center-of-mass location, moment of inertia, and expected changes of these are included in the archive.

The archive is allowed to accumulate entries until near full. A utility program periodically erases old entries.

3.2.1 Input Subsystem

All input to the system is accomplished using the FORTRAN NAMELIST feature. In addition to the FORTRAN NAMELIST, the history data and the observed attitude data will be inputted as formatted tables which can be filled from the Command History and/or Attitude History archives.

3.2.2 Attitude Prediction Subsystem

The attitude prediction subsystem simulates changes in spin-axis attitudes and spin rates. The simulation algorithms are based on the assumption that nutation is of negligible magnitude, and that collinearity is therefore maintained between the spin-axis direction and the spacecraft angular momentum vector. Attitude-dependent disturbance torques are computed in the simulation and numerically integrated to predict changes in the spacecraft angular momentum magnitude and direction.

All disturbance torque calculations are made at user option. Included are gravity gradient, aerodynamic, magnetic, direct solar radiation pressure, and thruster torques.

The predictor also monitors day/night conditions to determine whether or not there is solar radiation pressure to be computed and to determine the magnetic moment strength during low voltage conditions.

It also simulates momentum transfers between the main body and wheel, as it is controlled by the onboard pitch feedback-control system.

3.2.3 Attitude Control Subsystem

This subsystem automatically computes the optimum commands subject to operator-specified constraints to precisely implement control functions. The types of commands automatically computed by this subsystem are as follows:

- time-optimal or energy-optimal spin-axis coil commands to bring the spin axis to a specified attitude
- momentum coil commands to bring the angular momentum magnitude to a specified value
- yaw thruster commands to bring the spin axis to a positive or negative orbit normal

- auto-roll commands to maintain the attitude near the orbit normal
- tachometer commands to achieve the desired body spin rate

3.2.4 Output Subsystem

The output subsystem writes the set of computed commands onto the AE Command History archive, produces printed output, and optionally writes an attitude history tape.

3.2.5 Parameter Estimation Subsystem

The parameter estimation subsystem is designed to provide a means of estimating nonmeasurable parameters necessary for torque computation, such as the value of the CP-CM offset, or the value of a residual magnetic dipole moment, etc. Such values are necessary to generate valid attitude predictions using the attitude prediction subsystem and are consequently necessary to plan a command sequence correctly.

This subsystem, KOPTIM, uses an operator-selected sequence of attitude determinations and spacecraft commands from the MSAP archives, then iteratively determines the values of a set of operator-specified MSAP parameters which minimize the weighted squared error between a set of observations and predictions at corresponding times. KOPTIM performs the following functions:

1. KOPTIM inputs information from MSAP that specifies which parameters are to be optimized. Then it converts these parameters into the state vector from subroutine KOPTM1, which is a pure function optimization program.

2. KPTIM calls subroutine KOPTM1, which generates a new set of state vectors according to the least-squares method.

3. KOPTIM converts the new set of state vectors to the parameter values of MSAP.

4. If the program satisfies the convergence criterion or exceeds an iteration limit, KOPTIM sends a signal to MSAP to terminate the computation.

The optimization technique used by KOPTM1 is a first-order adaptive method to find a local minimum of the nonlinear objective function. The original method was developed by Gauss and Newton and is obtained from a Taylor series expansion of the model through the linear terms. Using the idea of Levenberg to control convergence, Marquardt and Kotsakis have introduced modifications to the basic method to achieve a nearly optimum convergence performance.

The advantages of KOPTM1 are as follows:

1. The objective function decreases monotonically from iteration to iteration. This implies that the set of parameters computed last is a better set over the previous iterations. This is an advantage if the computation has to be terminated prior to the ultimate convergence.

2. An optimum interpolation between the gradient and Gauss-Newton method is chosen adaptively by the algorithm whereby a proper direction and magnitude for the correct vector is automatically computed to yield rapid convergence. (Mathematically this is controlled by the value of λ_i in Equation (3-3).)

A brief summary of the KOPTM1 algorithm is as follows:

Let the prediction vector to be fitted to a set of data points (t_j , Z_j), $j = 1, 2, \ldots, n$ be

$$\underline{Y} = f(t , X_1 , X_2 , \ldots , X_{np}) \equiv \underline{f}(t , \underline{X}) \qquad (3\text{-}1)$$

where χ is a parameter vector to be estimated. Also, let the weighted least-squared function be

$$Q(\underline{\chi}) = [\underline{Z} - \underline{Y}]^T W [\underline{Z} - \underline{Y}] \tag{3-2}$$

The KOPTM1 algorithm to minimize this objective function $Q(\chi)$ is the recursion

$$\begin{aligned} \underline{\chi}_i &= \underline{\chi}_0 \\ \delta\underline{\chi}_i &= \left[J_i^T W J_i + \lambda_i I\right]^{-1} J_i^T W [\underline{Z} - \underline{f}(t, \underline{\chi}_i)] \\ \underline{\chi}_{i+1} &= \underline{\chi}_i + \delta\underline{\chi}_i \qquad\qquad i = 1, 2, \ldots, np \end{aligned} \tag{3-3}$$

where J_i is the $n \times np$ Jacobian matrix of the first partial derivative of $\underline{f}(t, \underline{\chi})$ evaluated at $\underline{\chi}_i$ and λ_i is a scalar, $\lambda_i \geq 0$.

It is shown that any value of λ_i such that

$$Q\left(\underline{\chi}_i + \delta\underline{\chi}(\lambda_i)\right) < Q(\underline{\chi}_i) \tag{3-4}$$

will ensure convergence and the choice of λ_i will affect the rate of convergence. Various strategies have been proposed to determine an "optimum" value of λ dynamically at each iteration.

KPTM1 uses the scheme modified by Marquardt and Kotsakis[2] to control the convergence of Equation (3-3).

---

[2] Computer Sciences Corporation, 9101-12300-02TM, Data Management in Atmosphere Explorer Support Software, G. Kotsakis, January 1973.

The convergence criteria used in KOPTM1 are as follows:

$$\left| \chi_i^{(K)} - \chi_i^{(K-1)} \right| < \rho \qquad \text{for } i = 1, 2$$

$$\left| \frac{\chi_i^{(K)} - \chi_i^{(K-1)}}{\chi_i^{(K-1)}} \right| < \rho' \qquad \text{for } i = 3, 4, \ldots, np \tag{3-5}$$

where K = iteration index

χ_1 , χ_2 = initial values of right ascension and declination (radians)

ρ , ρ' = the order of accuracies desired for convergence

The maximum number of KOPTM1 iterations depends on the accuracy desired for the convergence. However, five iterations should be sufficient for most cases. One KOPTM1 iteration requires (np + 2) function evaluations (MSAP predictions), where np is the number of parameters being optimized.

SECTION 4 - OPERATIONS PLAN

This section presents nominal procedures and schedules for several operations:

- launch sequence
- perigee lowering
- apogee restoration
- normal operations
- low perigee operations
- magnetic inversion
- yaw thruster firing
- system momentum determination

4.1 LEAD TIME GROUND RULES

The following ground rules have been established for the lead time required for commands being sent through AEOCC:

- In general, a 6-hour lead time is required
- A 10- to 12-hour lead time is required before each OAPS burn
- Only a 1.5-hour lead time is required for apogee restorations when performed sequentially (on every second or third perigee)

On the schedules presented on the following pages, station coverage is indicated by orbit number, which is incremented each time the spacecraft goes through the ascending node. The letter P indicates perigee passes and A indicates apogee passes. The orbit number is indicated by the numbers following the P and the A. These numbers are representative.

NOMINAL LAUNCH SEQUENCE

SPACECRAFT EVENTS	STATION COVERAGE	ATTITUDE OPERATIONS
LAUNCH, INJECTION, YAW TO NEGATIVE ORBIT NORMAL SPINUP TO 10 RPM SEPARATION		
(SANTIAGO PASS)	P0	ATTITUDE DETERMINATION (AD) USING DSAI-BHS-MAGS; CHECK SPIN RATE USING MAGS
PRELIMINARY ELEMENTS		
(TANANARIVE PASS)	A0	AD; DETERMINE NUTATION AMPLITUDE
UPDATED ELEMENTS		REPROCESS WITH UPDATED ELEMENTS; ATTITUDE PREDICTION (AP) FOR QOMAC AND MASC COMMANDS TO BE LOADED ON A2
	A1	AD; CHECK NUTATION DAMPING; DETERMINE MOMENTUM MAGNITUDE
ORBIT TAPE		
SPINUP MWA IN TACH LOOP; LOAD QOMAC AND MASC COMMANDS		
	A2	AD USING WHS-DSAI-MAGS; DETERMINE MOMENTS OF INERTIA
PRECESS TO ORBIT NORMAL		
	A3	AD; EVALUATE DRIFT RATES AND OA BIASES
		AP FOR QOMAC AND AUTOROLL FOR LOADING ON A5
CLOSE PITCH LOOP	A4	AD; CHECK 4-RPM MODE
LOAD QOMAC AND AUTOROLL COMMANDS	A5	AD; CHECK AUTOROLL PROGRAMMER
COMMAND MEMORY LOAD AND DUMP	A6	AD; READOUT FOR ATTITUDE CONTROL
	A7	AD
		AP; QOMAC TO PRECESS TO ORBIT NORMAL BEFORE AND AFTER OAPS BURN FOR LOADING ON A11
	A8	AD
	A9	AD
COMMAND DESPIN	A10	AD; CHECK DESPIN MODE AND PITCH OFFSET MOMENTS-OF-INERTIA DETERMINATION
LOAD QOMAC COMMANDS	A11	AD; END DRIFT ANALYSIS
PRECESS TO ORBIT NORMAL		
OAPS CALIBRATION BURN	A12	AD; NOMINAL ELEMENTS AND UPDATED ELEMENTS
PRECESS TO ORBIT NORMAL		
	A13	AD
ORBIT TAPE		AP; QOMAC FOR LOADING ON A16
	A14	

NOMINAL PERIGEE LOWERING

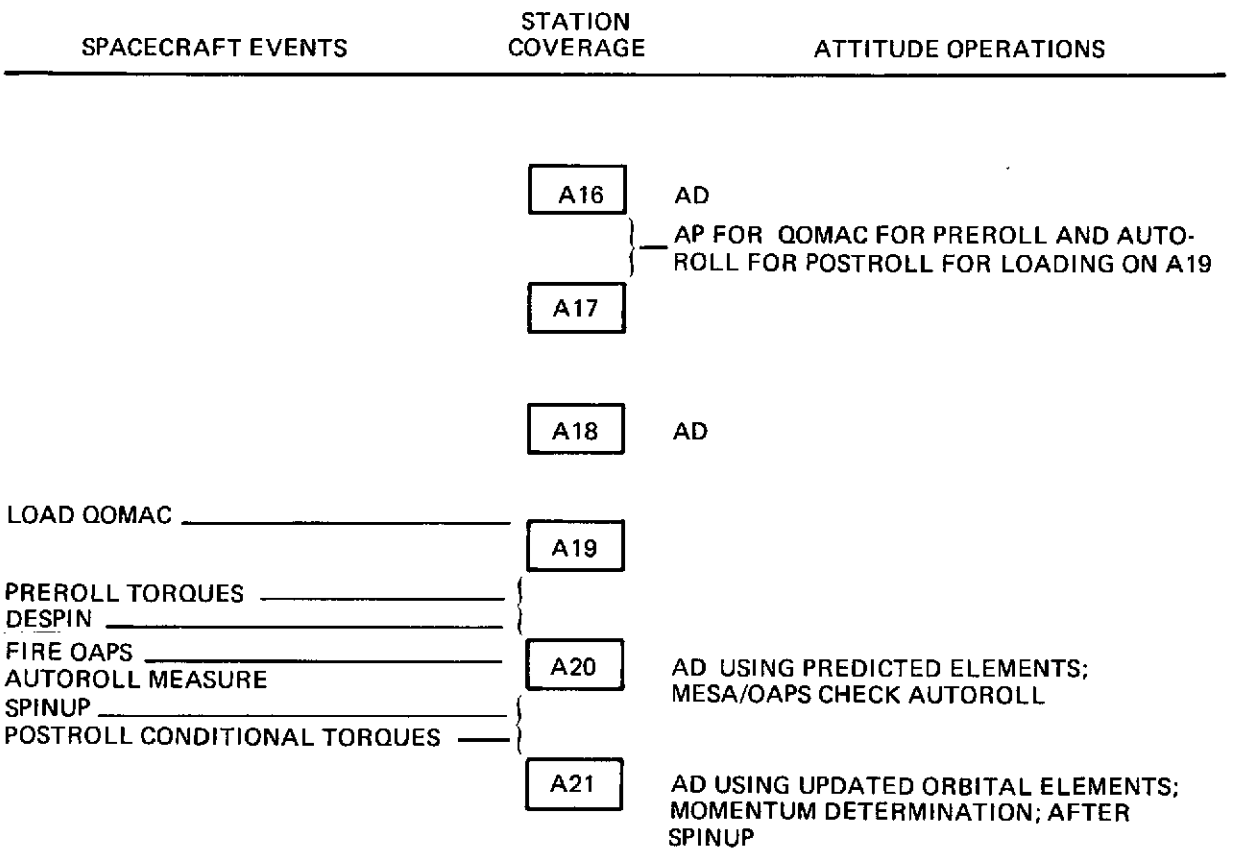

NOMINAL APOGEE RESTORATION OPERATIONS (SEQUENTIAL)

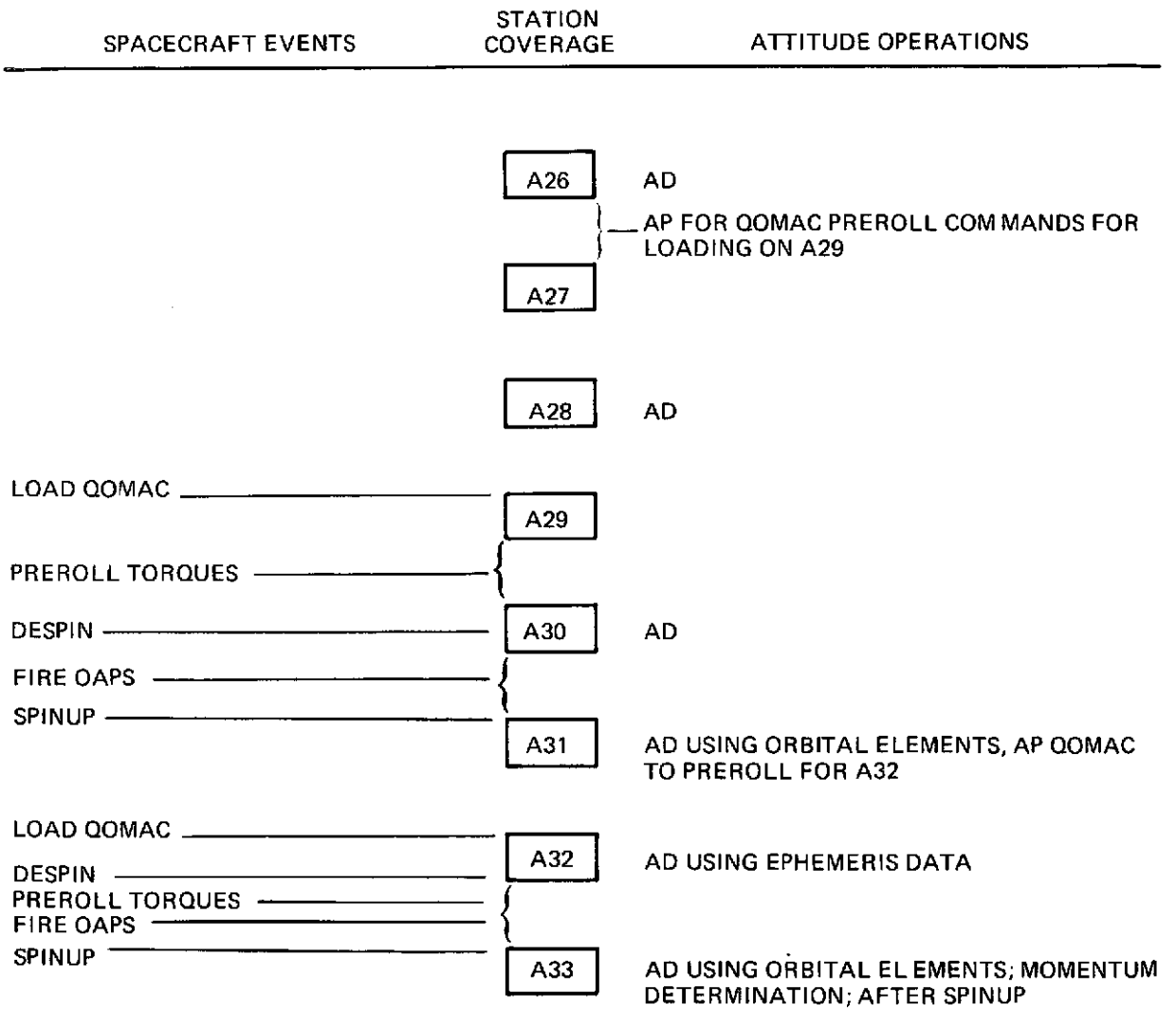

NORMAL OPERATIONS

SPACECRAFT EVENTS	STATION COVERAGE	ATTITUDE OPERATIONS
	A41	AD
		AP FOR QOMAC AND MASC COMMANDS FOR 24 HOURS FOR LOADING ON A44
	A42	
	A43	
LOAD COIL COMMANDS	A44	AD
COIL TORQUES TO		
	P45	
OVERSHOOT ORBIT NORMAL		
	A45	
	A46	AD
	A47	
	A48	
	A49	AD
COIL TORQUES IF REQUIRED FOR PERIGEE BELOW 140 KM		
	A50	
	A51	
RECEIVE NEW EPHEMERIS		

NOMINAL LOW PERIGEE OPERATIONS

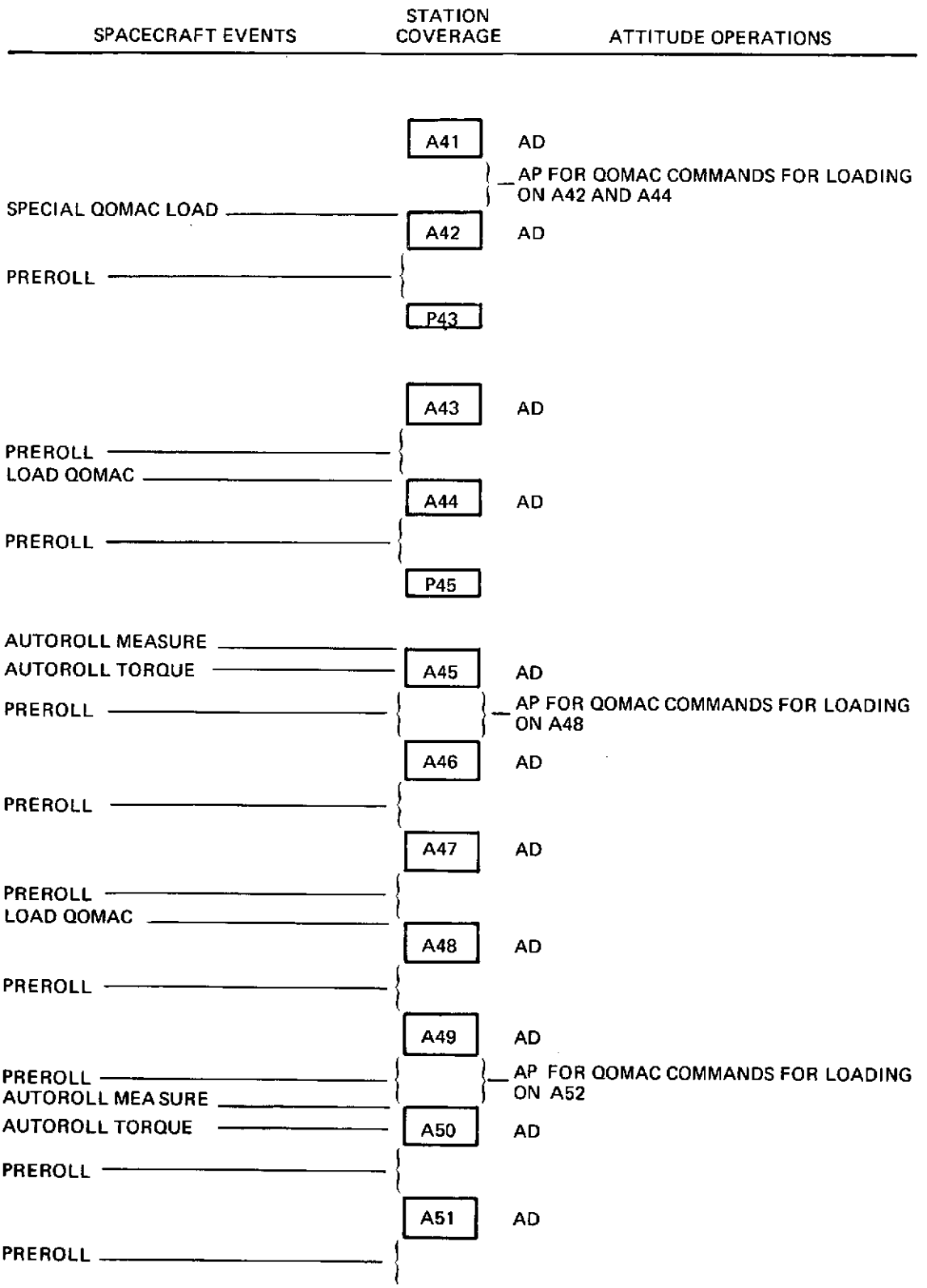

NOMINAL MAGNETIC INVERSION OPERATIONS

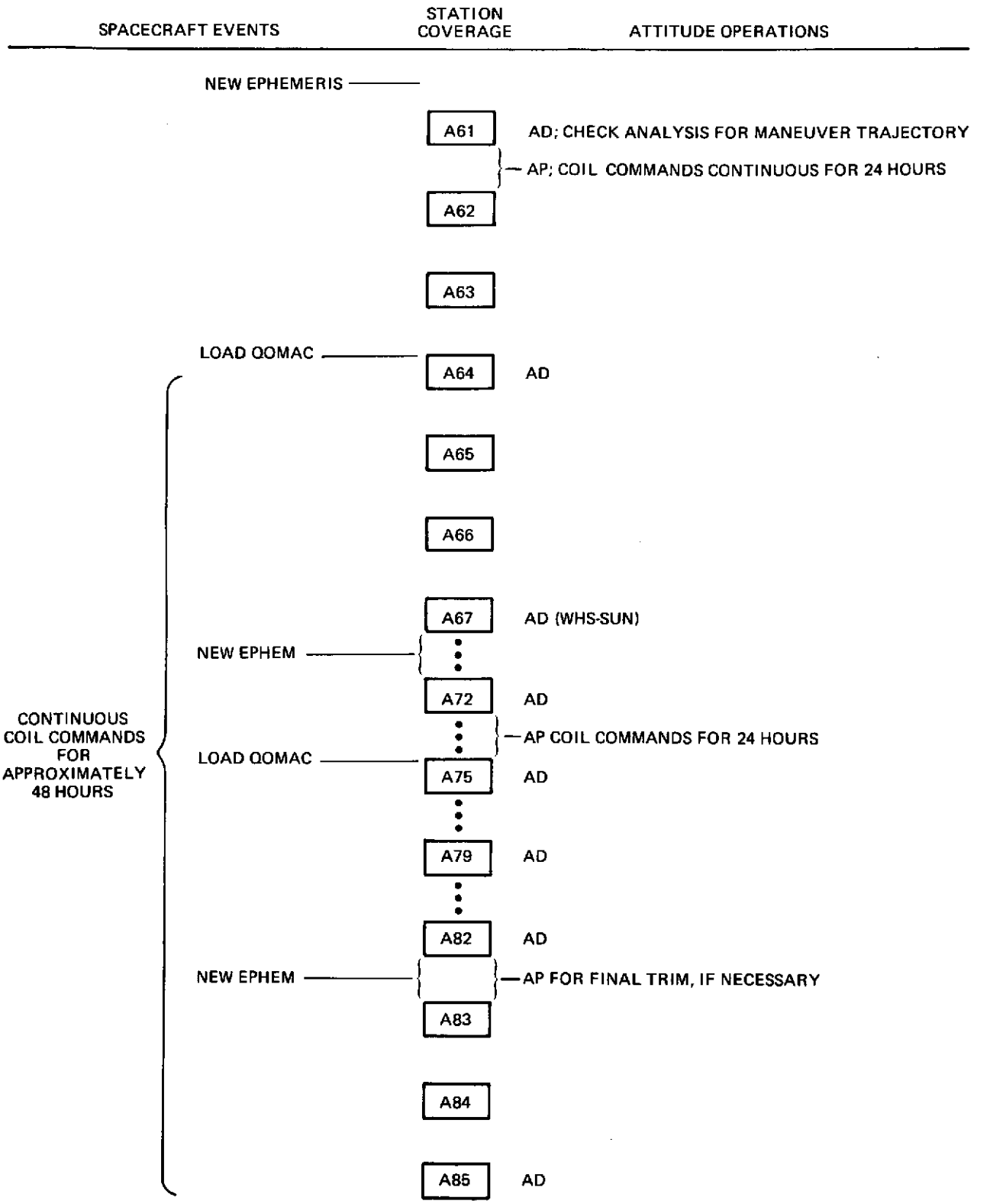

NOMINAL YAW THRUSTER FIRING

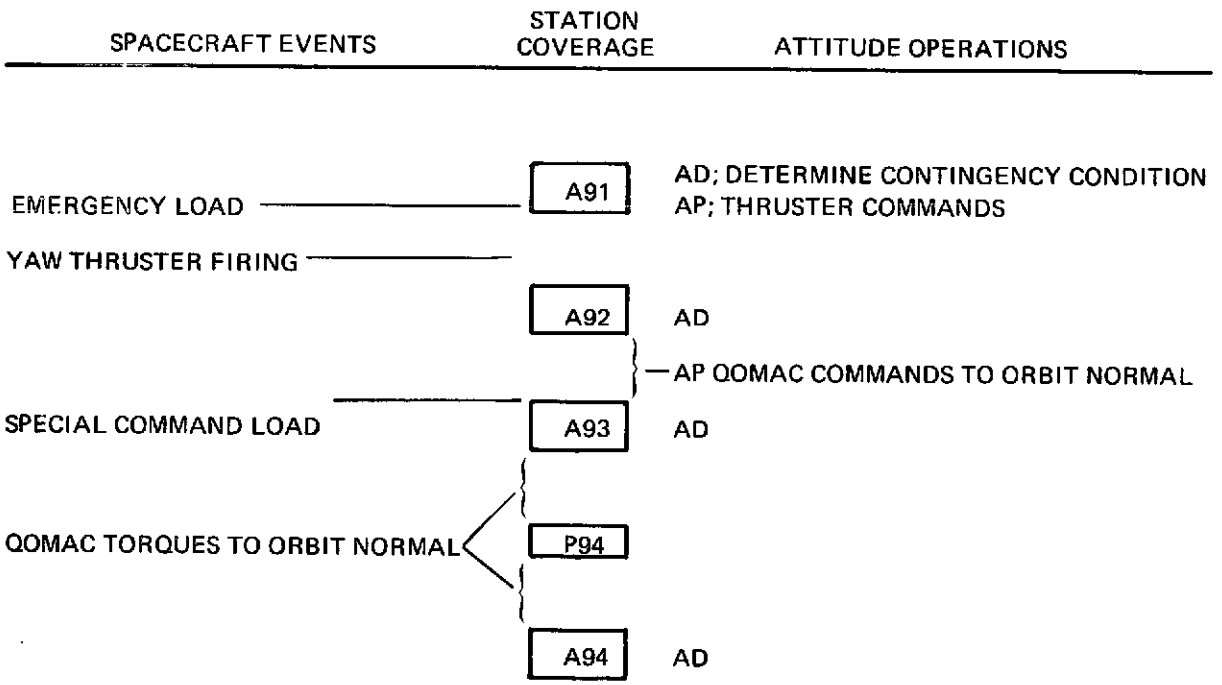

MOMENTS-OF-INERTIA DETERMINATION (AFTER PERIGEE LOWERING)

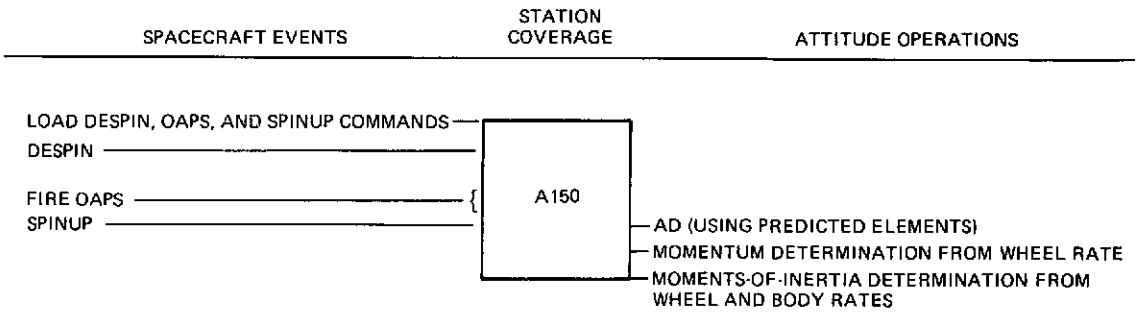

4.2 DETERMINING SYSTEM MOMENTUM

4.2.1 Initial Determination

Current launch plans call for the PCE to be off for the first couple of orbits. The wheel is expected to spin up to the body rate of about 10 rpm:

$$\vec{H} = I\,\vec{\omega}$$

After nutation has damped down, most of the momentum will be about the z-axis:

$$H_{TOT} \cong H_3 = I_{33}\,\omega_3$$

where I_{33} is well known and includes the flywheel, and ω_3 can be determined from Sun times (inertial), BHS leading edge times (Earth referenced), or magnetometer azimuth angles (B-field referenced).

If there is a 1-percent error in I_{33}, however, there will be a 1-percent error in H_{TOT}. When a subsequent despin is performed, this error will limit the accuracy of measurement of the wheel moment of inertia.

4.2.2 Subsequent Determinations

After a firing, the body moments of inertia will change and an accurate determination of system momentum will require more than just wheel and body rates. The recommended procedure is as follows:

- Despin the spacecraft
- Determine the wheel spin rate
- Calculate the total momentum
- Command body to a high spin rate (4 to 6 rpm)
- Calculate body (I_{33}) moment of inertia from total momentum

SECTION 5 - DYNAMICS MODELING AND DATA CHARACTERISTICS

5.1 INVESTIGATION OF BODY DYNAMICS

For a better understanding of the complicated dynamics expected on AE, the Continuous System Modeling Program (CSMP) was used to simulate the spacecraft's motion. This package, which is available on the S/360-95, is especially useful because of the ease of development, modification, and output. The features listed below have been implemented.

AE-C is modeled as a rigid body with

- Momentum wheel, which can be offset from the Z-axis
- PCE tachometer loop at a commanded rate, including electronic gains and delays
- Fluid loop nutation damper, modeled as 10 concentric flow rings
- External torques (only aerodynamic torques are computed at present)

Aerodynamic drag force is computed inertially and rotated into body coordinates for torque computation:

- Euler summetric parameters are integrated to provide the rotation matrix
- Parameters are renormalized to improve accuracy
- Drag force model has a constant inertial wind direction, an amplitude which is Gaussian in time, scaled according to the instantaneous area presented to the wind
- Spacecraft is modeled as a cylinder with a variable center of pressure (CP) offset according to CP = 0.25 inch $\pm$0.1 inch per degree yaw
- Accelerations are computed at each integration step

To improve computational speed, there are branches around the computations of aerodynamic torque and accelerometer output when not required.

Sample MSAD plots are shown of the body motion in Figures 5-1 through 5-4 before the aerodynamic torque is applied. Figure 5-1 shows the cone angle between the angular momentum vector and the Z-axis versus time, Figures 5-2, 5-3, and 5-4 show the Euler angles, θ , φ , ψ , versus time.

5.2 DATA CHARACTERISTICS

A telemetry simulator (TELSIM) was built to test the Telemetry Processor and Attitude Determination Subsystem. It has the capability of simulating either telemetry frames or cone angles derived from the data. It can simulate various types of noise and bias, including the quantization of the telemetered values, which has been extremely useful in anticipating the actual data characteristics.

Figures 5-5 through 5-9 are MSAD plots of typical expected data. Figure 5-5 is a plot of the raw magnetometer cone angles before fitting (notice horizontal predicted line) of data. Figure 5-6 is a plot of the raw magnetometer cone angles after being smoothed. In addition, this plot shows the large change in cone angle at apogee caused by a bucket change in the Z-magnetometer reading. Note that Figures 5-5 and 5-6 are for two different time periods. Figure 5-7 shows typical examples of a continuous batch of WHS data after being smoothed. Figure 5-8 is used to determine if the spacecraft is spinning in the proper direction. Figure 5-9 shows the single- versus the dual-scanner nadir angle solutions. It is possible to identify each scanner solution (plot) by operator intervention.

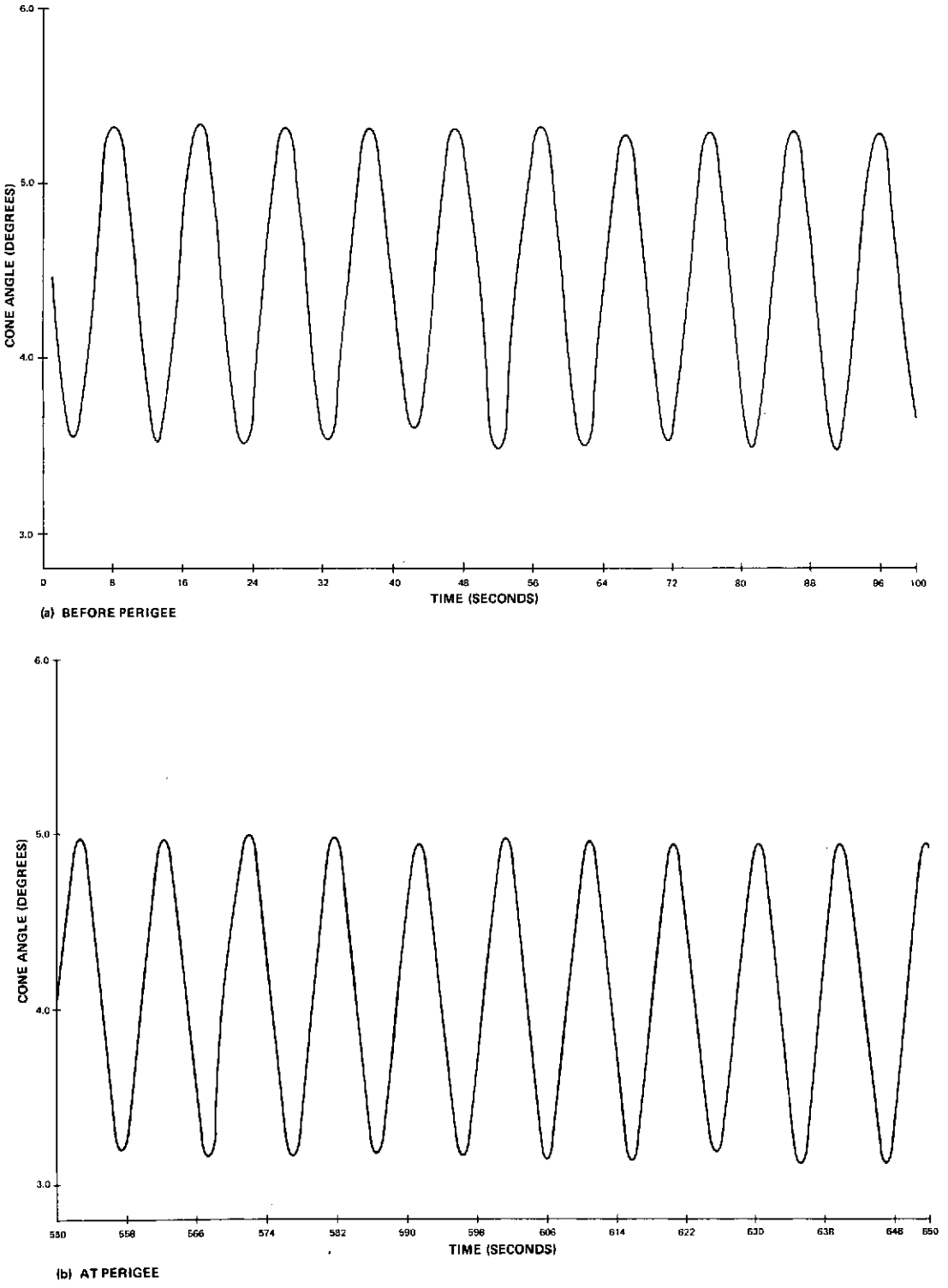

Figure 5-1. Cone Angle (Between Body Z-Axis and Angular Momentum Vector) Versus Time Before and at Perigee

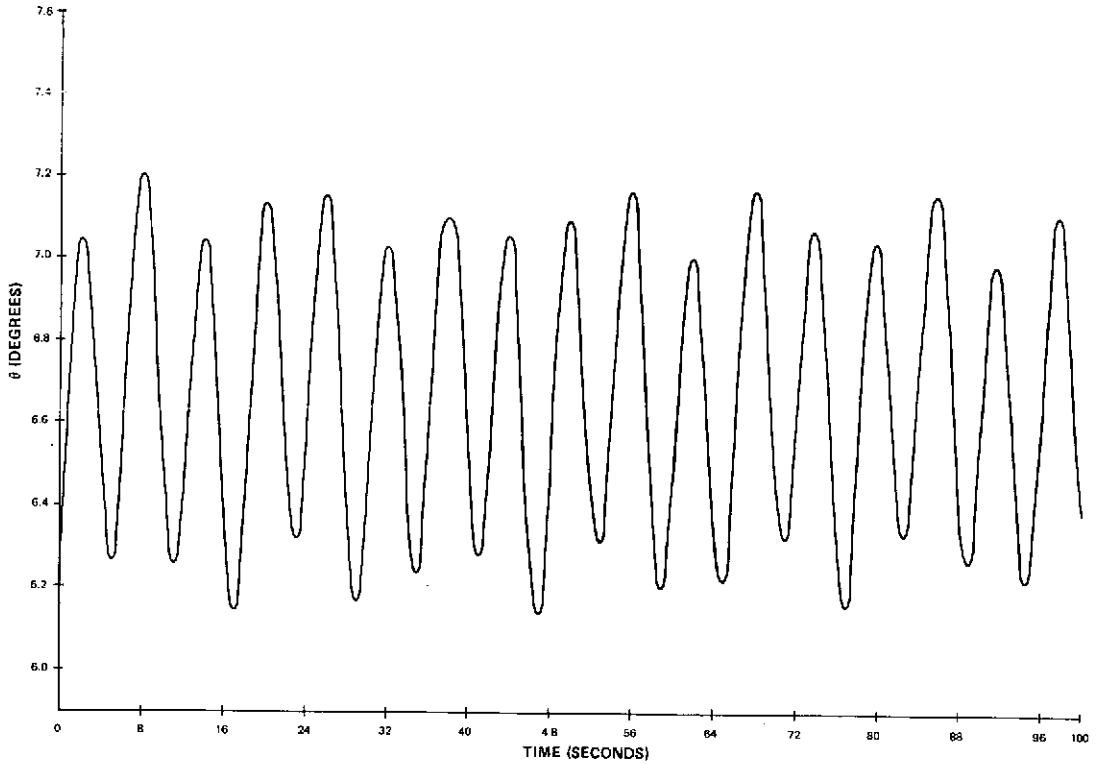

(a) BEFORE PERIGEE

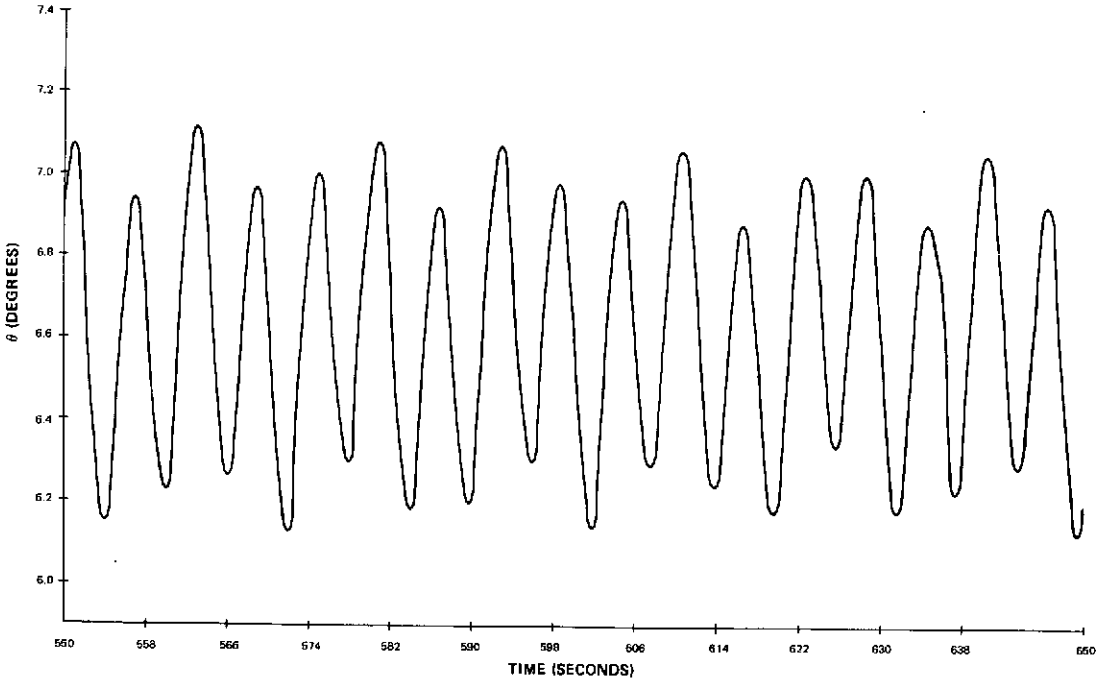

(b) AT PERIGEE

Figure 5-2. Theta Versus Time Before and at Perigee

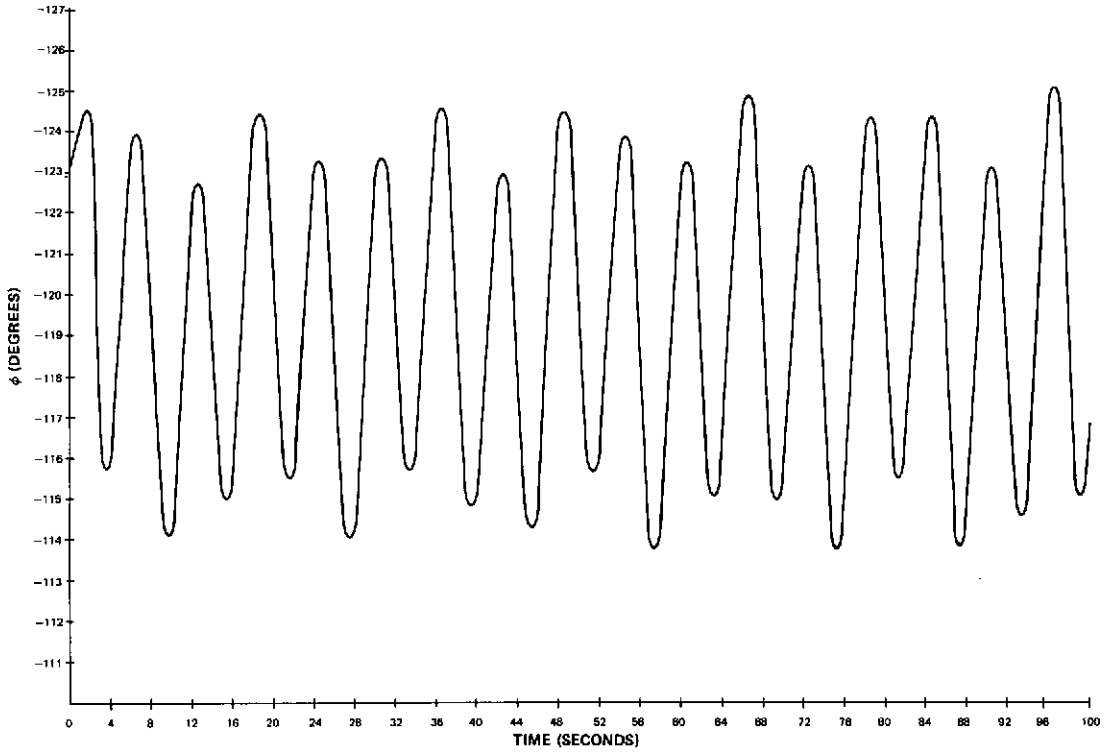

(a) BEFORE PERIGEE

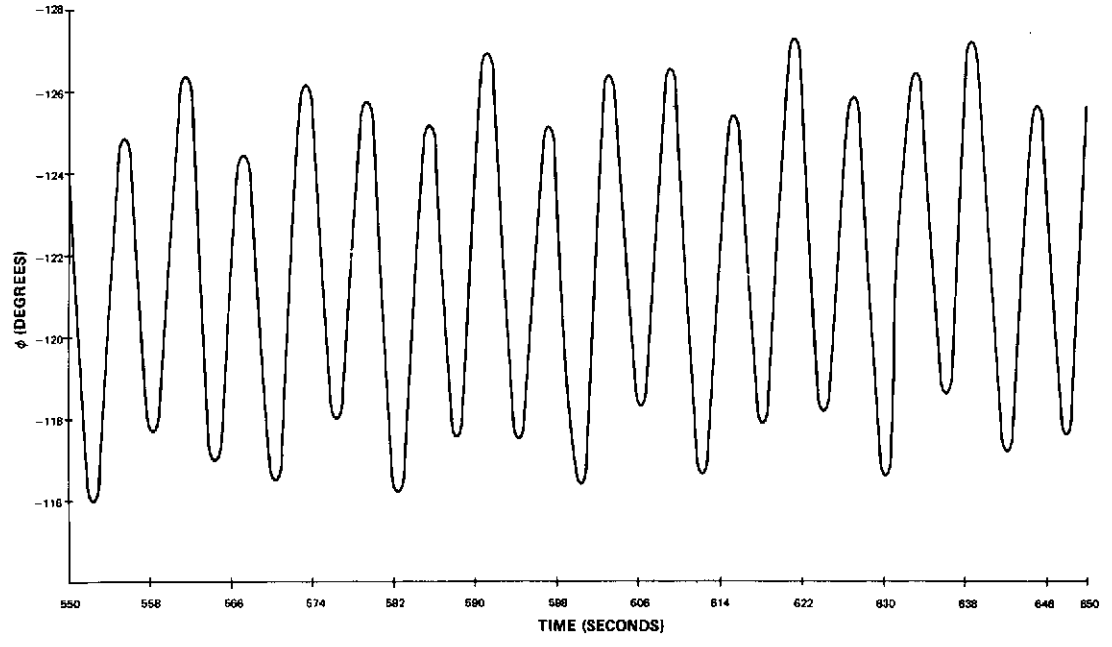

(b) AT PERIGEE

Figure 5-3. Phi Versus Time Before and at Perigee

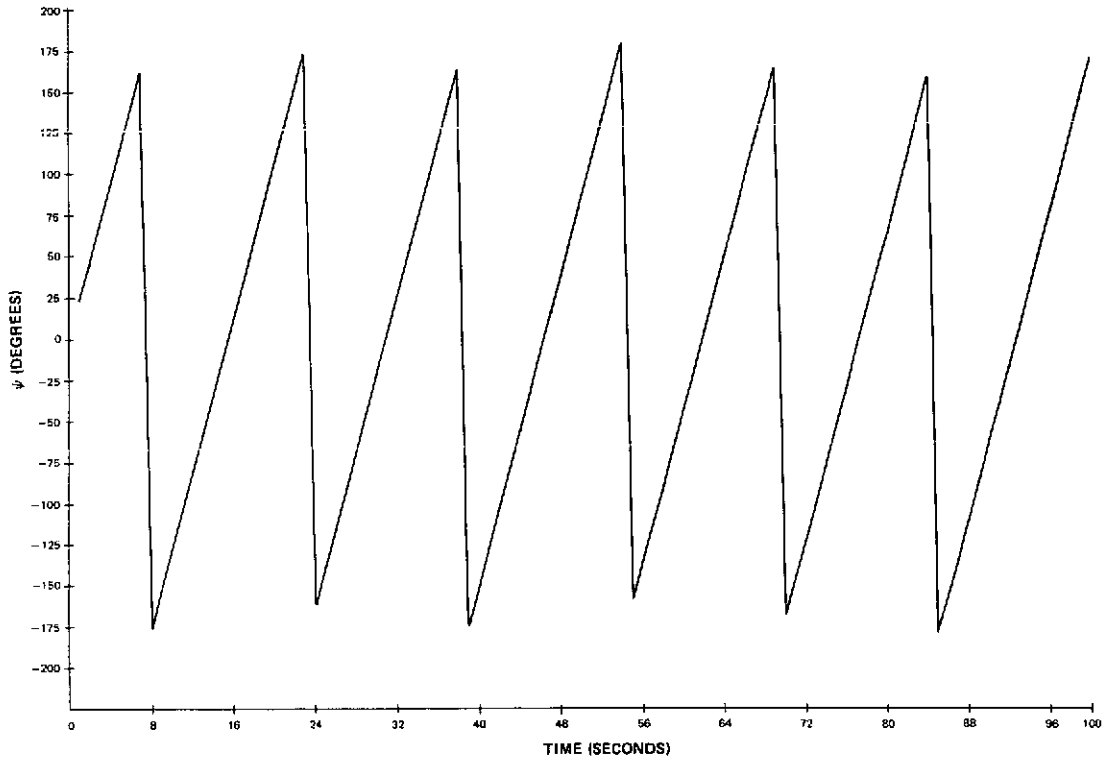

(a) BEFORE PERIGEE

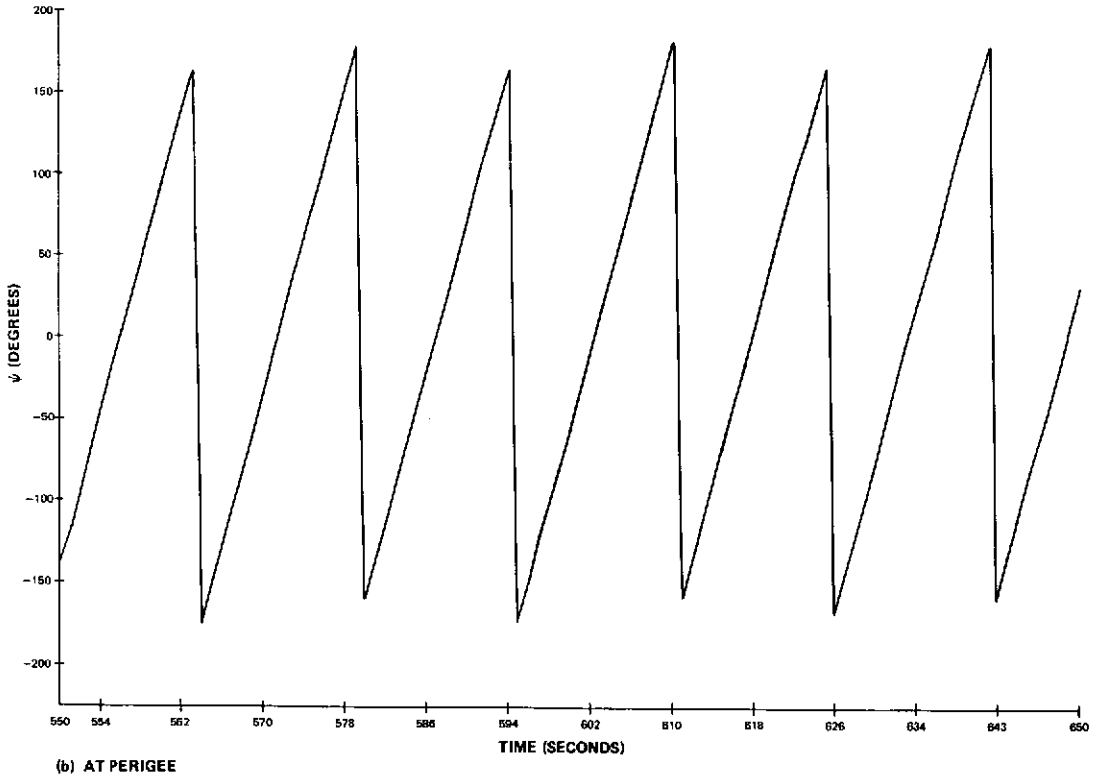

(b) AT PERIGEE

Figure 5-4. Psi Versus Time Before and at Perigee

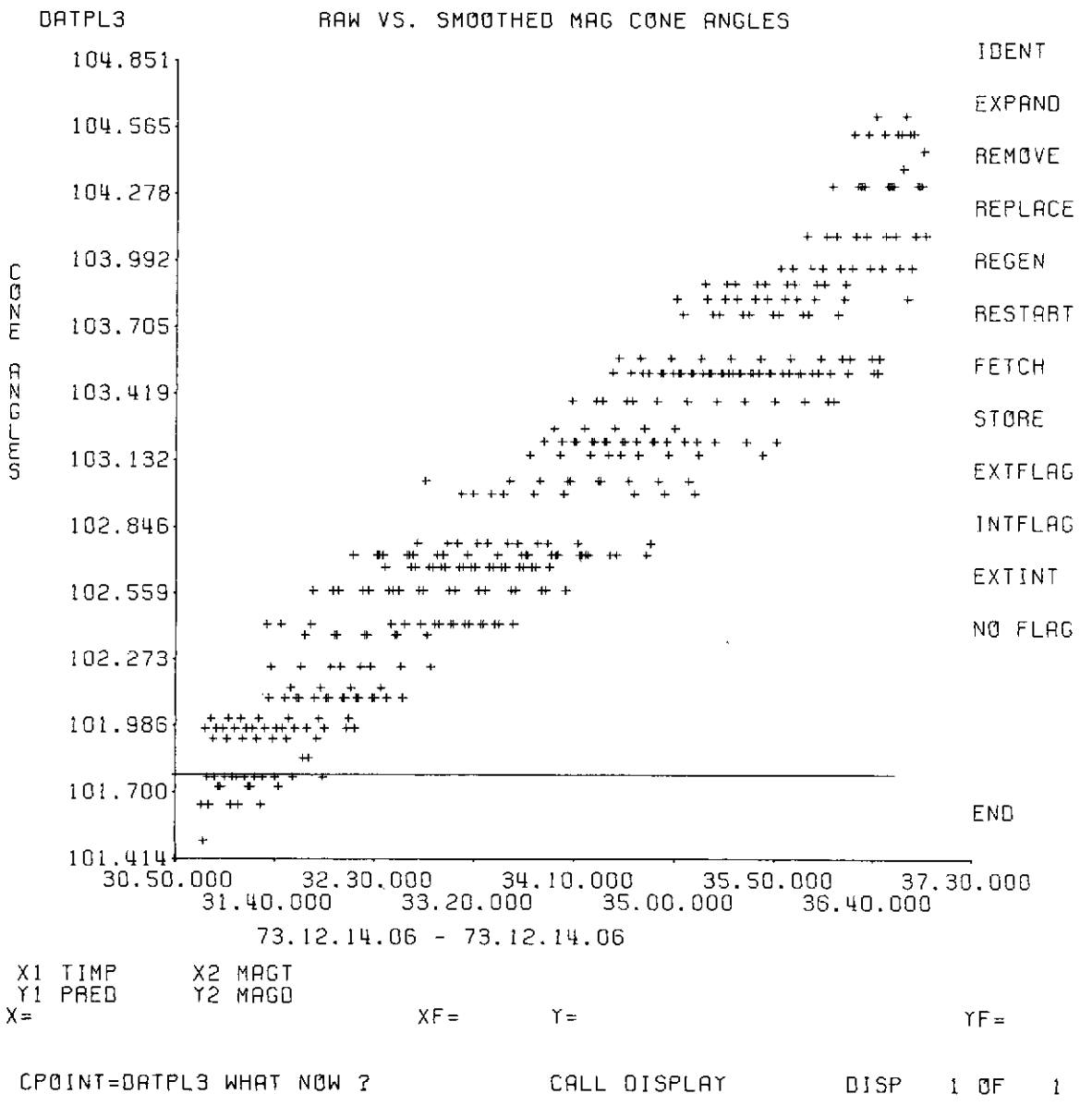

Figure 5-5. Raw Versus Smoothed Magnetic Cone Angles Before Smoothing

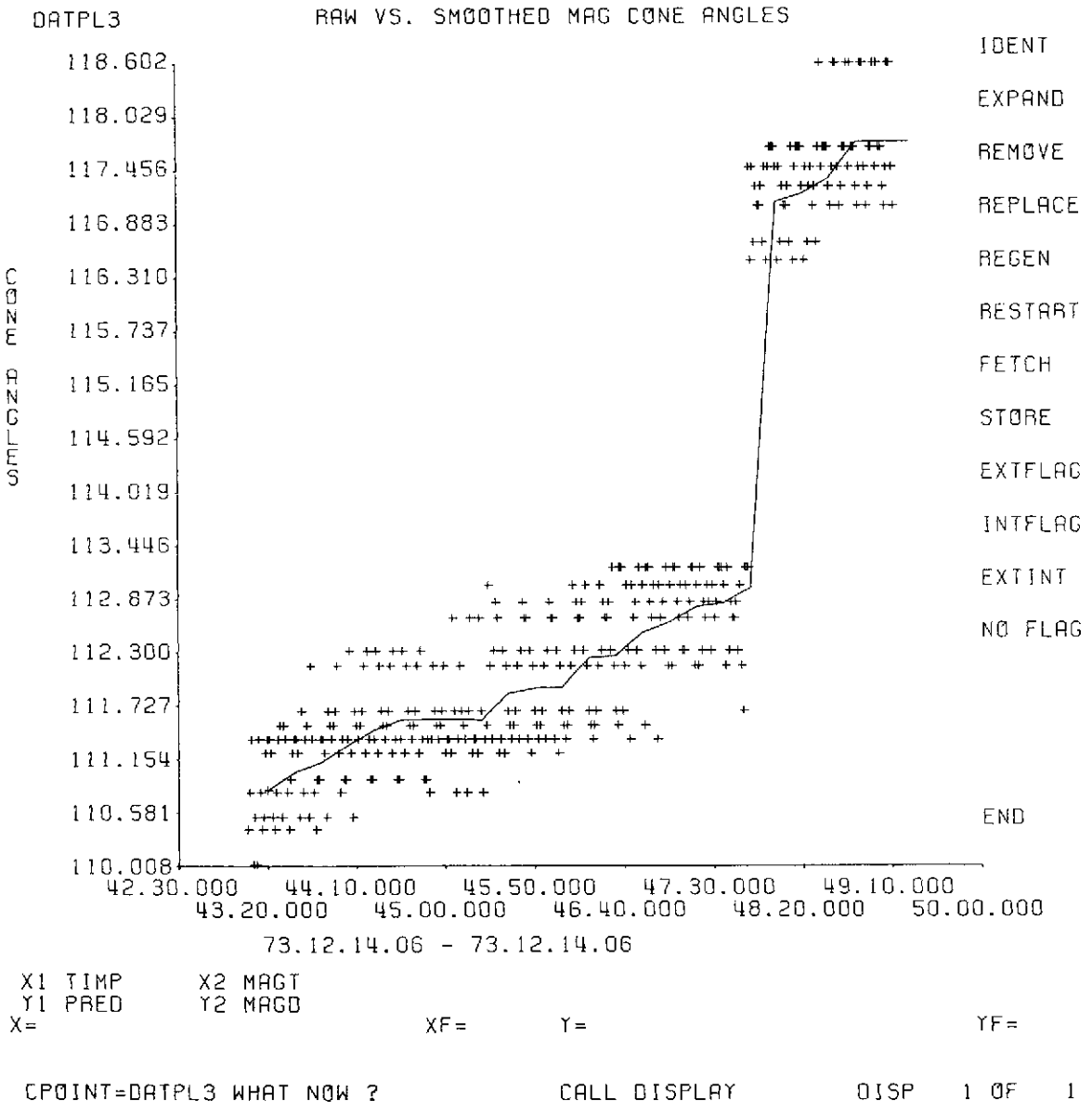

Figure 5-6. Raw Versus Smoothed Magnetic Cone Angles After Smoothing

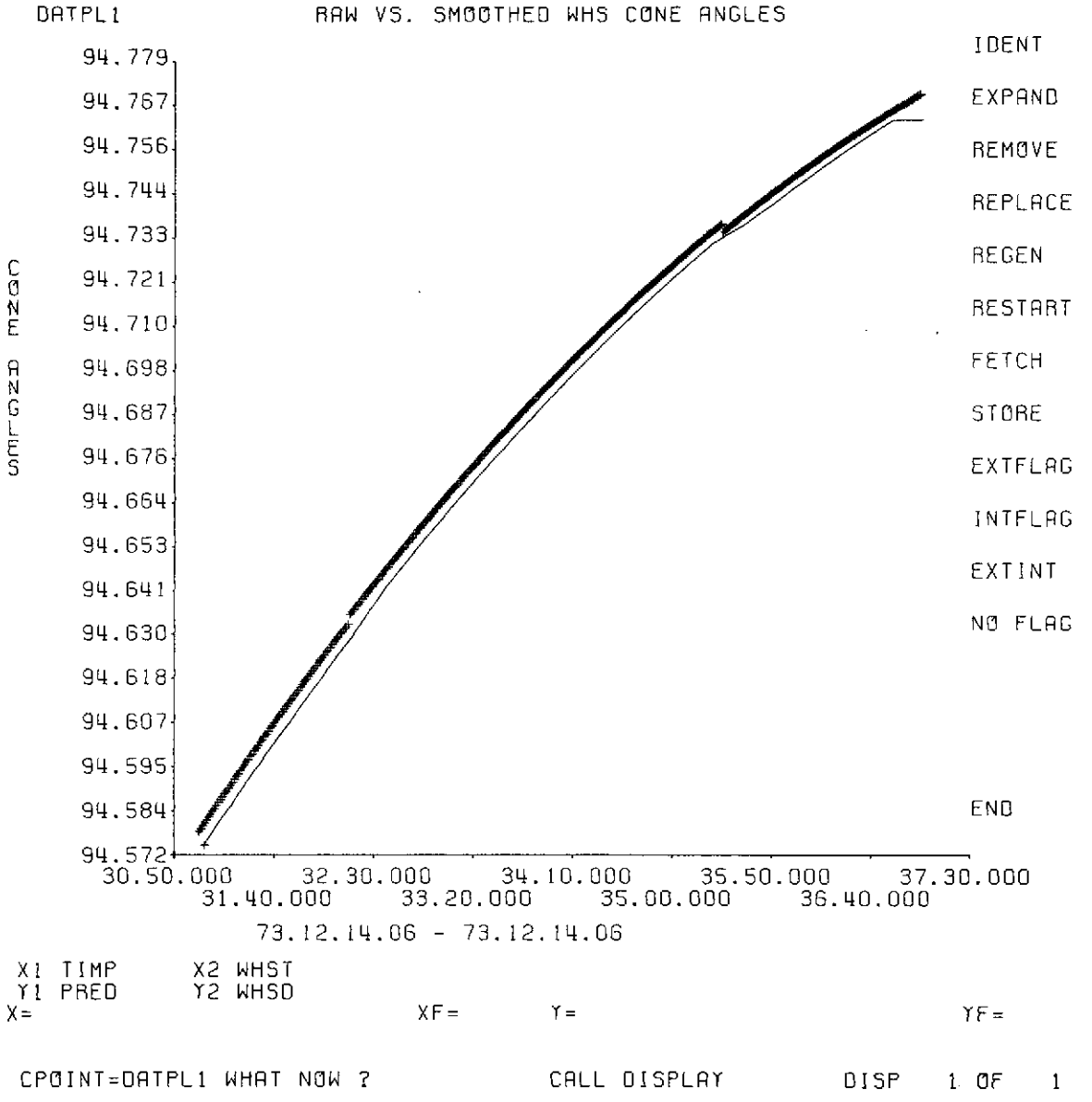

Figure 5-7. Raw Versus Smoothed WHS Cone Angles After Smoothing (1 of 2)

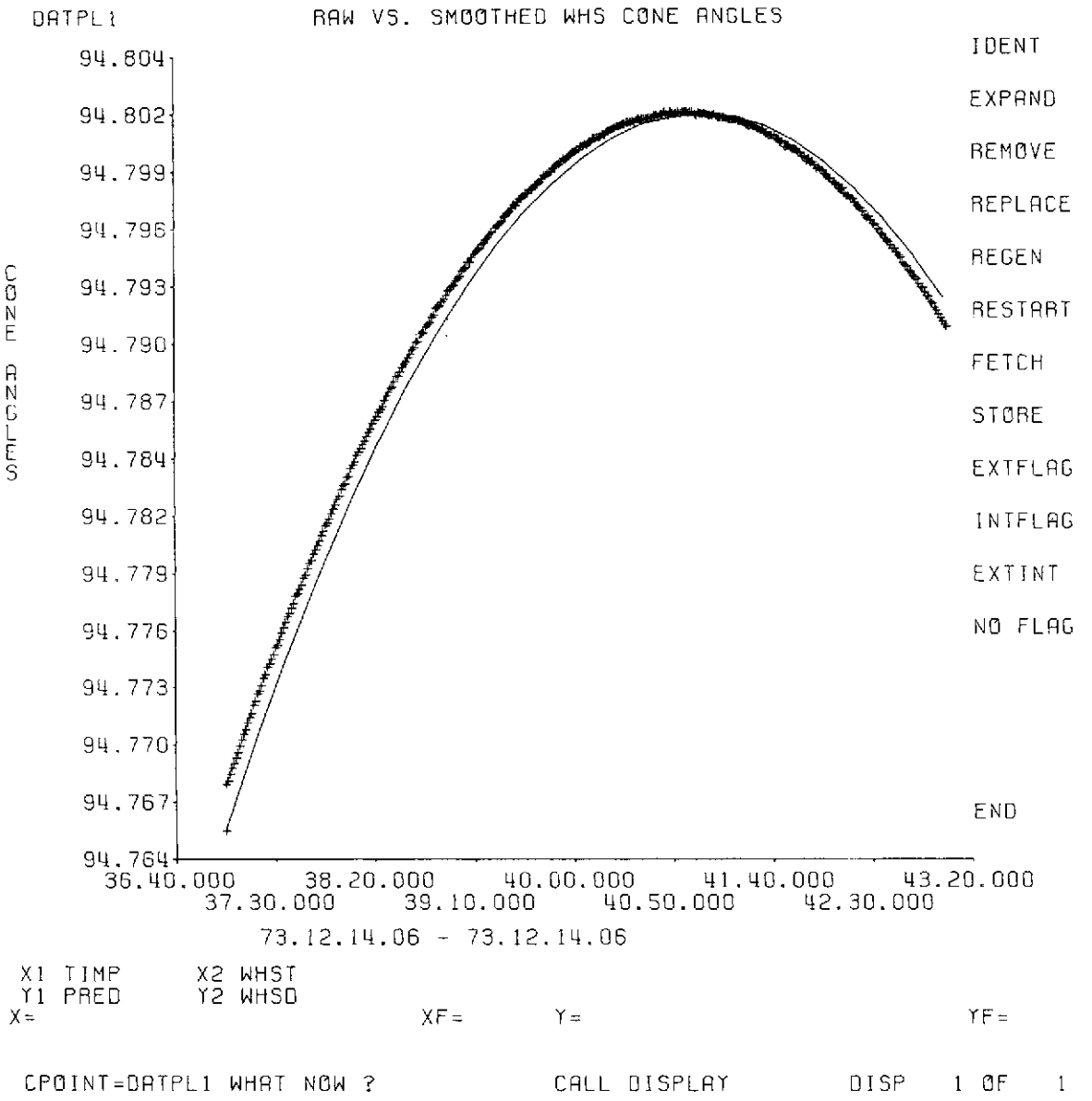

Figure 5-7. Raw Versus Smoothed WHS Cone Angles After Smoothing (2 of 2)

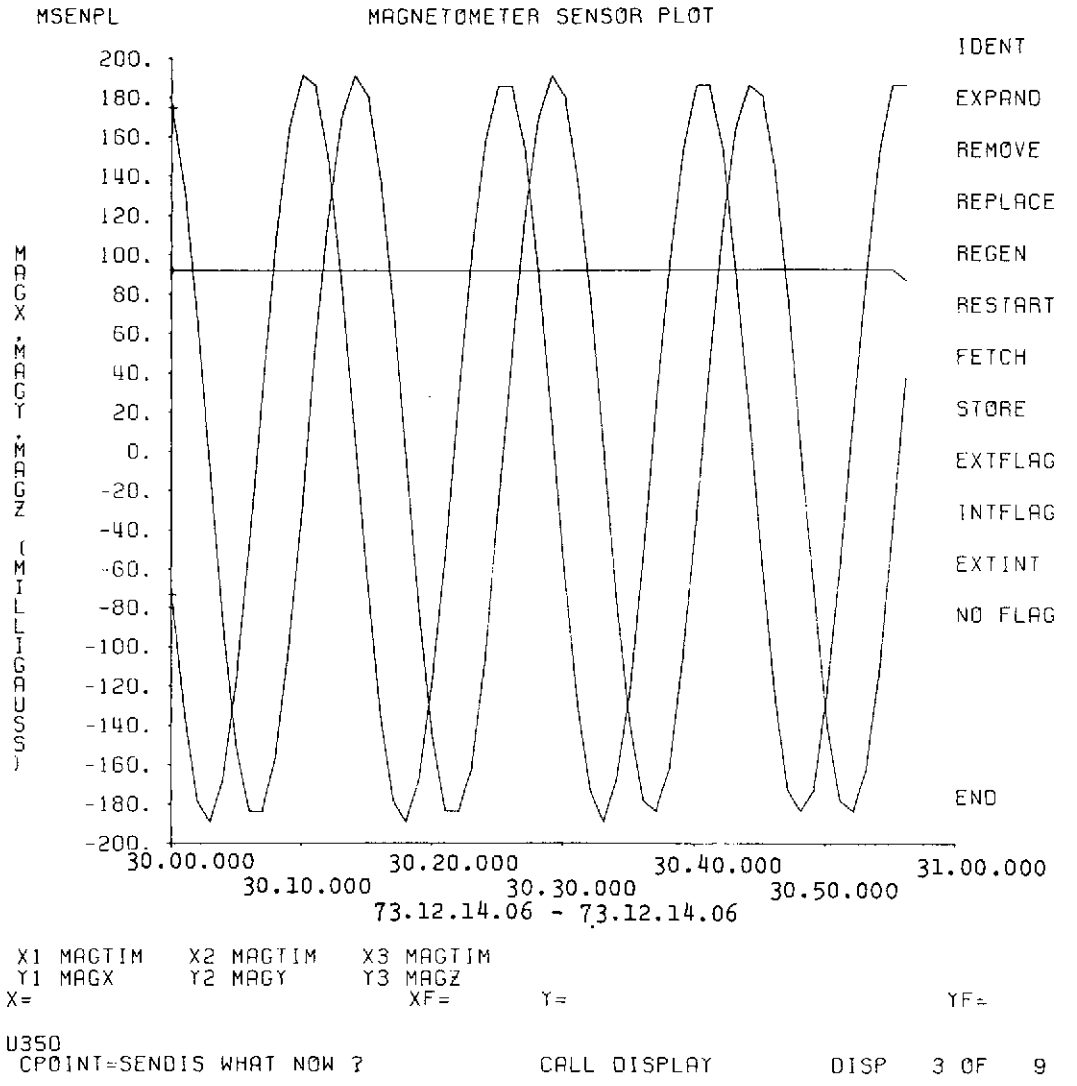

Figure 5-8. Magnetometer Sensor Plot

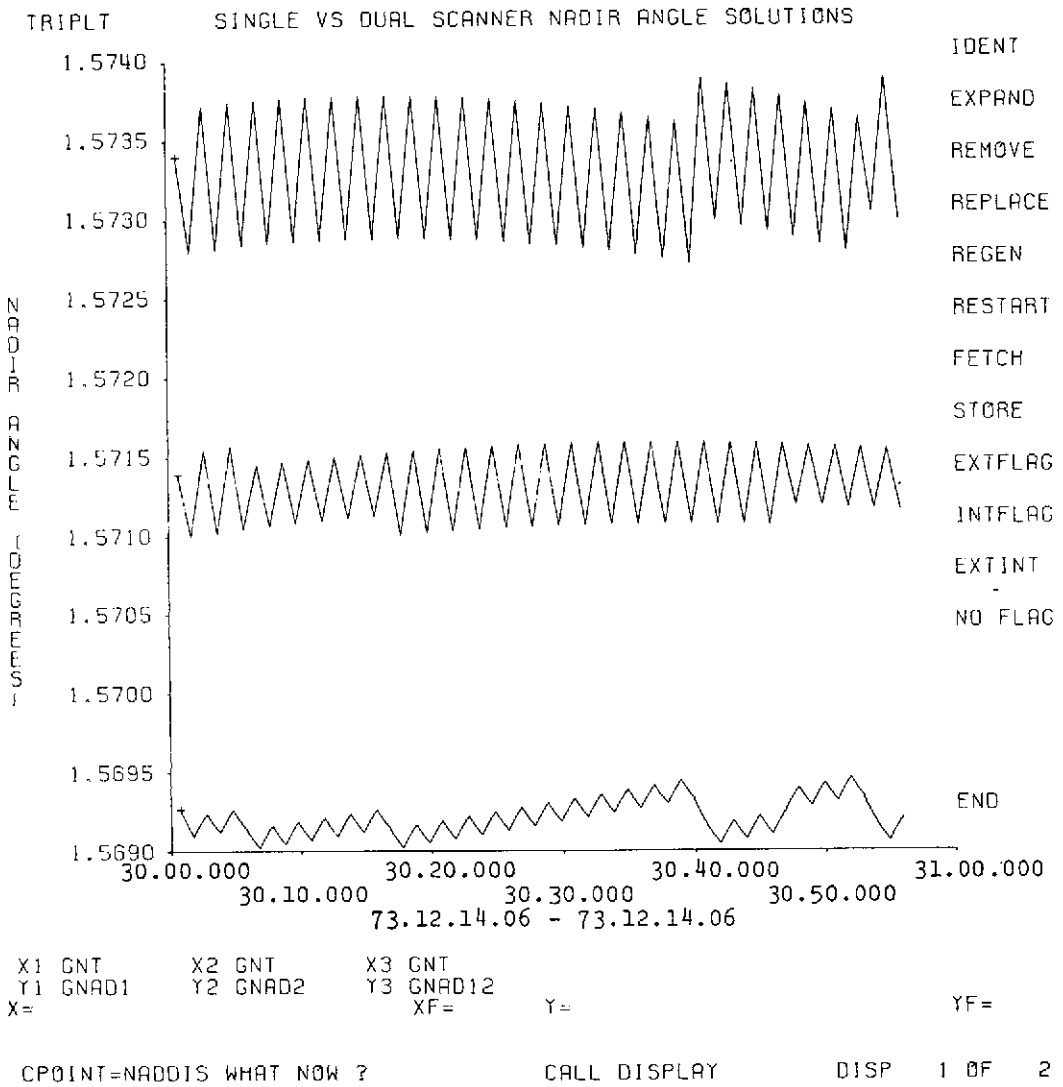

Figure 5-9. Single- Versus Dual-Scanner Nadir Angle Solutions

APPENDIX A - ORBITAL ELEMENTS FOR AE-C

Epoch	06 hours 23 minutes GMT on December 14, 1973
Semimajor axis	8614.0 kilometers
Eccentricity	0.2414
Inclination	68.1 degrees $\pm$0.1 degree (3σ)
Mean anomaly	359.2 degrees
Argument of perigee	166.0 degrees
Right ascension of ascending node	251.4 degrees
Height of perigee	156 kilometers $\pm$16 kilometers (3σ)
Height of apogee	4300 kilometers $\pm$30 kilometers (3σ)

APPENDIX B - AERODYNAMIC DRIFT

The following printouts are representative of the predicted AE-C spacecraft drift behavior due to aerodynamic torques at a low perigee of 120 kilometers.

The CM-CP offset is the radius vector from the center of mass to the center of pressure. This version of MSAP approximates the AE configuration as a right circular cylinder with the center of pressure at the centroid of the projected area, which is taken as the origin of the spacecraft reference system. The CM-CP offset in this case is due to having the CM location offset from the center of the reference system.

Figure B-1 shows a plot of the AE-C spacecraft declination versus right ascension due to aerodynamic torques with a CM-CP offset of 0.1 inches at a low perigee of 120 kilometers.

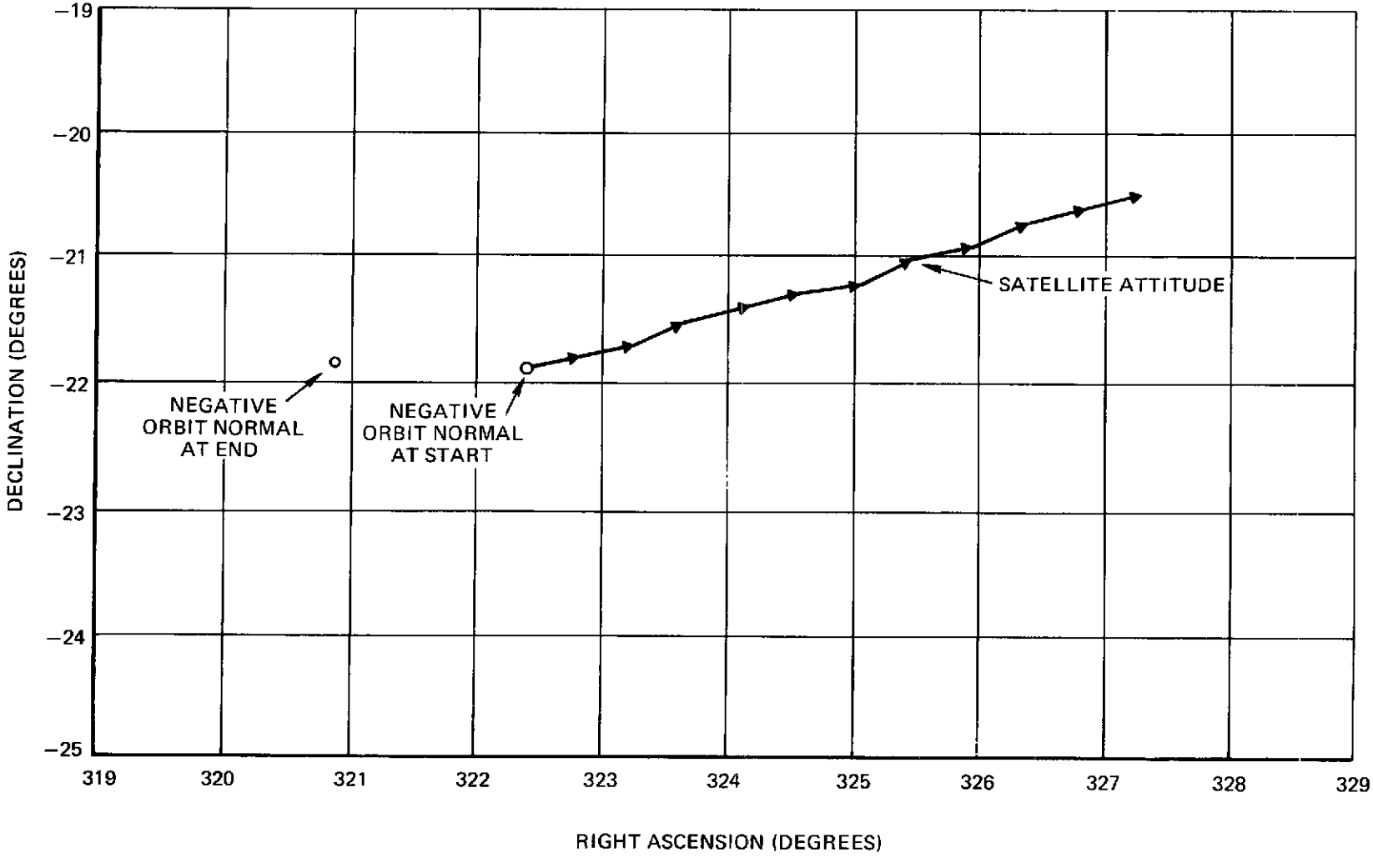

Figure B-1. Plot for One Day of AE-C Spacecraft Declination Versus Right Ascension Due to Aerodynamic Torques

MSAP SATELLITE INDEPENDENT INPUTS.

KSTART = 73 12 10 5 53 0		PREDICTOR START TIME (YR.,MO.,DA.,HR.,MIN.,SEC.).
KSTOP = 73 12 11 5 53 0		PREDICTOR STOP TIME (YR.,MO.,DA.,HR.,MIN.,SEC.).
NUMINT =	30	NUMBER OF INTEGRATIONS PER ORBIT.
NUMOUT =	30	NUMBER OF OUTPUT POINTS PER ORBIT.
MPEROD =	132	ORBITAL PERIOD IN MINUTES.
MDTORQ =	90	TORQUE COMPUTATION STEP SIZE (SEC.).
ALPHA =	322.40	INITIAL RIGHT ASCENSION OF SPIN AXIS (DEG.).
DELTA =	-21.90	INITIAL DECLINATION OF SPIN AXIS (DEG.).
OMEGA =	4.00	INITIAL SPIN RATE OF SPIN AXIS (RPM.).
RMAX =	300.00	ALTITUDE ABOVE WHICH AERODYNAMIC TORQUE MAY BE NEGLECTED (KM.).
DRAGB =	0.0	BROUWER DRAG TERM (RAD./SEC.**2).
IPRINT =	6	STANDARD PRINTED OUTPUT DSRN.
INCARD =	73	CARD INPUT DSRN.
ITAPE =	10	RESERVED FOR FUTURE DSRN.
ICRB1 =	0	ORB1 TAPE DSRN.
IDUMP =	78	INTERMEDIATE PRINTED OUTPUT DSRN.
IEPHEM =	0	EPHEMERIS TAPE DSRN.
MSGIN =	13	ERROR MESSAGE DATA SET INPUT DSRN.
MSGOUT =	6	ERROR MESSAGE DATA SET OUTPUT DSRN.
OEPOCH =	731207.00	EPOCH DATE OF ORBITAL ELEMENTS (YYMMDD.0).
OTIME =	21180.00	EPOCH TIME OF ORBITAL ELEMENTS (SECONDS).
OAXIS =	6625.12	SEMI-MAJOR AXIS (KM.).
OEPSLN =	0.242183	ECCENTRICITY.
OIOTA =	68.11	INCLINATION (DEG.).
OUPSLN =	359.41	MEAN ANOMALY (DEG.).
OOMEGA =	165.75	ARGUMENT OF PERIGEE (DEG.).
OALPHA =	236.90	RIGHT ASCENSION OF ASCENDING NODE (DEG.).
OMOREF =	731210.00	REFERENCE DATE FOR LONGITUDE OF GREENWICH (YYMMDD.0).
OLAMDA =	78.53	LONGITUDE OF GREENWICH REFERENCED TO PREDICTOR START DATE (DEG.).

NSAP SATELLITE DEPENDENT INPUT

IATARC	0	ATTITUDE ARCHIVE OPTION INDICATOR (0=NO)
IMSARC	0	MSAP ARCHIVE OPTION INDICATOR (0=NO)
IOFF(1)	1	MAGNETIC TORQUE CALC. INDICATOR (1=OFF)
IOFF(2)	1	GRAVITY GRADIENT TORQUE CALC. INDICATOR (1=OFF)
IOFF(3)	1	GRAVITY TORQUE CALC. INDICATOR (1=OFF)
IOFF(4)	0	AERO TORQUE CALC. INDICATOR (1=OFF)
IOFF(5)	1	SOLAR TORQUE CALC. INDICATOR (1=OFF)
IPREC	20	PERCENT OF COIL REDUCTION DURING NIGHT
ISPMOD	4	SPIN MODE (0=DESPIN 4=4RPM,10-41=TACH)
IPANGL	0	PITCH MODE (0-359=PITCH ANGLE)
NSTEP1	4	CONTROL SEARCH STEP SIZE(FORWARD)
NSTEP2	4	CONTROL SEARCH STEP SIZE(BACKWARD)
NATAPE	0	ATTITUDE TAPE (0=NO TAPE,XX=DSRN)
IPERIN	30	PERIGEE INTEGRATION STEP SIZE (SECS)
IPER	1	CONTROL DISTURBANCE TORQUE OPTION(0=OFF)
MINPER	20	NUM. MIN. NO CONTROL EITHER SIDE PERIGEE
XCMOFF	0.0	X CENTER OF MASS OFFSET (INCHES)
YCMOFF	0.100	Y CENTER OF MASS OFFSET (INCHES)
ZCMOFF	0.100	Z CENTER OF MASS OFFSET (INCHES)
XBIAS	0.0	X-DIRECTED MAGNETIC BIAS (POLE-CM)
YBIAS	0.0	Y-DIRECTED MAGNETIC BIAS (POLE-CM)
ZBIAS	0.0	Z-DIRECTED MAGNETIC BIAS (POLE-CM)
XMOIWH	17974848.000	WHEEL X MOMENT OF INERTIA (GM-CM**2)
YMOIWH	17974848.000	WHEEL Y MOMENT OF INERTIA (GM-CM**2)
ZMOIWH	36926208.000	WHEEL Z MOMENT OF INERTIA (GM-CM**2)
WHMASS	18662.086	WHEEL MASS (GM)
XMOINS	957059364.000	BODY X MOMENT OF INERTIA (GM-CM**2)
YMOINS	9232C3584.000	BODY Y MOMENT OF INERTIA (GM-CM**2)

ZMOINS	1088275456.000	BODY Z MOMENT OF INERTIA (GM-CM**2)
AMASSN	456038.313	BODY MASS (GM)
COIL1	58000.000	SPIN AXIS COIL STRENGTH (POLE-CM)
COIL2	13000.000	SPIN RATE COIL STRENGTH (POLE-CM)
YTHRST	3.000	THRUST OF YAW THRUSTER (LBS)
DELV1	5.000	THRUST OF DELTA-V1 ROCKET (LBS)
DELV2	5.000	THRUST OF DELTA-V2 ROCKET (LBS)
WHLSPN	25.132	WHEEL SPIN RATE (RPMS)
GDT	7920	GRAPHICS TIME INCREMENT (MIN)
ALT	170.000	ALTITUDE FOR PERIGEE TORQUE CALC. (KM)
CLOSE1	0.100	ARC ERROR REORIENTATION CRITERA (DEG.)
NP		NUMBER OF PARAMETERS OPTIMZED
IPSCDE		PARAMETER OPTIMIZATION CODE
CD	2.000	AERO DRAG COEFFICIENT

AE - C ATTITUDE SUMMARY PREDICTOR START TIME = DEC 10 73

DATE	TIME	RIGHT ASCENSION (DEGREES)	DECLINATION (DEGREES)	SPIN RATE (RPM*6)	MOMENTUM IN.LB.SC	GAMMA (DEG.)	LAMDA (DEG.)	PHIMAX (DEG.)
DEC 10 73	5:53: 0	322.4	-21.9	3.9998	1202.6	59.9	351.6	179.9
DEC 10 73	5:57:25	322.4	-21.9	3.9932	1202.6	59.9	354.1	179.9
DEC 10 73	6: 1:50	322.4	-21.9	3.9925	1202.6	59.9	357.1	179.9
DEC 10 73	6: 6:15	322.4	-21.9	3.9917	1202.6	59.9	0.4	180.0
DEC 10 73	6:10:40	322.4	-21.9	3.9907	1202.6	59.9	3.1	180.0
DEC 10 73	6:15: 5	322.4	-21.9	3.9896	1202.6	59.9	2.6	180.0
DEC 10 73	6:19:30	322.4	-21.9	3.9885	1202.6	59.9	0.0	180.0
DEC 10 73	6:23:55	322.4	-21.9	3.9875	1202.6	59.9	0.0	180.0
DEC 10 73	6:28:20	322.5	-21.9	3.9871	1202.9	60.0	173.4	179.9
DEC 10 73	6:32:45	322.8	-21.8	3.9872	1195.5	60.3	166.8	179.6
DEC 10 73	6:37:10	322.8	-21.8	3.9879	1195.6	60.3	166.7	179.6
DEC 10 73	6:41:35	322.8	-21.8	3.9890	1195.6	60.3	166.0	179.6
DEC 10 73	6:46: 0	322.8	-21.8	3.9901	1195.6	60.3	165.4	179.6
DEC 10 73	6:50:25	322.8	-21.8	3.9912	1195.6	60.3	165.0	179.6
DEC 10 73	6:54:50	322.8	-21.8	3.9921	1195.6	60.3	165.0	179.5
DEC 10 73	6:59:15	322.8	-21.8	3.9928	1195.6	60.3	165.2	179.5
DEC 10 73	7: 3:40	322.8	-21.8	3.9935	1195.6	60.3	165.5	179.5
DEC 10 73	7: 8: 5	322.8	-21.8	3.9940	1195.6	60.3	165.9	179.5
DEC 10 73	7:12:30	322.8	-21.8	3.9943	1195.6	60.3	166.3	179.5
DEC 10 73	7:16:55	322.8	-21.8	3.9946	1195.6	60.3	166.7	179.5
DEC 10 73	7:21:20	322.8	-21.8	3.9948	1195.6	60.3	167.0	179.6
DEC 10 73	7:25:45	322.8	-21.8	3.9950	1195.6	60.3	167.3	179.5
DEC 10 73	7:30:10	322.8	-21.8	3.9951	1195.6	60.3	167.5	179.5
DEC 10 73	7:34:35	322.8	-21.8	3.9951	1195.6	60.3	167.7	179.5
DEC 10 73	7:39: 0	322.8	-21.8	3.9951	1195.6	60.3	167.8	179.5
DEC 10 73	7:43:25	322.8	-21.8	3.9950	1195.6	60.3	167.8	179.5
DEC 10 73	7:47:50	322.8	-21.8	3.9949	1195.6	60.3	167.8	179.5
DEC 10 73	7:52:15	322.8	-21.8	3.9947	1195.6	60.3	167.8	179.5
DEC 10 73	7:56:40	322.8	-21.8	3.9945	1195.6	60.3	167.6	179.5
DEC 10 73	8: 1: 5	322.8	-21.8	3.9941	1195.6	60.3	167.4	179.5
DEC 10 73	8: 5:30	322.8	-21.8	3.9937	1195.6	60.3	167.2	179.5
DEC 10 73	8: 9:55	322.8	-21.8	3.9931	1195.6	60.3	166.9	179.5
DEC 10 73	8:14:20	322.8	-21.8	3.9924	1195.6	60.3	166.6	179.5
DEC 10 73	8:18:45	322.8	-21.8	3.9916	1195.6	60.3	166.5	179.5
DEC 10 73	8:23:10	322.8	-21.8	3.9906	1195.6	60.2	166.6	179.5
DEC 10 73	8:27:35	322.8	-21.8	3.9894	1195.6	60.2	167.0	179.5
DEC 10 73	8:32: 0	322.8	-21.8	3.9883	1195.6	60.2	167.8	179.5
DEC 10 73	8:36:25	322.8	-21.8	3.9875	1195.6	60.2	168.8	179.5
DEC 10 73	8:40:50	322.9	-21.7	3.9871	1196.1	60.3	167.7	179.4
DEC 10 73	8:45:15	323.3	-21.7	3.9873	1189.5	60.7	167.3	179.0
DEC 10 73	8:49:40	323.3	-21.7	3.9880	1189.6	60.7	167.2	179.0
DEC 10 73	8:54: 5	323.3	-21.7	3.9891	1189.6	60.7	166.9	179.0
DEC 10 73	8:58:30	323.3	-21.7	3.9902	1189.6	60.7	166.6	179.0
DEC 10 73	9: 2:55	323.3	-21.7	3.9913	1189.6	60.6	166.5	179.0
DEC 10 73	9: 7:20	323.3	-21.7	3.9922	1189.6	60.6	166.5	179.0
DEC 10 73	9:11:45	323.3	-21.7	3.9929	1189.6	60.6	166.6	179.0
DEC 10 73	9:16:10	323.3	-21.7	3.9935	1189.6	60.6	166.7	179.0
DEC 10 73	9:20:35	323.3	-21.7	3.9940	1189.6	60.6	166.9	179.0
DEC 10 73	9:25: 0	323.3	-21.7	3.9944	1189.6	60.6	167.1	179.0
DEC 10 73	9:29:25	323.3	-21.7	3.9947	1189.6	60.6	167.2	179.0

AE - C ATTITUDE SUMMARY PREDICTOR START TIME = DEC 10 73

DATE	TIME	RIGHT ASCENSION (DEGREES)	DECLINATION (DEGREES)	SPIN RATE (RPM*S)	MOMENTUM IN-LB-SC	GAMMA (DEG.)	LAMDA (DEG.)	PHIMAX (DEG.)
DEC 10 73	9:33:50	323.3	-21.7	3.9949	1189.6	60.6	167.4	179.0
DEC 10 73	9:38:15	323.3	-21.7	3.9950	1189.6	60.6	167.5	179.0
DEC 10 73	9:42:40	323.3	-21.7	3.9951	1189.6	60.6	167.6	179.0
DEC 10 73	9:47: 5	323.3	-21.7	3.9951	1189.6	60.6	167.7	179.0
DEC 10 73	9:51:30	323.3	-21.7	3.9951	1189.6	60.6	167.7	179.0
DEC 10 73	9:55:55	323.3	-21.7	3.9950	1189.6	60.6	167.8	179.0
DEC 10 73	10: 0:20	323.3	-21.7	3.9949	1189.6	60.6	167.8	179.0
DEC 10 73	10: 4:45	323.3	-21.7	3.9947	1189.6	60.6	167.7	179.0
DEC 10 73	10: 9:10	323.3	-21.7	3.9944	1189.6	60.6	167.6	179.0
DEC 10 73	10:13:35	323.3	-21.7	3.9941	1189.6	60.6	167.5	179.0
DEC 10 73	10:18: 0	323.3	-21.7	3.9936	1189.6	60.6	167.4	179.0
DEC 10 73	10:22:25	323.3	-21.7	3.9931	1189.6	60.6	167.3	179.0
DEC 10 73	10:26:50	323.3	-21.7	3.9923	1189.6	60.6	167.2	179.0
DEC 10 73	10:31:15	323.3	-21.7	3.9915	1189.6	60.6	167.1	178.9
DEC 10 73	10:35:40	323.3	-21.7	3.9904	1189.6	60.6	167.2	178.9
DEC 10 73	10:40: 5	323.3	-21.7	3.9893	1189.6	60.6	167.4	178.9
DEC 10 73	10:44:30	323.3	-21.7	3.9882	1189.6	60.6	167.8	178.9
DEC 10 73	10:48:55	323.3	-21.7	3.9874	1189.6	60.6	168.3	178.9
DEC 10 73	10:53:20	323.5	-21.6	3.9870	1189.9	60.7	167.4	178.7
DEC 10 73	10:57:45	323.7	-21.5	3.9873	1184.9	61.0	167.4	178.5
DEC 10 73	11: 2:10	323.7	-21.5	3.9881	1185.0	61.0	167.3	178.5
DEC 10 73	11: 6:35	323.7	-21.5	3.9892	1185.0	61.0	167.1	178.5
DEC 10 73	11:11: 0	323.7	-21.5	3.9903	1185.0	61.0	167.0	178.5
DEC 10 73	11:15:25	323.7	-21.5	3.9914	1185.0	61.0	166.9	178.5
DEC 10 73	11:19:50	323.7	-21.5	3.9923	1185.0	61.0	166.9	178.4
DEC 10 73	11:24:15	323.7	-21.5	3.9930	1185.0	61.0	167.0	178.4
DEC 10 73	11:28:40	323.7	-21.5	3.9936	1185.0	61.0	167.1	178.4
DEC 10 73	11:33: 5	323.7	-21.5	3.9940	1185.0	61.0	167.2	178.4
DEC 10 73	11:37:30	323.7	-21.5	3.9944	1185.0	61.0	167.3	178.4
DEC 10 73	11:41:55	323.7	-21.5	3.9947	1185.0	61.0	167.4	178.4
DEC 10 73	11:46:20	323.7	-21.5	3.9949	1185.0	61.0	167.5	178.4
DEC 10 73	11:50:45	323.7	-21.5	3.9950	1185.0	61.0	167.6	178.4
DEC 10 73	11:55:10	323.7	-21.5	3.9951	1185.0	61.0	167.6	178.4
DEC 10 73	11:59:35	323.7	-21.5	3.9951	1185.0	61.0	167.7	178.4
DEC 10 73	12: 4: 0	323.7	-21.5	3.9951	1185.0	61.0	167.7	178.4
DEC 10 73	12: 8:25	323.7	-21.5	3.9950	1185.0	60.9	167.7	178.4
DEC 10 73	12:12:50	323.7	-21.5	3.9949	1185.0	60.9	167.7	178.4
DEC 10 73	12:17:15	323.7	-21.5	3.9947	1185.0	60.9	167.7	178.4
DEC 10 73	12:21:40	323.7	-21.5	3.9944	1185.0	60.9	167.6	178.4
DEC 10 73	12:26: 5	323.7	-21.5	3.9940	1185.0	60.9	167.6	178.4
DEC 10 73	12:30:30	323.7	-21.5	3.9936	1185.0	60.9	167.5	178.4
DEC 10 73	12:34:55	323.7	-21.5	3.9930	1185.0	60.9	167.4	178.4
DEC 10 73	12:39:20	323.7	-21.5	3.9922	1185.0	60.9	167.3	178.4
DEC 10 73	12:43:45	323.7	-21.5	3.9914	1185.0	60.9	167.3	178.4
DEC 10 73	12:48:10	323.7	-21.5	3.9903	1185.0	60.9	167.3	178.4
DEC 10 73	12:52:35	323.7	-21.5	3.9892	1185.0	60.9	167.5	178.4
DEC 10 73	12:57: 0	323.7	-21.5	3.9881	1185.0	60.9	167.8	178.4
DEC 10 73	13: 1:25	323.7	-21.5	3.9873	1185.0	60.9	168.1	178.4
DEC 10 73	13: 5:50	324.0	-21.5	3.9870	1184.6	61.2	167.4	178.1
DEC 10 73	13:10:15	324.2	-21.4	3.9874	1181.4	61.3	167.5	177.9

AE-C ATTITUDE SUMMARY — PREDICTED STARTING TIME — DEC 10 — V5

DATE	TIME	RIGHT ASCENSION (DEGREES)	DECLINATION (DEGREES)	SPIN RATE (RPM)	MOMENTUM (N-M-SEC)	GAMMA (DEG)	LAMDA (DEG)	PHIMAX (DEG)
DEC 10 73	13:14:40	324.2	-21.4	3.9902	1181.4	61.3	167.4	177.9
DEC 10 73	13:19: 5	324.2	-21.4	3.9895	1181.4	61.3	167.2	177.9
DEC 10 73	13:23:30	324.2	-21.4	3.9905	1181.4	61.3	167.1	177.9
DEC 10 73	13:27:55	324.2	-21.4	3.9915	1181.4	61.3	167.1	177.9
DEC 10 73	13:32:20	324.2	-21.4	3.9924	1181.4	61.3	167.1	177.9
DEC 10 73	13:36:45	324.2	-21.4	3.9931	1181.4	61.3	167.1	177.9
DEC 10 73	13:41:10	324.2	-21.4	3.9936	1181.4	61.3	167.2	177.9
DEC 10 73	13:45:35	324.2	-21.4	3.9941	1181.4	61.3	167.3	177.9
DEC 10 73	13:50: 0	324.2	-21.4	3.9944	1181.4	61.3	167.4	177.9
DEC 10 73	13:54:25	324.2	-21.4	3.9947	1181.4	61.3	167.5	177.9
DEC 10 73	13:58:50	324.2	-21.4	3.9949	1181.4	61.3	167.6	177.9
DEC 10 73	14: 3:15	324.2	-21.4	3.9950	1181.4	61.3	167.6	177.9
DEC 10 73	14: 7:40	324.2	-21.4	3.9951	1181.4	61.3	167.6	177.9
DEC 10 73	14:12: 5	324.2	-21.4	3.9951	1181.4	61.3	167.7	177.9
DEC 10 73	14:16:30	324.2	-21.4	3.9951	1181.4	61.3	167.7	177.9
DEC 10 73	14:20:55	324.2	-21.4	3.9950	1181.4	61.3	167.7	177.9
DEC 10 73	14:25:20	324.2	-21.4	3.9949	1181.4	61.3	167.7	177.9
DEC 10 73	14:29:45	324.2	-21.4	3.9947	1181.4	61.3	167.7	177.9
DEC 10 73	14:34:10	324.2	-21.4	3.9944	1181.4	61.3	167.6	177.9
DEC 10 73	14:38:35	324.2	-21.4	3.9940	1181.4	61.3	167.6	177.9
DEC 10 73	14:43: 0	324.2	-21.4	3.9935	1181.4	61.3	167.5	177.9
DEC 10 73	14:47:25	324.2	-21.4	3.9929	1181.4	61.3	167.5	177.9
DEC 10 73	14:51:50	324.2	-21.4	3.9922	1181.4	61.3	167.4	177.8
DEC 10 73	14:56:15	324.2	-21.4	3.9913	1181.4	61.3	167.4	177.8
DEC 10 73	15: 0:40	324.2	-21.4	3.9902	1181.4	61.3	167.4	177.8
DEC 10 73	15: 5: 5	324.2	-21.4	3.9891	1181.4	61.3	167.6	177.8
DEC 10 73	15: 9:30	324.2	-21.4	3.9880	1181.4	61.3	167.8	177.8
DEC 10 73	15:13:55	324.2	-21.4	3.9873	1181.4	61.3	168.0	177.8
DEC 10 73	15:18:20	324.5	-21.3	3.9870	1179.7	61.6	167.4	177.6
DEC 10 73	15:22:45	324.6	-21.3	3.9875	1178.0	61.7	167.5	177.4
DEC 10 73	15:27:10	324.6	-21.3	3.9884	1178.0	61.7	167.4	177.4
DEC 10 73	15:31:35	324.6	-21.3	3.9895	1178.0	61.7	167.3	177.4
DEC 10 73	15:36: 0	324.6	-21.3	3.9906	1178.0	61.7	167.2	177.4
DEC 10 73	15:40:25	324.6	-21.3	3.9916	1178.0	61.7	167.2	177.3
DEC 10 73	15:44:50	324.6	-21.3	3.9924	1178.0	61.7	167.2	177.3
DEC 10 73	15:49:15	324.6	-21.3	3.9931	1178.0	61.7	167.2	177.3
DEC 10 73	15:53:40	324.6	-21.3	3.9937	1178.0	61.7	167.3	177.3
DEC 10 73	15:58: 5	324.6	-21.3	3.9941	1178.0	61.7	167.4	177.3
DEC 10 73	16: 2:30	324.6	-21.3	3.9945	1178.0	61.6	167.4	177.3
DEC 10 73	16: 6:55	324.6	-21.3	3.9947	1178.0	61.6	167.5	177.3
DEC 10 73	16:11:20	324.6	-21.3	3.9949	1178.0	61.6	167.6	177.3
DEC 10 73	16:15:45	324.6	-21.3	3.9950	1178.0	61.6	167.6	177.3
DEC 10 73	16:20:10	324.6	-21.3	3.9951	1178.0	61.6	167.6	177.3
DEC 10 73	16:24:35	324.6	-21.3	3.9951	1178.0	61.6	167.7	177.3
DEC 10 73	16:29: 0	324.6	-21.3	3.9951	1178.0	61.6	167.7	177.3
DEC 10 73	16:33:25	324.6	-21.3	3.9950	1178.0	61.6	167.7	177.3
DEC 10 73	16:37:50	324.6	-21.3	3.9948	1178.0	61.6	167.7	177.3
DEC 10 73	16:42:15	324.6	-21.3	3.9946	1178.0	61.6	167.7	177.3
DEC 10 73	16:46:40	324.6	-21.3	3.9943	1178.0	61.6	167.6	177.3
DEC 10 73	16:51: 5	324.6	-21.3	3.9939	1178.0	61.6	167.6	177.3

AE-C ATTITUDE SUMMARY PREDICTOR START TIME = DEC 10 73

DATE	TIME	RIGHT ASCENSION (DEGREES)	DECLINATION (DEGREES)	SPIN RATE (RPM*S)	MOMENTUM (N-L-S-C)	GAMMA (DEG.)	LAMDA (DEG.)	PHIMAX (DEG.)
DEC 10 73	16:55:30	324.6	-21.3	3.9935	1178.0	61.6	167.5	177.3
DEC 10 73	16:59:55	324.6	-21.3	3.9928	1178.0	61.6	167.5	177.3
DEC 10 73	17: 4:20	324.6	-21.3	3.9921	1178.0	61.6	167.5	177.3
DEC 10 73	17: 8:45	324.6	-21.3	3.9911	1178.0	61.6	167.4	177.3
DEC 10 73	17:13:10	324.6	-21.3	3.9901	1178.0	61.6	167.5	177.3
DEC 10 73	17:17:35	324.6	-21.3	3.9889	1178.0	61.6	167.6	177.3
DEC 10 73	17:22: 0	324.6	-21.3	3.9879	1178.0	61.6	167.8	177.3
DEC 10 73	17:26:25	324.6	-21.3	3.9872	1178.0	61.6	168.0	177.2
DEC 10 73	17:30:50	325.0	-21.2	3.9871	1174.8	62.0	167.4	176.9
DEC 10 73	17:35:15	325.1	-21.2	3.9875	1174.0	62.0	167.5	176.8
DEC 10 73	17:39:40	325.1	-21.2	3.9885	1174.0	62.0	167.5	176.8
DEC 10 73	17:44: 5	325.1	-21.2	3.9896	1174.0	62.0	167.4	176.8
DEC 10 73	17:48:30	325.1	-21.2	3.9907	1174.0	62.0	167.3	176.8
DEC 10 73	17:52:55	325.1	-21.2	3.9917	1174.0	62.0	167.3	176.8
DEC 10 73	17:57:20	325.1	-21.2	3.9925	1174.0	62.0	167.3	176.8
DEC 10 73	18: 1:45	325.1	-21.2	3.9932	1174.0	62.0	167.3	176.8
DEC 10 73	18: 6:10	325.1	-21.2	3.9938	1174.0	62.0	167.4	176.8
DEC 10 73	18:10:35	325.1	-21.2	3.9942	1174.0	62.0	167.4	176.8
DEC 10 73	18:15: 0	325.1	-21.2	3.9945	1174.0	62.0	167.5	176.8
DEC 10 73	18:19:25	325.1	-21.2	3.9948	1174.0	62.0	167.5	176.7
DEC 10 73	18:23:50	325.1	-21.2	3.9949	1174.0	62.0	167.6	176.7
DEC 10 73	18:28:15	325.1	-21.2	3.9951	1174.0	62.0	167.6	176.7
DEC 10 73	18:32:40	325.1	-21.2	3.9951	1174.0	62.0	167.6	176.7
DEC 10 73	18:37: 5	325.1	-21.2	3.9951	1174.0	62.0	167.7	176.7
DEC 10 73	18:41:30	325.1	-21.2	3.9951	1174.0	62.0	167.7	176.7
DEC 10 73	18:45:55	325.1	-21.2	3.9950	1174.0	62.0	167.7	176.7
DEC 10 73	18:50:20	325.1	-21.2	3.9948	1174.0	62.0	167.7	176.7
DEC 10 73	18:54:45	325.1	-21.2	3.9946	1174.0	62.0	167.7	176.7
DEC 10 73	18:59:10	325.1	-21.2	3.9943	1174.0	62.0	167.6	176.7
DEC 10 73	19: 3:35	325.1	-21.2	3.9939	1174.0	62.0	167.6	176.7
DEC 10 73	19: 8: 0	325.1	-21.2	3.9934	1174.0	62.0	167.6	176.7
DEC 10 73	19:12:25	325.1	-21.2	3.9928	1174.0	62.0	167.5	176.7
DEC 10 73	19:16:50	325.1	-21.2	3.9920	1174.0	62.0	167.5	176.7
DEC 10 73	19:21:15	325.1	-21.2	3.9910	1174.0	61.9	167.5	176.7
DEC 10 73	19:25:40	325.1	-21.2	3.9900	1174.0	61.9	167.5	176.7
DEC 10 73	19:30: 5	325.1	-21.2	3.9888	1174.0	61.9	167.6	176.7
DEC 10 73	19:34:30	325.1	-21.2	3.9878	1174.0	61.9	167.8	176.7
DEC 10 73	19:38:55	325.1	-21.1	3.9871	1174.0	61.9	167.9	176.7
DEC 10 73	19:43:20	325.5	-21.0	3.9871	1169.3	62.3	167.6	176.3
DEC 10 73	19:47:45	325.5	-21.0	3.9876	1169.0	62.4	167.5	176.2
DEC 10 73	19:52:10	325.5	-21.0	3.9886	1169.0	62.4	167.6	176.2
DEC 10 73	19:56:35	325.5	-21.0	3.9897	1169.0	62.4	167.4	176.2
DEC 10 73	20: 1: 0	325.5	-21.0	3.9908	1169.0	62.4	167.3	176.2
DEC 10 73	20: 5:25	325.5	-21.0	3.9918	1169.0	62.4	167.3	176.2
DEC 10 73	20: 9:50	325.5	-21.0	3.9926	1169.0	62.4	167.2	176.2
DEC 10 73	20:14:15	325.5	-21.0	3.9933	1169.0	62.4	167.4	176.2
DEC 10 73	20:18:40	325.5	-21.0	3.9938	1169.0	62.4	167.4	176.2
DEC 10 73	20:23: 5	325.5	-21.0	3.9942	1169.0	62.3	167.5	176.2
DEC 10 73	20:27:30	325.5	-21.0	3.9946	1169.0	62.3	167.5	176.2

AE - C ATTITUDE SUMMARY PREDICTOR START TIME = DEC 10 73

DATE	TIME	RIGHT ASCENSION (DEGREES)	DECLINATION (DEGREES)	SPIN RATE (RPMIS)	MOMENTUM IN-LB-SC	GAMMA (DEG.)	LAMDA (DEG.)	PHIMAX (DEG.)
DEC 10 73	20:31:55	326.5	-21.0	3.9948	1169.0	62.3	167.6	176.2
DEC 10 73	20:36:20	325.5	-21.0	3.9949	1169.0	62.3	167.6	176.2
DEC 10 73	20:40:45	326.6	-21.0	3.9951	1169.0	62.3	167.6	176.2
DEC 10 73	20:45:10	325.5	-21.0	3.9951	1169.0	62.3	167.7	176.2
DEC 10 73	20:49:35	326.6	-21.0	3.9951	1169.0	62.3	167.7	176.2
DEC 10 73	20:54: 0	325.5	-21.0	3.9951	1169.0	62.3	167.7	176.2
DEC 10 73	20:58:25	326.5	-21.0	3.9950	1169.0	62.3	167.7	176.2
DEC 10 73	21: 2:50	325.5	-21.0	3.9948	1169.0	62.3	167.7	176.2
DEC 10 73	21: 7:16	326.6	-21.0	3.9946	1169.0	62.3	167.7	176.2
DEC 10 73	21:11:40	325.5	-21.0	3.9942	1169.0	62.3	167.6	176.2
DEC 10 73	21:16: 5	326.5	-21.0	3.9938	1169.0	62.3	167.6	176.2
DEC 10 73	21:20:30	325.5	-21.0	3.9933	1169.0	62.3	167.6	176.2
DEC 10 73	21:24:55	326.6	-21.0	3.9927	1169.0	62.3	167.5	176.2
DEC 10 73	21:29:20	325.5	-21.0	3.9919	1169.0	62.3	167.5	176.2
DEC 10 73	21:33:45	325.5	-21.0	3.9909	1169.0	62.3	167.6	176.2
DEC 10 73	21:38:10	325.5	-21.0	3.9898	1169.0	62.3	167.6	176.1
DEC 10 73	21:42:35	326.5	-21.0	3.9887	1169.0	62.3	167.7	176.1
DEC 10 73	21:47: 0	325.5	-21.0	3.9877	1169.0	62.3	167.8	176.1
DEC 10 73	21:51:25	325.5	-21.0	3.9871	1169.0	62.3	167.9	176.1
DEC 10 73	21:55:50	325.9	-20.9	3.9871	1163.0	62.7	167.5	175.7
DEC 10 73	22: 0:15	326.0	-20.9	3.9877	1162.9	62.7	167.6	175.7
DEC 10 73	22: 4:40	326.0	-20.9	3.9887	1162.9	62.7	167.5	175.7
DEC 10 73	22: 9: 5	326.0	-20.9	3.9899	1162.9	62.7	167.4	175.7
DEC 10 73	22:13:30	326.0	-20.9	3.9910	1162.9	62.7	167.4	175.7
DEC 10 73	22:17:55	326.0	-20.9	3.9919	1162.9	62.7	167.4	175.6
DEC 10 73	22:22:20	326.0	-20.9	3.9927	1162.9	62.7	167.4	175.6
DEC 10 73	22:26:45	326.0	-20.9	3.9933	1162.9	62.7	167.4	175.6
DEC 10 73	22:31:10	326.0	-20.9	3.9939	1162.9	62.7	167.5	175.6
DEC 10 73	22:35:35	326.0	-20.9	3.9943	1162.9	62.7	167.5	175.6
DEC 10 73	22:40: 0	326.0	-20.9	3.9946	1162.9	62.7	167.5	175.6
DEC 10 73	22:44:25	326.0	-20.9	3.9948	1162.9	62.7	167.6	175.6
DEC 10 73	22:48:50	326.0	-20.9	3.9950	1162.9	62.7	167.6	175.6
DEC 10 73	22:53:15	326.0	-20.9	3.9951	1162.9	62.7	167.6	175.6
DEC 10 73	22:57:40	326.0	-20.9	3.9951	1162.9	62.7	167.7	175.6
DEC 10 73	23: 2: 5	326.0	-20.9	3.9951	1162.9	62.7	167.7	175.6
DEC 10 73	23: 6:30	326.0	-20.9	3.9951	1162.9	62.7	167.7	175.6
DEC 10 73	23:10:55	326.0	-20.9	3.9949	1162.9	62.7	167.7	175.6
DEC 10 73	23:15:20	326.0	-20.9	3.9948	1162.9	62.7	167.7	175.6
DEC 10 73	23:19:45	326.0	-20.9	3.9945	1162.9	62.7	167.7	175.6
DEC 10 73	23:24:10	326.0	-20.9	3.9942	1162.9	62.7	167.6	175.6
DEC 10 73	23:28:35	326.0	-20.9	3.9938	1162.9	62.7	167.6	175.6
DEC 10 73	23:33: 0	326.0	-20.9	3.9933	1162.9	62.7	167.6	175.6
DEC 10 73	23:37:25	326.0	-20.9	3.9926	1162.9	62.7	167.6	175.6
DEC 10 73	23:41:50	326.0	-20.9	3.9918	1162.9	62.7	167.5	175.6
DEC 10 73	23:46:15	326.0	-20.9	3.9908	1162.9	62.7	167.5	175.6
DEC 10 73	23:50:40	326.0	-20.9	3.9897	1162.9	62.6	167.6	175.6
DEC 10 73	23:55: 5	326.0	-20.9	3.9886	1162.9	62.6	167.7	175.6
DEC 10 73	23:59:30	326.0	-20.9	3.9876	1162.9	62.6	167.8	175.6
DEC 11 73	0: 3:55	326.0	-20.9	3.9871	1163.4	62.7	167.8	175.5
DEC 11 73	0: 8:20	326.4	-20.8	3.9871	1156.6	63.1	167.6	175.1

AE - C ATTITUDE SUMMARY PREDICTOR START TIME = DEC 10 73

DATE	TIME	RIGHT ASCENSION (DEGREES)	DECLINATION (DEGREES)	SPIN RATE (RPM'S)	MOMENTUM IN-LB-SC	GAMMA (DEG.)	LAMDA (DEG.)	PHIMAX (DEG.)
DEC 11 73	0:12:45	326.4	-20.7	3.9878	1156.6	63.1	167.6	175.1
DEC 11 73	0:17:10	326.4	-20.7	3.9888	1156.6	63.1	167.5	175.1
DEC 11 73	0:21:35	326.4	-20.7	3.9900	1156.6	63.1	167.5	175.1
DEC 11 73	0:26: 0	326.4	-20.7	3.9911	1156.6	63.1	167.4	175.1
DEC 11 73	0:30:25	326.4	-20.7	3.9920	1156.6	63.1	167.4	175.1
DEC 11 73	0:34:50	326.4	-20.7	3.9928	1156.6	63.1	167.4	175.1
DEC 11 73	0:39:15	326.4	-20.7	3.9934	1156.6	63.1	167.5	175.1
DEC 11 73	0:43:40	326.4	-20.7	3.9939	1156.6	63.1	167.5	175.1
DEC 11 73	0:48: 5	326.4	-20.7	3.9943	1156.6	63.0	167.5	175.1
DEC 11 73	0:52:30	326.4	-20.7	3.9946	1156.6	63.0	167.6	175.1
DEC 11 73	0:56:55	326.4	-20.7	3.9948	1156.6	63.0	167.6	175.1
DEC 11 73	1: 1:20	326.4	-20.7	3.9950	1156.6	63.0	167.6	175.1
DEC 11 73	1: 5:45	326.4	-20.7	3.9951	1156.6	63.0	167.7	175.1
DEC 11 73	1:10:10	326.4	-20.7	3.9951	1156.6	63.0	167.7	175.1
DEC 11 73	1:14:35	326.4	-20.7	3.9951	1156.6	63.0	167.7	175.1
DEC 11 73	1:19: 0	326.4	-20.7	3.9950	1156.6	63.0	167.7	175.1
DEC 11 73	1:23:25	326.4	-20.7	3.9949	1156.6	63.0	167.7	175.1
DEC 11 73	1:27:50	326.4	-20.7	3.9947	1156.6	63.0	167.7	175.1
DEC 11 73	1:32:15	326.4	-20.7	3.9945	1156.6	63.0	167.7	175.1
DEC 11 73	1:36:40	326.4	-20.7	3.9942	1156.6	63.0	167.7	175.1
DEC 11 73	1:41: 5	326.4	-20.7	3.9937	1156.6	63.0	167.6	175.0
DEC 11 73	1:45:30	326.4	-20.7	3.9932	1156.6	63.0	167.6	175.0
DEC 11 73	1:49:55	326.4	-20.7	3.9926	1156.6	63.0	167.6	175.0
DEC 11 73	1:54:20	326.4	-20.7	3.9917	1156.6	63.0	167.6	175.0
DEC 11 73	1:58:45	326.4	-20.7	3.9907	1156.6	63.0	167.6	175.0
DEC 11 73	2: 3:10	326.4	-20.7	3.9896	1156.6	63.0	167.6	175.0
DEC 11 73	2: 7:35	326.4	-20.7	3.9885	1156.6	63.0	167.7	176.0
DEC 11 73	2:12: 0	326.4	-20.7	3.9875	1156.6	63.0	167.8	175.0
DEC 11 73	2:16:25	326.5	-20.7	3.9870	1157.4	63.1	167.7	174.9
DEC 11 73	2:20:50	326.9	-20.6	3.9872	1150.3	63.4	167.6	174.6
DEC 11 73	2:25:15	326.9	-20.6	3.9879	1150.4	63.4	167.6	174.6
DEC 11 73	2:29:40	326.9	-20.6	3.9890	1150.4	63.4	167.5	174.5
DEC 11 73	2:34: 5	326.9	-20.6	3.9901	1150.4	63.4	167.5	174.5
DEC 11 73	2:38:30	326.9	-20.6	3.9912	1150.4	63.4	167.4	174.5
DEC 11 73	2:42:55	326.9	-20.6	3.9921	1150.4	63.4	167.4	174.5
DEC 11 73	2:47:20	326.9	-20.6	3.9929	1150.4	63.4	167.5	174.5
DEC 11 73	2:51:45	326.9	-20.6	3.9935	1150.4	63.4	167.5	174.5
DEC 11 73	2:56:10	326.9	-20.6	3.9940	1150.4	63.4	167.5	174.5
DEC 11 73	3: 0:35	326.9	-20.6	3.9943	1150.4	63.4	167.6	174.5
DEC 11 73	3: 5: 0	326.9	-20.6	3.9946	1150.4	63.4	167.6	174.5
DEC 11 73	3: 9:26	326.9	-20.6	3.9948	1150.4	63.4	167.6	174.5
DEC 11 73	3:13:50	326.9	-20.6	3.9950	1150.4	63.4	167.6	174.5
DEC 11 73	3:18:15	326.9	-20.6	3.9951	1150.4	63.4	167.7	174.5
DEC 11 73	3:22:40	326.9	-20.6	3.9951	1150.4	63.4	167.7	174.5
DEC 11 73	3:27: 5	326.9	-20.6	3.9951	1150.4	63.4	167.7	174.5
DEC 11 73	3:31:30	326.9	-20.6	3.9950	1150.4	63.4	167.7	174.5
DEC 11 73	3:35:55	326.9	-20.6	3.9949	1150.4	63.4	167.7	174.5
DEC 11 73	3:40:20	326.9	-20.6	3.9947	1150.4	63.4	167.7	174.5
DEC 11 73	3:44:45	326.9	-20.6	3.9945	1150.4	63.4	167.7	174.5
DEC 11 73	3:49:10	326.9	-20.6	3.9941	1150.4	63.4	167.7	174.5

AE - C ATTITUDE SUMMARY PREDICTOR START TIME = DEC 10 73

DATE	TIME	RIGHT ASCENSION (DEGREES)	DECLINATION (DEGREES)	SPIN RATE (RPM'S)	MOMENTUM IN-LB-SC	GAMMA (DEG.)	LAMDA (DEG.)	PHIMAX (DEG.)
DEC 11 73	3:53:35	326.9	-20.6	3.9937	1150.4	63.4	167.6	174.5
DEC 11 73	3:58: 0	326.9	-20.6	3.9931	1150.4	63.4	167.6	174.5
DEC 11 73	4: 2:25	326.9	-20.6	3.9925	1150.4	63.4	167.6	174.5
DEC 11 73	4: 6:50	326.9	-20.6	3.9918	1150.4	63.4	167.6	174.5
DEC 11 73	4:11:15	326.9	-20.6	3.9906	1150.4	63.4	167.6	174.5
DEC 11 73	4:15:40	326.9	-20.6	3.9895	1150.4	63.3	167.6	174.4
DEC 11 73	4:20: 5	326.9	-20.6	3.9883	1150.4	63.3	167.7	174.4
DEC 11 73	4:24:30	326.9	-20.6	3.9874	1150.4	63.3	167.8	174.4
DEC 11 73	4:28:55	327.0	-20.6	3.9870	1151.4	63.6	167.7	174.3
DEC 11 73	4:33:20	327.3	-20.5	3.9872	1144.9	63.8	167.6	174.0
DEC 11 73	4:37:45	327.3	-20.5	3.9880	1144.9	63.8	167.6	174.0
DEC 11 73	4:42:10	327.3	-20.5	3.9891	1144.9	63.8	167.5	174.0
DEC 11 73	4:46:35	327.3	-20.5	3.9902	1144.9	63.8	167.6	174.0
DEC 11 73	4:51: 0	327.3	-20.5	3.9913	1144.9	63.8	167.5	174.0
DEC 11 73	4:55:25	327.3	-20.5	3.9922	1144.9	63.8	167.5	173.9
DEC 11 73	4:59:50	327.3	-20.5	3.9929	1144.9	63.8	167.5	173.9
DEC 11 73	5: 4:15	327.3	-20.5	3.9936	1144.9	63.8	167.5	173.9
DEC 11 73	5: 8:40	327.3	-20.5	3.9940	1144.9	63.8	167.5	173.9
DEC 11 73	5:13: 5	327.3	-20.5	3.9944	1144.9	63.8	167.6	173.9
DEC 11 73	5:17:30	327.3	-20.5	3.9946	1144.9	63.8	167.6	173.9
DEC 11 73	5:21:55	327.3	-20.5	3.9949	1144.9	63.7	167.6	173.9
DEC 11 73	5:26:20	327.3	-20.5	3.9950	1144.9	63.7	167.6	173.9
DEC 11 73	5:30:45	327.3	-20.5	3.9951	1144.9	63.7	167.7	173.9
DEC 11 73	5:35:10	327.3	-20.5	3.9951	1144.9	63.7	167.7	173.9
DEC 11 73	5:39:35	327.3	-20.5	3.9951	1144.9	63.7	167.7	173.9
DEC 11 73	5:44: 0	327.3	-20.5	3.9950	1144.9	63.7	167.7	173.9
DEC 11 73	5:48:25	327.3	-20.5	3.9949	1144.9	63.7	167.7	173.9
DEC 11 73	5:52:50	327.3	-20.5	3.9947	1144.9	63.7	167.7	173.9
DEC 11 73	5:53: 0	327.3	-20.5	3.9947	1144.9	63.7	167.7	173.9

APPENDIX C - OPTIMAL ATTITUDE CONTROL

COMPUTER SIMULATION FOR TIME OPTIMAL OR ENERGY OPTIMAL ATTITUDE CONTROL OF SPIN-STABILIZED SPACECRAFT

Robert D. Woolley
(Computer Sciences Corporation, Silver Spring, Md.)
Roger D. Werking
(NASA-Goddard Space Flight Center, Greenbelt, Md.)

SUMMARY

An original technique for determining the optimal magnetic torque strategy for control of the attitude of spin stabilized spacecraft is presented. By employing Lagrange multipliers and the Calculus of Variations, optimal control equations are derived which define minimum time and minimum energy attitude maneuvers. Computer program algorithms to numerically solve these optimal control equations are also described. The performance of this technique is compared with a commonly employed planning method.

INTRODUCTION

For several years, the orientation of most near-earth spacecraft has been controlled by the interactions of magnetic fields. Figure 1 illustrates a controllable electromagnetic coil whose axis is parallel to the axis of rotation (spin axis) of the spacecraft on which it is mounted. When electric current flows through this coil, the resultant magnetism interacts with the earth's magnetic field to produce a torque on the spacecraft. By controlling the magnitude and polarity of the electric current, controlled torques are produced which change the spin axis orientation.

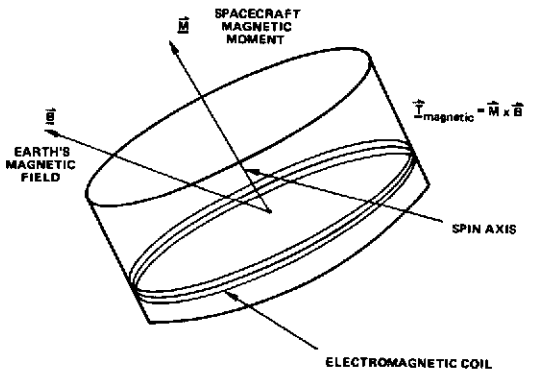

Figure 1. A Spin-Stabilized Spacecraft Employing Magnetic Attitude Control

In early missions, commanded changes of this electric current were limited by the necessity for ground station contacts at the times of change. The magnetic control systems were left in a given state for a period of orbits or days. During this time, the spin axis would precess at a very slow average rate. These early control systems were intended to maintain spacecraft sun angles and compensate for unavoidable environmental disturbance torques.

The launch of TIROS IX introduced an innovation in magnetic control system design. It was known that a more efficient control system would switch the coil polarity four times per orbit [1], [2], [3]. This system, depicted in Figure 2, was called Quarter Orbit Magnetic Attitude Control (QOMAC). The quarter orbit switching was accomplished by an onboard timer which reduced the reliance on ground station contact. The QOMAC maneuver continued as long as was necessary to achieve the desired spin axis precession. Control capabilities increased dramatically from a few degrees per week to about five degrees per orbit.

Recently designed spacecraft are being equipped with command memories. With this capability, the exact time at which a coil state should change can be preloaded into the command memory. This has added tremendous flexibility to the use of magnetic control systems and has improved the efficiency of these systems even further. This is especially true for eccentric orbits and low inclination orbits where QOMAC is not readily adaptable. With this increased flexibility, control planning processes become more complicated.

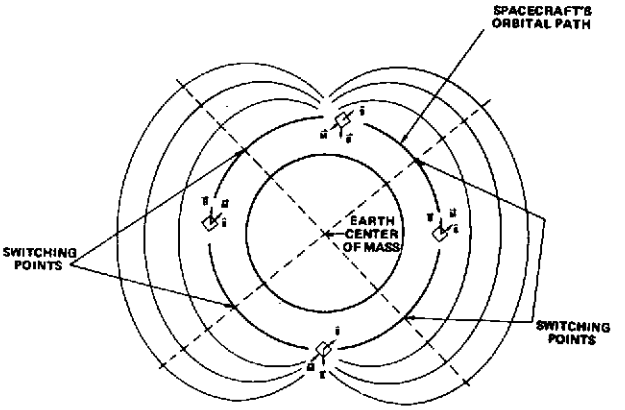

Figure 2. QOMAC Coil Switching Technique

This paper presents a technique to mechanize the control planning process using high-speed computers and optimal control theory. The computer program developed for this technique will be used to support the Atmosphere Explorer (AE) and Orbiting Solar Observatory (OSO) satellites. It will minimize either the coil energy or the elapsed time required to complete maneuvers between specified attitudes. The option selected depends on the immediate mission requirements.

THE ATTITUDE STATE EQUATION

Consider a spin stabilized spacecraft system containing a nutation damping system. This system maintains collinearity between the spacecraft's angular velocity vector and one of its principal body axes. Defining the spin axis as their common direction, the angular momentum is

$$\underline{H} = H\hat{\underline{S}} \tag{1}$$

where H is the magnitude of the spacecraft's angular momentum, and $\hat{\underline{S}}$ is a unit vector in the direction of the spin axis, expressed in an inertial coordinate system.

Spin-stabilized spacecraft utilizing magnetic attitude control are designed and built with the axis of an onboard bidirectional electromagnet aligned to the spacecraft spin axis. The polarity of the resulting magnetic moment is determined by the direction of electrical current through the coil; the magnitude of magnetic moment is determined by the magnitude of coil current. These design characteristics are summarized by the following equations.

$$\underline{M} = \hat{\underline{S}}mu \tag{2}$$

$$-1 \le u \le +1 \tag{3}$$

where $\underline{M}$ is the electromagnet's magnetic moment, m is the maximum magnitude of the magnetic moment (possibly a function of time), and u is the normalized remotely commanded coil state.

The external torque on the spacecraft resulting from the interaction of the onboard electromagnet with the earth's magnetic field is

$$\underline{T}_{magnetic} = \underline{M} \times \underline{B} = \hat{\underline{S}} \times m\underline{B}u \tag{4}$$

where $\underline{B}$ is the inertial representation of the local external magnetic flux density in the vicinity of the spacecraft. In near-earth space, the magnetic field is approximately equal to the geomagnetic field. This field is mathematically characterized to sufficient accuracy by a spherical harmonic expansion in terms of latitude, longitude, and altitude [4], [5]. Thus, for a satellite in a known near-earth orbit, the local external magnetic flux density, $\underline{B}$, can be obtained as a function of time alone.

The spin axis state equation is governed by Newton's second law applied to the rotational motion of the spacecraft in inertial space. Thus

$$\frac{d}{dt}(H\underline{\hat{s}}) = \underline{\hat{s}} \times m\underline{B}u + \underline{T}_d \tag{5}$$

where $\underline{T}_d$ is the vector sum of environmental disturbance torques acting on the spacecraft. Significant disturbance torques are caused by the interaction of the residual magnetic moment of the spacecraft with the earth's magnetic field, and by offsets between the spacecraft center-of-mass and the lines of action of solar pressure, aerodynamic drag pressure, and gravity. These offsets and residual magnetic moments tend to rotate with the spacecraft, so that their effective average direction is approximately aligned with the spin axis. The disturbance torques can thus be approximated by

$$\underline{T}_d = \underline{\hat{s}} \times \underline{D} \tag{6}$$

where $\underline{D}$ is the sum of the average generalized forces multiplied by their offsets along the spin axis.

Spin stabilized spacecraft generally have extremely small variations in the magnitude of the angular momentum vector. This is partially because spin axis components of environmental torques tend to cancel themselves effectively during each spin rotation period, and partially because the angular momentum magnitude is generally quite large. Since angular momentum magnitude is maintained within a close tolerance of a nominal value by periodic actions of a different onboard torquing system, it is considered to be a constant or a known time function. Thus we have the following spin axis attitude state equation:

$$\frac{d\underline{\hat{s}}}{dt} = \underline{\hat{s}} \times \left[\frac{m}{H}\underline{B}u + \frac{1}{H}\underline{D}\right] \tag{7}$$

For most spin-stabilized spacecraft, the coil controlling onboard electronics do not allow continuous variation of coil current magnitude. Instead, the coil current may be off or on with either polarity at a designed value. For these spacecraft, Equation (3) is replaced by

$$u = -1,\ 0,\ \text{or}\ +1 \tag{8}$$

THE CONTROL PLANNING PROBLEM

The attitude state equation, Equation (7), is time varying, nonlinear, and not totally controllable. The time-varying nature of the magnetic and disturbance vectors, $\underline{B}$ and $\underline{D}$, preclude the use of classical controls techniques which employ frequency domain analysis. Nonlinear effects arise because the control variable, u, and the attitude, $\underline{\hat{s}}$, are multiplied together in Equation (7). The attitude is not totally controllable because instantaneous disturbances and the desired attitude motion possess two degrees of freedom while the instantaneous commandable torque has only one. Therefore, it is theoretically impossible to precisely follow many continuously specified attitude trajectories. The addition of the control constraints in either Equation (3) or Equation (8) to Equation (7) almost guarantees the fruitlessness of an intuitive approach to control planning.

Attitude control planning may be accomplished with time domain analysis if some additional constraint is placed on the control beyond those of Equations (7) and (8). For instance, the QOMAC method constrains the coil to remain energized throughout an active control period, alternating polarity at precise quarter-orbit intervals. Thus, the QOMAC control problem is reduced to determining the desired duration of the active control period and the constant relative phasing between the orbit and coil alternations.

An optimal control law adds the constraint that a physically significant cost function is minimized. The objective of the control technique to be presented is to determine the discrete $u(t)$ control history which causes the spin axis attitude to change from $\underline{\hat{s}}_1$ to $\underline{\hat{s}}_2$ in an optimal manner. The direction, $\underline{\hat{s}}(t)$, must always satisfy Equation (7), and the sense of optimality is either minimum time or minimum electrical energy to activate the electromagnet. Minimum time maneuvers achieve greater attitude motion during a limited period than any other maneuvers. Hence, rapid attitude changes are accomplished most effectively. Minimum energy maneuvers achieve a desired final attitude in a specified time period, with as little coil energy expenditure as possible.

THE OPTIMAL CONTROL EQUATIONS

In view of Equation (8), the amount of energy used by the coil for a given maneuver is proportional to the functional

$$J_1 = \int_{t_1}^{t_f} |u|\,dt \tag{9}$$

The elapsed time for a maneuver is the functional

$$J_2 = \int_{t_1}^{t_f} dt = t_f - t_1 \tag{10}$$

Using the definitions

$$L_1 = |u| \tag{11}$$

$$L_2 = 1 \tag{12}$$

the performance functions which are to be separately minimized may be compactly expressed by the single integral equation

$$J_i = \int_{t_1}^{t_f} L_i\,dt \tag{13}$$

The quantity being minimized, J_i, is augmented by the state and control equations as follows:

$$J_i = \int_{t_1}^{t_f} \left[L_i + \underline{\lambda}^T\left(\underline{\hat{s}} \times \left[\frac{m}{H}\underline{B}u + \frac{1}{H}\underline{D}\right] - \frac{d\underline{\hat{s}}}{dt}\right) + \mu(u^2 - 1)\right] dt \tag{14}$$

where $\underline{\lambda}$ and μ are Lagrange multipliers with

$$\mu \begin{cases} > 0 \text{ if } u^2 - 1 = 0 \\ = 0 \text{ if } u^2 - 1 < 0 \end{cases} \tag{15}$$

Equation (14) is integrated by parts and its first variation set to zero as a necessary condition for minimization of J_i. Since the endpoint conditions are fixed, and the Lagrange multipliers are selected so that the remaining terms in the first variation of J_i with respect to variations in the control, u, and the attitude, $\underline{\hat{s}}$, are zero, any optimal maneuver minimizing Equation (14) must satisfy the following Euler-Lagrange vector equations [6]:

$$\frac{\partial}{\partial u}\left\{L_i + \underline{\lambda}^T\left[\underline{\hat{s}} \times \left(\frac{m}{H}\underline{B}u + \frac{1}{H}\underline{D}\right)\right] + \left(\frac{d}{dt}\underline{\lambda}^T\right)\underline{\hat{s}} + \mu(u^2 - 1)\right\} = 0 \tag{16}$$

$$\frac{\partial}{\partial \underline{\hat{s}}}\left\{L_i + \underline{\lambda}^T\left[\underline{\hat{s}} \times \left(\frac{m}{H}\underline{B}u + \frac{1}{H}\underline{D}\right)\right] + \left(\frac{d}{dt}\underline{\lambda}^T\right)\underline{\hat{s}} + \mu(u^2 - 1)\right\} = \underline{0}^T \tag{17}$$

The Lagrange multipliers, the attitude, and the disturbance torques are not explicitly functions of the coil state, u; therefore, partial derivatives of $\underline{\lambda}$, μ, $\underline{\hat{s}}$, and $\underline{D}$ with respect to u are zero. Coil control histories for minimum energy and minimum time maneuvers are defined as $u_1(t)$ and $u_2(t)$, respectively. Equations (11), (12), (15), and (16) are combined to produce

$$u_1 = -\text{DEZ}\left[\frac{m}{H}\underline{\lambda}^T(\underline{\hat{s}} \times \underline{B})\right] \tag{18}$$

$$u_2 = -\text{SGN}\left[\frac{m}{H}\underline{\lambda}^T(\underline{\hat{s}} \times \underline{B})\right] \tag{19}$$

where DEZ represents the deadzone function

$$\text{DEZ}(x) = \begin{cases} +1 \text{ if } 1 < x \\ 0 \text{ if } -1 \le x \le +1 \\ -1 \text{ if } x < -1 \end{cases} \tag{20}$$

and where SGN represents the signum function

$$SGN(x) = \begin{cases} +1 \text{ if } 0 < x \\ 0 \text{ if } x = 0 \\ -1 \text{ if } x < 0 \end{cases} \qquad (21)$$

The variables L_i , $\underline{\lambda}$, u , and μ are not explicitly functions of the attitude; therefore, their partial derivatives with respect to $\hat{\underline{s}}$ are zero. For either the minimum time or the minimum energy optimal maneuvers, Equation (17) is reduced to

$$\frac{d}{dt}\underline{\lambda} = \underline{\lambda} \times \left[\frac{m}{H}\underline{Bu} + \frac{1}{H}\underline{D}\right] + \left[\frac{\partial \underline{D}}{\partial \hat{\underline{s}}}\right](\hat{\underline{s}} \times \underline{\lambda}) \qquad (22)$$

Equations (7), (18), and (22) or Equations (7), (19), and (22) define minimum energy or minimum time optimal maneuvers, respectively, in the presence of any normal disturbance torques. However, for certain types of disturbance torques, such as those caused by residual dipole moment or aerodynamic forces, the vector $\underline{D}$ is approximately a function of time only, independent of $\hat{\underline{s}}$. For these types of disturbance torques, Equation (22) becomes

$$\frac{d}{dt}\underline{\lambda} = \underline{\lambda} \times \left[\frac{m}{H}\underline{Bu} + \frac{1}{H}\underline{D}\right] \qquad (23)$$

Equations (7) and (23) maintain both a constant magnitude of $\underline{\lambda}$ and a constant angle between $\underline{\lambda}$ and $\hat{\underline{s}}$. Since the component of $\underline{\lambda}$ along $\hat{\underline{s}}$ does not affect u through either Equation (18) or (19), that component may be arbitrarily set to zero. The resulting $\underline{\lambda}$ has a magnitude and a direction perpendicular to $\hat{\underline{s}}$ which define

$$C = \frac{1}{\sqrt{\underline{\lambda}^T\underline{\lambda}}} \qquad (24)$$

$$\hat{\underline{q}} = \hat{\underline{s}} \times \underline{\lambda}C \qquad (25)$$

By the definition of the signum function given in Equation (21), the coil control for a minimum time optimal maneuver is not influenced by the magnitude of $\underline{\lambda}$, only by the direction of $\underline{\lambda}$. Furthermore, as the magnitude of $\underline{\lambda}$ approaches infinity, Equations (18) and (19) become equivalent. With the above considerations and a specification of required initial and final attitudes, Equations (24) and (25) are substituted into Equations (18) and (23). The following resultant optimal equations define both minimum time and minimum energy optimum maneuvers:

$$\frac{d}{dt}\hat{\underline{s}} = \hat{\underline{s}} \times \left[\frac{m}{H}\underline{Bu} + \frac{1}{H}\underline{D}\right] \qquad (7)$$

$$\frac{d}{dt}\hat{\underline{q}} = \hat{\underline{q}} \times \left[\frac{m}{H}\underline{Bu} + \frac{1}{H}\underline{D}\right] \qquad (26)$$

$$u = \begin{cases} +1 \text{ if } C < \frac{m}{H}\underline{B}\cdot\hat{\underline{q}} \text{ and } t \le t_f \\ 0 \text{ if } -C \le \frac{m}{H}\underline{B}\cdot\hat{\underline{q}} \le C \text{ or } t_f < t \\ -1 \text{ if } \frac{m}{H}\underline{B}\cdot\hat{\underline{q}} < -C \text{ and } t \le t_f \end{cases} \qquad (27)$$

$$\hat{\underline{q}}(t_1)\cdot\hat{\underline{s}}(t_1) = 0 \qquad (28)$$

$$t_1 \ , \ \hat{\underline{s}}(t_1) = \hat{\underline{s}}_1 \quad \text{specified} \qquad (29)$$

$$t_2 \ , \ \hat{\underline{s}}(t_2) = \hat{\underline{s}}_2 \quad \text{specified} \qquad (30)$$

$$\begin{aligned} &t_f = t_2 \ , \ C \ge 0 \quad \text{if minimum energy} \\ &C = 0 \ , \ t_1 \le t_f \le t_2 \quad \text{if minimum time} \end{aligned} \qquad (31)$$

Since Equations (7) and (26) have identical form, they can both be numerically solved in one attitude simulation program. Equation (29) fixes the initial attitude $\hat{\underline{s}}(t_1)$ and Equation (28) constrains the initial pseudo-attitude $\hat{\underline{q}}(t_1)$ to be perpendicular to $\hat{\underline{s}}(t_1)$. Equation (27) gives the algorithm used for computing the optimal coil control throughout the simulation.

COMPUTER ALGORITHMS

The optimal control equations have two undetermined parameters which must be correctly selected in order to achieve the final attitude specified by Equation (30). One of the parameters appears explicitly in Equation (31), the other parameter is implicit in Equation (28). To express this other parameter in equation form, a right-handed system is defined about the initial attitude. Introducing two mutually perpendicular unit vectors, $\hat{\underline{a}}_1$ and $\hat{\underline{a}}_2$, which are perpendicular to the initial attitude vector, i.e.,

$$\hat{\underline{a}}_1\cdot\hat{\underline{a}}_2 = 0 \qquad (32)$$

$$\hat{\underline{s}}(t_1)\cdot(\hat{\underline{a}}_1 \times \hat{\underline{a}}_2) = +1 \qquad (33)$$

Equation (28) can be replaced by

$$\hat{\underline{q}}(t_1) = \hat{\underline{a}}_1 \cos\phi + \hat{\underline{a}}_2 \sin\phi \ , \ 0 \le \phi < 2\pi \qquad (34)$$

The two undetermined parameters are then C and ϕ for the minimum energy case, and t_f and ϕ for the minimum elapsed time case.

Because the boundary conditions of Equations (29) and (30) are split between the initial and final endpoints, no explicit equations are employed to determine the parameters ϕ and C or t_f . Instead, Equations (7), (26) through (29), and (31) are successively solved by a fast simulation routine. A two-dimensional numerical search algorithm drives this routine, varying values of the appropriate parameters on successive simulations to converge on the final attitude specified by Equation (30). Computer time economy dictates that both the fast simulation and the two-dimensional search be as efficient as possible.

The commandable magnetic precession vector appearing in Equation (27) is a function of time alone, independent of attitude. The geomagnetic flux density vector, $\underline{B}$, is a known function of the spacecraft's position with respect to the rotating earth; the spacecraft's inertial position-time dependence is given by non-Keplerian formulas which include effects of terrestial oblateness and atmospheric drag. The commandable magnetic moment, m , is a function of the voltage available to power the onboard electromagnet. This voltage may have a different value when the spacecraft's position is in the earth's shadow than when the spacecraft's position is in sunlight, because of differing characteristics of batteries and solar arrays. The commandable magnetic moment may also be set to zero during any portion of the period of interest in order to mechanize requirements that the coil be off during those periods (see Equation 27).

Although the commandable magnetic precession vectors could be recomputed during each execution of the fast simulation routine, much computer time is saved (at the expense of some storage space) by initially filling a 3-by-N array with N computed 3-by-1 commandable precession vectors for each N integration time step spanning the period of interest. The fast simulation routine is further streamlined by the use of a direct precession vector integration scheme. Equations (7) and (26) may be rewritten as

$$\frac{d}{dt}\hat{\underline{s}} = \tilde{\underline{s}} \times \left[\frac{m}{H}\underline{Bu} + \frac{1}{H}\underline{D}\right] + (\hat{\underline{s}} - \tilde{\underline{s}}) \times \left[\frac{m}{H}\underline{Bu} + \frac{1}{H}\underline{D}\right] \qquad (35)$$

$$\frac{d}{dt}\hat{\underline{q}} = \tilde{\underline{q}} \times \left[\frac{m}{H}\underline{Bu} + \frac{1}{H}\underline{D}\right] + (\hat{\underline{q}} - \tilde{\underline{q}}) \times \left[\frac{m}{H}\underline{Bu} + \frac{1}{H}\underline{D}\right] \qquad (36)$$

where $\tilde{\underline{s}}$ and $\tilde{\underline{q}}$ may be arbitrary. For a constant coil control period where

$$u(t) = u_j \ , \ t_j < t < t_{j+1} \qquad (37)$$

they are selected as

$$\tilde{\underline{s}} = \hat{\underline{s}}(t_j) \qquad (38)$$

$$\tilde{\underline{q}} = \hat{\underline{q}}(t_j) \qquad (39)$$

Equations (35) through (39) are combined, neglecting the small terms in Equations (35) and (36), and integrated to yield

$$\underline{s}(t_{j+1}) \cong \hat{\underline{s}}(t_j) + \underline{\hat{s}}(t_j) \times \left[U_j \left(\int_{t_1}^{t_{j+1}} \frac{m}{H} \underline{B} dt - \int_{t_1}^{t_j} \frac{m}{H} \underline{B} dt \right) + \int_{t_1}^{t_{j+1}} \frac{1}{H} \underline{D} dt - \int_{t_1}^{t_j} \frac{1}{H} \underline{D} dt \right] \tag{40}$$

$$\underline{g}(t_{j+1}) \cong \hat{\underline{g}}(t_j) + \hat{\underline{g}}(t_j) \times \left[U_j \left(\int_{t_1}^{t_{j+1}} \frac{m}{H} \underline{B} dt - \int_{t_1}^{t_j} \frac{m}{H} \underline{B} dt \right) + \int_{t_1}^{t_{j+1}} \frac{1}{H} \underline{D} dt - \int_{t_1}^{t_j} \frac{1}{H} \underline{D} dt \right] \tag{41}$$

Analysis of the approximations, Equations (40) and (41), shows that the directional approximation errors can be kept extremely small while maintaining appreciable time steps between t_j and t_{j+1}. For small motions through an angle $\Delta\psi$ (radians), the per unit directional error introduced by Equations (40) and (41) is

$$\frac{\text{ERROR } (\Delta\psi)}{\Delta\psi} = \frac{(\Delta\psi)^2}{3} \tag{42}$$

For example, a 90-degree attitude maneuver simulated using these approximations and $\Delta\psi$ as large as one degree would be in error by about one hundredth of a degree. Of course, each application of Equations (40) and (41) is followed by unitizing the results to form $\hat{\underline{s}}(t_{j+1})$, $\hat{\underline{g}}(t_{j+1})$.

Since the integrals in Equations (40) and (41) do not involve the attitude, it is not necessary that they be recomputed in each execution of the fast simulation program. Much computer time is saved by initially filling a pair of 3-by-(N+1) arrays with the (N+1) computed 3-by-1 integral commandable precession vectors and the (N+1) computed 3-by-1 integral disturbance precession vectors for each of the N+1 integration time points spanning the period of interest. These integral commandable and disturbance precession vectors are directly computed as the Riemann integral of the commandable and disturbance precession vectors. Position and time dependent parameters essential to compute the commandable and disturbance precession vectors are provided by a call to an external routine.

The fast simulation program steps through every entry of its commandable precession vector table, using Equation (27) in every case to determine the instantaneous commanded coil state. Equations (40) and (41) are applied every M entries to avoid excessive approximation error. Whenever a coil state change is detected, a search is instituted using Equations (41) and (27) to determine the precise switching time. After it is located, both Equations (40) and (41) are applied before continuing to step through the table, checking Equation (27).

The two-dimensional numerical search algorithm which calls the fast simulation program is based on a variable separation technique. A right-handed system is defined about the final attitude resulting from no control, such that

$$\underline{\hat{s}}(t_2)_{\text{NO CONTROL}} \times (\hat{\underline{b}}_1 \times \hat{\underline{b}}_2) = +1 \tag{43}$$

$$\hat{\underline{b}}_1 \times \hat{\underline{b}}_2 = 0 \tag{44}$$

Then for any other final attitude, $\hat{\underline{s}}_k(t_2)$, we can define angles ρ_k and θ_k such that

$$\hat{\underline{s}}_k(t_2) = \underline{\hat{s}}(t_2)_{\text{NO CONTROL}} \cos\rho_k + \hat{\underline{b}}_1 \cos\theta_k \sin\rho_k + \hat{\underline{b}}_2 \sin\theta_k \sin\rho_k \tag{45}$$

For both the minimum elapsed time case and the minimum coil time case, it is assumed that θ is monotonically related to ϕ. We also assume that ρ is monotonically related to C in the minimum energy case, and to t_f in the minimum time case. The search technique, making use of these assumptions tries to adjust ϕ and either C or t_f in order to drive θ and ρ to the desired θ and ρ. The adjustments are made in embedded bracket-method, one-dimensional searches. These assumptions have been justified by the convergence of the search algorithm for all tested cases.

The inner search algorithm adjusts only the value of C (or t_f), utilizing in its calls to the fast simulation routine the ϕ passed to it from the outer search. It initially tries C = 0 (or $t_f = t_2$) to establish whether or not an angular motion of ρ_{DESIRED} can be achieved. If the resultant ρ computed by the fast simulation routine is less than the desired ρ, control is passed back to the outer search. If, however, the desired magnitude of motion can be achieved, the inner search successively increases C (or decreases t_f) until a ρ less than the desired ρ results. Having bracketed the desired amount of motion with two values of C (or t_f), the inner search iteratively converges on a value producing the desired motion by repetitively testing values in the interval and letting them replace the appropropriate upper or lower bracket value to reduce the bracket size. Control is passed back to the outer search algorithm after the bracket size is reduced to the computer's numerical precision size.

The outer search algorithm starts with an initial estimate of the correct value of ϕ, then passes control to the inner search algorithm. After the inner search algorithm has returned control to the outer search, θ is computed and compared with the desired θ. Then ϕ is either increased or decreased in repetitive calls to the inner search, until the outer search has established a pair of ϕ-values with associated θ-values bracketing the desired θ. After bracketing is achieved, convergence proceeds similar to the inner search, by repetitively subdividing the interval, down to the numerical precision of the computer. Upon convergence of the outer search, the desired attitude maneuver has been obtained. The coil state history is that determined during the last execution of the fast simulation routine.

The average number of fast simulations executed to achieve ultimate convergence is approximately the product of the average number of bracket subdivisions performed in each of the two one-dimensional searches. Thus, the required computer time is quite sensitive to the method of subdividing the intervals. The conservative approach of interval halving requires 25 steps per one-dimensional search. Use of this method requires about 625 fast simulations for ultimate convergence. A linear interpolation approach can complete a one-dimensional search in as few as 4 steps if the linearity assumption is approximately valid, requiring about 16 fast simulations for ultimate convergence. Drastic departures from the assumed linearity can make this method even less efficient than the interval halving method.

The bracket subdivision algorithm used in the developed program is a weighted average between linear interpolation and interval halving. Weighting factors are redetermined prior to each iteration on the basis of the departure from linearity detected in the previous iteration. This self-adaptive feature results in consistent achievement of the ultimate convergence within 20 to 50 fast simulations.

If the desired final attitude is unachievable during the period of interest, this search scheme converges to a final attitude on a great circle connecting the desired final attitude with the "no control" final attitude, as close as possible to the desired final attitude. However, this program can also identify the set of achievable final attitudes when operating it in a different mode.

The set of all final attitudes achievable during a control period is bounded by the set of all final attitudes achievable using maximal time optimal control throughout the period. Thus, by setting

$$C = 0 \tag{46}$$

$$t_f = t_2 \tag{47}$$

and stepping ϕ from 0 to 360 degrees on successive executions of the fast simulation program, a contour passing through the successive attitudes encloses all possible final attitudes achievable during the control period utilizing any magnetic attitude control planning scheme.

EVALUATION OF OPTIMAL MAGNETIC ATTITUDE CONTROL

Practical application of optimal control to real attitude control planning tasks necessitates access to a computer. Although the time required for the computer solution is minimal, a manual numerical calculation of an optimal attitude maneuver would be prohibitively time consuming. This computer requirement compares unfavorably with previously employed planning methods. Approximate algebraic formulas exist for both QOMAC and continuous control maneuvers, allowing an analyst to manually plan maneuvers with few numerical calculations. But the benefits gained from optimal maneuvers warrant computer availability.

Optimal magnetic attitude control has two main advantages. Coil utilization is more efficient for optimal control maneuvers than for any other type of maneuver. Also, the use of optimal control automates the planning process, thus reducing the analyst's involvement below the necessary levels of involvement characteristic of other planning methods [7].

Coil utilization is significantly more efficient for optimal control than for QOMAC, over a large class of orbits. The only cases where the improvements in efficiency are sometimes small are with low altitude polar orbits. In those cases, optimal maneuvers are similar or identical to QOMAC-generated maneuvers.

Table 1 compares minimum time and minimum energy optimal maneuvers with a QOMAC maneuver.

Table 1. Performance Comparison of Optimal and QOMAC Maneuvers

MANEUVER TYPE	MANEUVER COMPLETION TIME	ENERGY (COIL ON-TIME)
MINIMUM TIME OPTIMAL	270 MINUTES	270 MINUTES
MINIMUM ENERGY OPTIMAL	457 MINUTES	174 MINUTES
QOMAC	457 MINUTES	457 MINUTES

The maneuvers are between identical attitudes and start at the same initial time in the same orbit (see Table 2).

Table 2. Parameter Values Used in Comparative Maneuvers

PLANNING PARAMETERS	
INITIAL TIME	DEC. 21, 1973; 0 HRS, 0 MIN, 0 SEC
INITIAL RIGHT ASCENSION OF SPIN AXIS	10 DEGREES
INITIAL DECLINATION OF SPIN AXIS	0 DEGREES
FINAL RIGHT ASCENSION OF SPIN AXIS	0 DEGREES
FINAL DECLINATION OF SPIN AXIS	0 DEGREES
SPACECRAFT PARAMETERS	
COMMANDABLE MAGNETIC MOMENT OF COIL	98 AMPERE-TURN-METER^2
ANGULAR MOMENTUM ABOUT SPIN AXIS	134.4 NEWTON-METER-SEC
ORBIT PARAMETERS	
ECCENTRICITY	0.002
SEMIMAJOR AXIS	6,700 KILOMETERS
INCLINATION	88 DEGREES
RIGHT ASCENSION OF ASCENDING NODE	0 DEGREES
ARGUMENT OF PERIGEE	0 DEGREES
MEAN ANOMALY	0 DEGREES
EPOCH	DEC. 21, 1973: 0 HRS, 0 MIN, 0 SEC

The chosen orbit is low altitude, nearly circular, and only 22 degrees away from a polar orbit, to present a case where QOMAC performs well. But the minimum time optimal maneuver (Figure 3) is still considerably faster than the QOMAC maneuver (Figure 5). The minimum energy optimal maneuver (Figure 4) was computed by allowing the same amount of time for maneuver completion as required by QOMAC. But the minimum energy optimal maneuver uses 60 percent less energy (coil-on-time) than the QOMAC maneuver. These improvements become considerably more dramatic with orbits of lower inclination, higher altitude, or greater eccentricity.

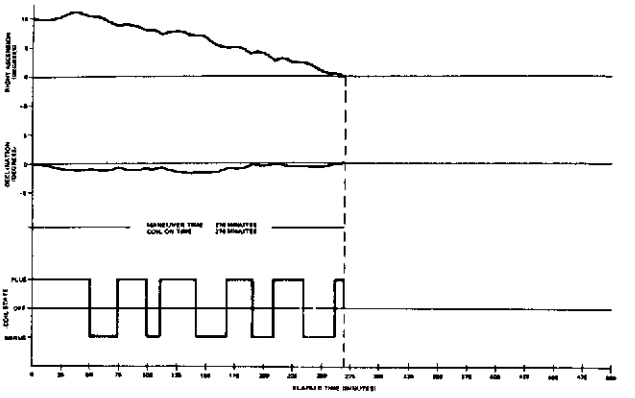

Figure 3. Minimum Time Optimal Maneuver

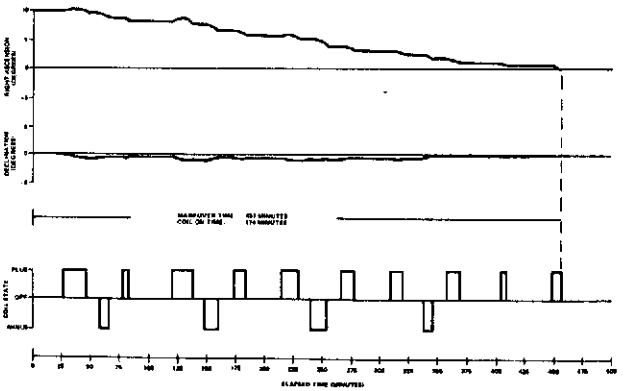

Figure 4. Minimum Energy Optimal Maneuver

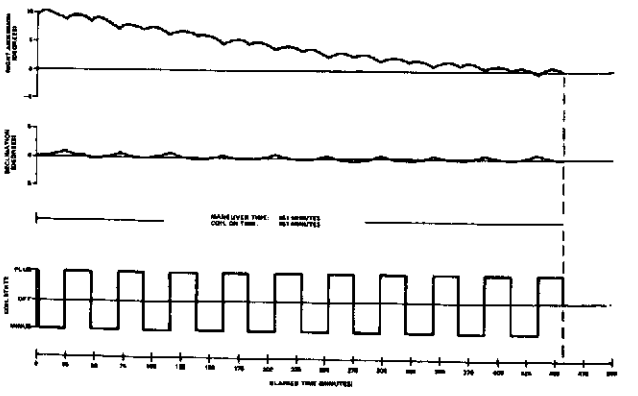

Figure 5. QOMAC Maneuver

Numerous modifications to the QOMAC method have been developed for special cases and used for control planning. These modifications attempt to improve the coil utilization efficiency with minimal change to the analytical approach of the basic QOMAC method. Of course, coil utilization efficiencies of these pseudo-QOMAC methods, even when applied to the special cases for which they were developed, can never surpass the coil efficiency of the optimal method.

Optimal magnetic attitude control automates the planning process through its algorithms' form and flexibility. The optimal control algorithms are orbit independent. They therefore apply directly to elliptical orbits. They can be used for a control period including only a portion of an orbit, or even for a control period which includes orbit adjustment maneuvers.

The optimal magnetic attitude control algorithms developed here compute a maneuver from the input specified initial attitude to precisely the input specified final attitude, if that final attitude is within the region achievable during the planning period. Planning methods utilizing an integer number of quarter-orbit coil pulses cannot, in general, precisely achieve a specified final attitude. The optimal control planning method eliminates the need for a "fine tuning" terminal portion of a maneuver as required by a modified QOMAC technique, thus reducing analyst requirements.

The commandable region boundary of achievable final attitudes may be automatically computed for any planning period, using the optimal control algorithms. An example of a commandable region boundary for an 8-hour control period using the parameters of Table 1 appears in Figure 6. None of the attitudes outside the boundary can be achieved during the control period using magnetic attitude control, no matter what method of planning is used. Any attitude inside the boundary can be achieved during the control period. Any attitude on the boundary itself can be achieved during the control period but only by employing optimal control.

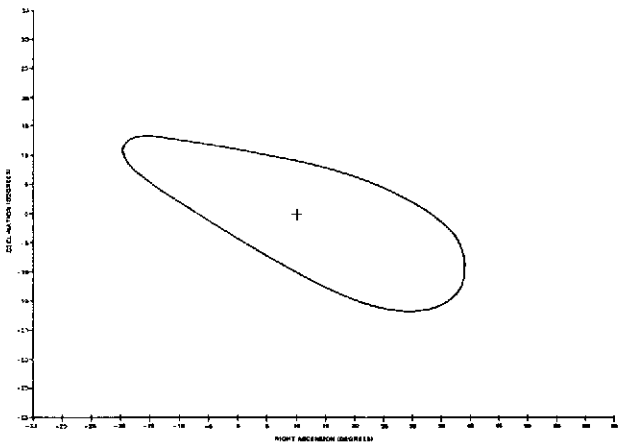

Figure 6. Commandable Region Boundary for an Eight-Hour Control Period

By providing the capability of computing the commandable region boundary for any control period, the optimal control algorithms succinctly display the set of available options to a program operator. This flexibility greatly reduces the analytical expertise necessary to select a desired final attitude, or a control period, or both.

Approximation errors in the optimal magnetic attitude control algorithms can be kept arbitrarily small. Consequently, any degree of desired planning accuracy can be achieved. An accurate geomagnetic field model can be used, as opposed to the canted dipole model assumed by most other methods. Different commandable coil strengths may be used for the sunlit and dark portions of a planning period. The effects of any modelled disturbance torques can be directly included. These characteristics of the optimal control algorithms can eliminate the discrepancies, innate in other control planning methods, between a control planning computer program, and an accurate attitude prediction (simulation) computer program. Elimination of the discrepancies reduces the need for analysis.

The optimal magnetic attitude control algorithms have the additional flexibility that a control period may include several input-specified, coil-off periods. A control program operator, knowing of scheduled spacecraft data collection periods during which the coil must be kept off, simply specifies those periods to the program. The commandable region boundary, and any optimal maneuvers, are then automatically computed by the program subject to the constraint that the coil be kept off during the specified coil-off portions of a control period.

By first presenting to an operator an accurate display of achievable final attitudes subject to any operator-specified time constraints, and then by generating a set of commands which precisely achieve the operator-selected final attitude, the optimal control algorithms effectively automate the control planning process. The generated set of commands minimize coil usage over all possible maneuvers meeting the operator-specified conditions.

REFERENCES

1. Attitude Handbook for the TIROS IX Meteorological Satellite Systems, RCA/Astro-Electronics Division, M-2036, October 7, 1964.

2. Sugaii, I., Kikkawa, S. and Werking, R., "Computer Simulation for Attitude Disturbance Torques for the Tiros Series," 1971 Summer Computer Simulation Conference, July 1971.

3. Bandeen, W. R. and Manger, W. P., Angular Motion of the Spin Axis of the TIROS-1 Meteorological Satellite due to Magnetic and Gravitational Torques, NASA TN D-571, April 1961.

4. Cain, J. C., Hendricks, S. J., Langel, R. A. and Hudson, W. V., "A Proposed Model for the International Geomagnetic Reference Field-1965," Journal of Geomagnetism and Geoelectricity, vol. 19, no. 4, 1967.

5. Hendricks, S. J. and Cain, J. C., "Magnetic Field Data for Trapped-Particle Evaluations," Journal of Geophysical Research, vol. 21, no. 1, January 1966.

6. Bryson, A. E. and Yu-Chi Ho, Applied Optimal Control, Ginn & Co., Waltham, Massachusetts, 1969, pp. 42-87.

7. Rosner, O., Parameter Determination for Roll/Yaw Control by Magnetics in Elliptical Orbit, RCA/Astro-Electronics Division, DN-1014-2.8/2.12(AE), March 1972.